



Co-funded by the
Erasmus+ Programme
of the European Union



University of Évora

ARCHMAT
(ERASMUS MUNDUS MASTER in ARCHaeological
MATerials Science)

Mestrado em Arqueologia e Ambiente (Erasmus Mundus – ARCHMAT)

**Characterization of mortars associated with the hydraulic
system of roman *villa* Horta da Torre (Fronteira, Portugal)**

Dulce Elizabeth Valdez Madrid
m40698

Patrícia Sofia Martins Moita
(Supervisor - Universidade de Évora)

Paula Cristina Gonçalves Pereira Galacho
(Co-supervisor - Universidade de Évora)

André Miguel Serra Pedreira Carneiro
(Co-supervisor - Universidade de Évora)

Évora, November 2019



SAPIENZA
UNIVERSITÀ DI ROMA



Co-funded by the
Erasmus+ Programme
of the European Union



Universidade of Évora

ARCHMAT
(ERASMUS MUNDUS MASTER in ARCHaeological
MATerials Science)

Mestrado em Arqueologia e Ambiente (Erasmus Mundus – ARCHMAT)

Caracterização de argamassas associadas ao sistema
hidráulico da *villa* romana Horta da Torre (Fronteira, Portugal)

Dulce Elizabeth Valdez Madrid
m40698

Patrícia Sofia Martins Moita
(Orientador - Universidade de Évora)

Paula Cristina Gonçalves Pereira Galacho
(Co-orientador - Universidade de Évora)

André Miguel Serra Pedreira Carneiro
(Co-orientador - Universidade de Évora)

Évora, Novembro 2019



PANEL OF JURY

President: Doctor Nicola Schiavon, Universidade de Évora.

Examiner: Doctor Carlos Ribeiro, Universidade de Évora.

Supervisor: Doctor Patrícia Moita, Universidade de Évora.

Partner member: Doctor Donatella Magri, Università di Roma.

ABSTRACT

Characterization of mortars associated with the hydraulic system of roman *villa* Horta da Torre (Fronreira, Portugal)

Villa Horta da Torre is an archaeological site from the 3rd – 4th century AD located in Fronreira, Portugal. In this Roman site, water plays an important role, due to the fact that the excavated buildings are comprised of a set of structures intended to store and channel water through a series of spaces and areas. This would create the most extraordinary displays to be viewed by a selected and privileged audience.

This research aimed to carry out the chemical, mineralogical and microstructural characterization of the lime mortars related to the hydraulic structures from the excavated *pars urbana* of the *villa*, in order provide evidence for the assessment of the raw materials used for their manufacture, as well as their provenance, and to establish a chronology amongst the structures. Moreover, valuable information concerning their production techniques was obtained and contrasted with the ancient recipes given by Vitruvius, which can be used for a future outlook with a view to their consolidation and repair.

A multianalytical approach was performed to conduct a complete and accurate characterization. Ten samples from hydraulic structures and two additional samples with a chromatic layer were analyzed by means of Optical Microscopy (Stereozoom and Petrographic microscope), X-ray Diffraction (XRD), Variable Pressure Scanning Electron Microscopy coupled to Energy Dispersive X-ray Spectroscopy (VP-SEM-EDS), Thermogravimetric analysis (TGA-DTG), Acid attack and Granulometric analysis.

Results demonstrated that the mortars analyzed present remarkable uniformity in terms of chemical, mineralogical and microstructural composition and according to their architectural purpose. There are no variations suggesting a different chronology of their manufacture, so it is assumed that they may be contemporaneous. In terms of production, it is evident that the Vitruvius rules were not followed. It can be implied that masons would have been familiarized with the ancient recipes for construction and the usefulness of ceramics, but this knowledge was always linked to their intuition and to the availability of the materials.

KEY WORDS Mortars; materials; archaeometry; Roman *villa*; provenance; ceramic aggregates.

RESUMO

Caracterização de argamassas associadas ao sistema hidráulico da *villa* romana Horta da Torre (Fronteira, Portugal)

A *villa* Horta da Torre é um sítio arqueológico do século III – IV DC, localizado em Fronteira, Portugal. Nesta *villa* romana, a água desempenhou um papel importante dado que os edifícios são compostos por um conjunto de estruturas destinadas a armazenar e canalizar a água através de uma série de espaços e áreas, o que criaria um ambiente cénico extraordinário para mostrar a um público selecionado e privilegiado.

Este estudo teve como objetivo a caracterização química e mineralógica das argamassas de cal relacionadas com as estruturas hidráulicas associadas à *pars urbana* da *villa*, a fim de fornecer evidências sobre as matérias-primas utilizadas para sua produção, bem como a sua proveniência, e para estabelecer uma cronologia entre as diferentes estruturas. Além disso, foram obtidas informações relevantes sobre as suas técnicas de produção que contrastam com as receitas antigas indicadas por Vitrúvio, que podem ser consideradas numa perspectiva futura de consolidação e reparação.

Efectuou-se uma abordagem multianalítica de modo a obter uma caracterização completa. Foram analisadas dez amostras de argamassas associadas a estruturas hidráulicas e duas amostras adicionais com uma camada cromática, através de Microscopia Óptica (Stereozoom e microscópio petrográfico), Difração de raios X (XRD), Microscopia eletrónica de Varrimento com Pressão Variável, acoplado a Espectroscopia de Energia Dispersiva de raio-X (VP-MEV-EDS), análise Termogravimétrica (ATG-DTG), ataque ácido e análise granulométrica.

Os resultados demonstraram que as argamassas estudadas apresentam uma notável uniformidade em termos de composição química, mineralógica e estrutural, e de acordo com seu propósito arquitetónico. Não havendo variações dentro de cada grupo funcional, o que poderia sugerir uma cronologia diferente na sua produção, assume-se que podem ser contemporâneos. Em termos de produção, é evidente que as regras Vitruvius não foram integralmente respeitadas. Os construtores estariam familiarizados com as antigas receitas romanas de construção e com a utilidade da cerâmica, mas esse conhecimento estava sempre ligado à sua intuição e à disponibilidade dos materiais.

PALAVRAS-CHAVE Argamassas; materiais; arqueometria; *villa* Romana; proveniências; cerâmicas

ACKNOWLEDGMENTS

The realization of this Master's thesis was possible thanks to the constant help and support of my family, friends and colleagues.

I would like to thank my supervisor Patrícia Moita and my co-supervisors Cristina Galacho and André Carneiro, for sharing their knowledge with me, for their feedback and for allowing me to be part of this project. Particularly, I want to thank my supervisor Patrícia Moita, and to Anna Tsoupra, for their continuous guidance, valuable advice, encouragement and patience throughout the process, and for giving me academic, practical, technical and moral support when I needed it. I would have never achieved this without them.

I would also like to thank the staff and researchers of the HERCULES Laboratory and the University of Évora for their technical and academic assistance, their advice, and for always be willing to help. I want to express my special thanks to Massimo Beltrame, Sandra Velez and Aida Graça, for their assistance and experience during the early stages of my work.

To Prof. Nick Schiavon and to the ARCHMAT EMMC International Selection Committee, for giving me the opportunity of participating in this program, and to the professors that inspired me and shared their knowledge and valuable instruction in archaeology and archaeometry that allowed me to perform this research.

I am extremely grateful to my colleagues and friends, who gave me their support, their constructive criticism and their company, but overall, I would like to express my deepest gratitude to my family, for their unconditional love and for giving me the motivation to keep growing. Thank you for everything.

INDEX

Abstract	I
Resumo	II
Acknowledgments	III
List of figures	VI
List of tables	IX
List of appendices	X
1 Introduction	1
1.1 Object of study	1
1.2 Mortars	2
1.2.1 Lime mortars	3
1.2.2 Mortars related to hydraulic structures	5
2 Archaeological context	6
2.1 Historical background	6
2.2 <i>Villa Horta da Torre</i>	8
2.2.1 Excavations	8
2.2.2 Configuration of the <i>villa</i>	9
2.2.3 Reoccupation of the site	13
2.3 Geological context	13
3 Samples and Methodology	15
3.1 Analytical techniques and methods	15
3.1.1 Visual inspection	16
3.1.2 Optical Microscopy (OM)	16
3.1.3 X-Ray Diffraction (XRD)	17
3.1.4 Thermogravimetric analysis (TGA-DTG)	19
3.1.5 Variable Pressure Scanning Electron Microscopy (VP-SEM-EDS)	20
3.1.6 Acid attack and Granulometric analysis	21
3.2 Sampling	22
3.3 Sample preparation	23
3.3.1 Cleaning for visual inspection	24
3.3.2 Sample preparation for Optical Microscopy and SEM-EDS – Cross and thin sections	24
3.3.3 Sample preparation for X-Ray Diffraction and Thermogravimetric Analysis – Powders (GF+FF)	26
3.3.4 Sample preparation for clay minerals identification	27
3.3.5 Sample preparation for Acid attack and Granulometric analysis – Fractions	28
3.4 Experimental conditions	29
3.4.1 Experimental conditions for Optical microscopy (OM)	29

3.4.2	Experimental conditions for X-Ray Diffraction (XRD).....	29
3.4.3	Experimental conditions for Thermogravimetric analysis (TGA-DTG)	29
3.4.4	Experimental conditions for Variable Pressure Scanning Electron Microscopy coupled to Energy Dispersive X-ray Spectrometry (VP-SEM-EDS)	30
3.4.5	Experimental conditions for Acid attack and Granulometric analysis	30
4	Results.....	31
4.1	Visual inspection.....	31
4.2	Optical microscopy (OM)	32
4.2.1	Stereozoom microscope.....	32
4.2.2	Petrographic microscope.....	37
4.3	X-ray Diffraction (XRD).....	38
4.3.1	Powder X-ray Diffraction (Powder XRD)	38
4.3.2	X-ray Diffraction in oriented mounts	42
4.4	Thermogravimetric Analysis (TGA)	43
4.5	Variable Pressure Scanning Electron Microscopy coupled to Energy Dispersive X-ray Spectroscopy (VP-SEM-EDS).....	45
4.6	Acid attack and Granulometric analysis	52
5	Discussion	57
5.1	Raw materials.....	58
5.1.1	Binder	58
5.1.2	Aggregates	60
5.2	Provenance	63
5.3	Production technology.....	64
6	Conclusions	69
	Bibliography.....	72
	Appendices.....	76

LIST OF FIGURES

Figure 1.1. The lime cycle. A) Calcination, B) hydration and C) carbonation.	3
Figure 2.1. a) Location of the Roman villa Horta da Torre in Portugal and b) relationship between villa Horta da Torre and the via XIV (dotted line), based on the routes proposed by André Carneiro in (Almeida et al, 2011). Base image taken from Google Earth Pro (12/2016).....	6
Figure 2.2. Preliminary results of the georadar prospection made in January 2018 by Lazaro Lagostena Barrios (Cadiz Univeristy), under the Fronteira Landscape Project (Universidade de Évora/Leiden University with funding from Prins Bernhard Cuulturfunds). André Carneiro's communication.....	9
Figure 2.3. Location of water bearing structures: a) double apse tank, b) triclinium water mirror, c) "Y" channel, d) tank 1, e) tank 2, f) unexcavated garden with surrounding water mirror (dashed lines), g) tank 3 (Bath) located approximately 65 meters towards NW. Orange arrows show the location of the pictures of Figure 5. Floorplan of villa Horta da Torre taken by geodrone, 2017, given by André Carneiro.	10
Figure 2.4. a) Probable water mirror surrounding the "garden" and the base of a column, and b) area comprising the Bath's structure (dashed line), showing colonization by trees. (Pictures taken by author, in March 12th, 2019).....	11
Figure 2.5. a) Stibadium, b) Mosque, c) bath wall, d) "Y" channel, e) tank 1 and f) tank 2 or peristylum. (Pictures taken by author, in March 12th, 2019).	12
Figure 2.6. Geological chart from Sousel (32-D) and Portalegre (32-B) geological maps, showing the limits of a 7km radius from the villa Horta da Torre. The vertical line depicts a fault across the geological units.....	14
Figure 3.1. Schematic representation of the interference process by waves produced by the ordered arrangement of atoms in a crystal (Stuart, 2007).....	18
Figure 3.2. Schematic diagram of a XRD diffractometer setup (Stuart, 2007).....	18
Figure 3.3. Illustrative pictures of the sampling: a) HHT-1 (double apse), b) HHT-8 (garden's water mirror) and c) HHT-11 (tank 3).....	22
Figure 3.4. Scheme showing the location of the samples in villa Horta da Torre. Base photogrammetric survey image taken from Carneiro (2017b), authorship of Carlos Carpetudo. The location of Tank 3 is schematic and out of scale.	23
Figure 3.5. Sample preparation diagram.....	24
Figure 3.6. Representative result of a a) thin section obtained from a b) cross section of the sample HHT-3.....	26

Figure 4.1. Types of ceramics found in each sample.....	36
Figure 4.2. Representative X-ray diffractograms of analysis performed in global and fine fraction powders of mortars from the hydraulic structures and mortars with chromatic layers.	41
Figure 4.3. Representative diffractograms of clay minerals identification of sample with chromatic layer.	42
Figure 4.4. Representative diffractogram of clay mineral identification of mortars related to hydraulic structures.....	43
Figure 4.5. Percentage of calculated CaCO_3 percentage in samples from villa Horta da Torre.	44
Figure 4.6. Representative thermograms depicting the different binder to aggregate ratios present in the samples.....	45
Figure 4.7. Representative elemental map of sample HHT-1 (hydraulic mortar). a) BSE image and arrows pointing at the surface in contact with water, b) ceramic and siliceous aggregates in a calcium enriched binder, with a lime lump enclosed in the dotted area, c) Mg and Ca elemental map, Mg related to ceramic aggregates, d) K and Na feldspars. Blue=Ca, yellow=Si, green=Mg, pink=K, orange=Al, red=Na.	46
Figure 4.8. Elemental map of sample HHT-2 with P enrichment in the contact surface. a) BSE image and b) P, Ca and Si elemental map, P present in a fine layer in the top. Blue=Ca, yellow=Si, pink=P.....	46
Figure 4.9. General elemental composition of sample PHHT-6 (mortar with a red chromatic layer). a) BSE image and recrystallization of calcite, b) relation between Si and Ca, c) Mg related to Si and Al, d) Fe enrichment in red chromatic layer. Blue=Ca, yellow=Si, green=Mg, orange=Al, red=Fe.....	47
Figure 4.10. Representative point analysis of a lime lump performed in sample HHT-1. a) BSE image of lime lump in Figure 7b, and b) point analysis spectrum of the spot marked in a.	47
Figure 4.11. Zoning around ceramic aggregate in thin section of sample HHT-3. a) BSE image, arrows point at zoning area, and dashed line indicates crack along the limit of the fragment. b) Elemental mapping of Ca and C, showing an enrichment of C along the crack and in zoned area of the ceramic, and an enrichment of Ca, in which “x” indicates the location of the point analysis of the binder (Fig. 12).....	48
Figure 4.12. Comparison between binder composition next to ceramic in thin section (TS) from sample HHT-3 (marked in Figure 11b) and binder matrix of cross section (CS) of the same sample.....	48
Figure 4.13. Representative multipoint analysis of a ceramic fragment performed in sample HHT-1. a) BSE image, b) spectrum of the area marked in a.	49

Figure 4.14. Comparison between yellowish (HHT-4) and reddish (HHT-9) ceramic fragments' composition.	49
Figure 4.15. Line analysis of the elemental composition of the ceramic-binder-ceramic transition in cross section of sample HHT-3. a) BSE image and b) spectra.	50
Figure 4.16. Representative point analysis of an amphibole performed in sample HHT-2. a) BSE image of amphibole, b) point analysis spectrum of the spot marked in a.	50
Figure 4.17. Representative point analysis of a pyroxene performed in sample HHT-1. a) BSE image of pyroxene, b) point analysis spectrum of the spot marked in a.	51
Figure 4.18. Representative elemental map of a K-feldspar with graphic texture performed in sample HHT-2. a) BSE image and b) Si (yellow) and K (pink) elemental maps. ...	51
Figure 4.19. Representative point analysis of a Na plagioclase (albite) performed in sample HHT-5. a) BSE image of plagioclase grain, b) point analysis spectrum of the spot marked in a.	52
Figure 4.20. Mean values obtained from the soluble and insoluble fractions of mortars after acid dissolution.	52
Figure 4.21. Particle size distribution of samples using the mean values. The rectangles indicate a similar distribution.	53
Figure 4.22. Gravel:mud:sand diagram from GRADISTAT.	55
Figure 5.1. Comparison between lime lumps composition present in the samples given by point analysis in EDS.	59
Figure 5.2. Comparison between ceramics composition of the samples by multipoint analysis in EDS.	62
Figure 5.3. CO ₂ to structurally bound water ratio in relation to CO ₂ %. Group 1a=orange; group 1b=yellow; group 2=green; group 3=blue.	68

LIST OF TABLES

Table 4.1. Results obtained from the microscopic observations of cross and thin sections of the samples. %= approximate percentage of aggregate within the binder matrix, CC= crushed ceramics.	32
Table 4.2. Particularities of representative samples observed under stereo microscope.	33
Table 4.3. Identification and description of the samples by visual inspection and microscopic observations of cross and thin sections.	34
Table 4.4. Types of ceramics found in cross sections of the samples from villa Horta da Torre.	36
Table 4.5. Distribution of frequency of ceramic fragment types found in samples of hydraulic mortars.	36
Table 4.6. Representative petrographic images of the general composition of mortars.	37
Table 4.7. Characteristic isolated minerals within the binder and ceramics.	38
Table 4.8. Mineralogical composition of the global fraction powders of mortars assessed by XRD.	39
Table 4.9. Mineralogical composition of the fine fractions of mortars assessed by XRD.	40
Table 4.10. TGA results. Record of the greater mass loss percentages during structurally bound water loss, decomposition of CO ₂ , CaCO ₃ percentage and estimated binder to aggregate ratio.	44
Table 4.11. Results from GRADISTAT based on Udden (1914) and Wentworth's (1922) classifications.	54
Table 4.12. Representative grain fraction results of samples related to hydraulic mortars (HHT-3 test HCl2).....	55
Table 4.13. Representative grain fraction results of mortar with chromatic layer (HHT-6 test HCl2).	56
Table 5.1. Subdivision of samples by groups used for the discussion of results.	57
Table 5.2. Sample composition (mass %) and binder to aggregate ratio (weight).....	66
Table 5.3. Weight loss percentages of structurally bound water in the temperature range 200-600 °C, and CO ₂ (600-900 °C) taken from Table x to calculate their ratio and the hydraulicity index (HI) of the mortars.	68

LIST OF APPENDICES

Appendix 1. Catalogue of collected samples and the fractions used for the elaboration of cross and thin sections.	76
Appendix 2. Thin-sections of the samples obtained from cross-sections for OM and VP-SEM-EDS analysis. The white dashed lines indicate the surface in contact with water, and the black dashed squares indicate the surfaces with a chromatic layer. The samples without indication were not in direct contact with water.	79
Appendix 3. Clay mineral identification flow diagram from USGS.	81
Appendix 4. Results of soluble and insoluble fractions after acid attack, and granulometric analysis performed in insoluble fractions.	82
Appendix 5. X-ray Diffractograms of the powdered samples from <i>villa</i> Horta da Torre. Relationship between global and fine fractions results.	83
Appendix 6. Thermograms of the results of the global fraction powders of the samples from <i>villa</i> Horta da Torre.	85
Appendix 7. X-ray diffractograms for clay mineral identification of the samples.	87
Appendix 8. Insoluble residues obtained after acid attack, observed by Stereozoom microscope.	90

1 INTRODUCTION

1.1 OBJECT OF STUDY

Built heritage is one of the most representative features that characterizes a civilization, their culture, traditions, beliefs, rites, social organization and technologies within their specific temporalities. Its analysis and understanding has become one of the most intensively studied areas throughout the world of science and cultural heritage in order to have a better understanding of the past and to formulate possible scenarios and interpretations of their evolution towards our modern technologies and societies.

This archaeometric study was undertaken at the HERCULES Laboratory of the University of Évora, Portugal, as part of the Erasmus Mundus Archaeological Materials Sciences Joint Master's Degree (ARCHMAT). The main goal of this study was the characterization of mortars related to hydraulic structures from the roman *villa* Horta da Torre, located near Cabeço de Vide in the municipality of Fronteira (Portalegre District of Alto Alentejo), Portugal, in order to provide information regarding their production technology and the raw materials used in their manufacture. Furthermore, this study intends to establish a chronology amongst the hydraulic structures of *villa* Horta da Torre and to gain an insight on the availability of the resources and the decisions taken in their manufacture. This has been achieved by the performance of a multianalytical approach to determine the mortars' chemical, mineralogical and microstructural composition.

Moreover, the acquired data was used to compare the mortars against ancient recipes for building materials preparation, as they were given by Vitruvius on his *Ten books on Architecture*, and to understand the importance of Horta da Torre and its relationship with the contemporary roman *villas*. Useful information about their production technologies has been deducted with a view to their consolidation and repair.

Ten samples of mortars from the *villa* Horta da Torre related to hydraulic structures were taken, in addition, two samples showing chromatic layers were analyzed for comparison. The samples were analyzed by means of Optical Microscopy (Stereozoom and Petrographic microscope), X-ray Diffraction (XRD, Powder XRD), Variable Pressure Scanning Electron Microscopy coupled to Energy Dispersive X-ray Spectroscopy (VP-SEM-EDS), Thermal Gravimetric Analysis (TGA-DTG), Acid attack and Granulometric analysis.

1.2 MORTARS

Mortars are widely spread binding materials used in built structures, and their composition varies depending on their specific function and the context of the construction. Their functions are numerous, such as structural foundations for walls to waterproofing, joining, rendering and finishing purposes (Elsen, 2006; Artioli, 2010). The raw material sources can be located in the immediate surroundings or can be taken from nearby areas (in most cases), and the techniques for the elaboration of mortars will change in function to the specific requirements of their application (Artioli, 2010).

Mortars are composed of a mixture of binder, aggregates, water and in some cases additives that help to enhance specific properties such as waterproofing. There are different types of binders, such as mud or clay, which have been used since 6,000 BC, followed by gypsum, considered as the first hydraulic binder developed since 7,000 BC (later replaced by natural cements) (Rodríguez-Navarro, 2009); and lime binders, which can be either hydraulic (hardens in contact with water) or aerial (hardens in contact with air).

Mortars are used as filling, joints and finishing or coatings since ancient times. The use of lime mortars is dated to the early sixth millennium B.C. in the archaeological site of Çatal Hüyük (Asia Minor), and their earliest use as binding material is dated to the third millennium B.C. in Egypt (Delatte, 2001). Nevertheless, previous research has demonstrated the early use of quicklime in the Hayonim Cave since 10,400 BC and lime-plaster in the Neolithic sites of Levant region since 8,700-7,000 BC (Artioli, 2010), and that most probably the lime-plaster diffusion was made through Greece to the Etruscans and then followed to the Roman Empire (Artioli, 2010).

In Roman times, the use of lime-based mortars and plasters was a very widespread practice. Scholars such as Vitruvius and Pliny, the Elder had written treatises such as *The ten books on Architecture* and *Natural history*, respectively, containing the recipes to achieve the best mixture for the different uses of the mortars, as well as the provenance and quality of the materials to be used. Both treatises mention the importance of the aging of the slaked lime from 2 to 3 years to produce a good quality binder, which is believed to be the key feature for the excellent quality of Roman mortars that are still solid and hard until now (Artioli, 2010). Additionally, in the Book II Chapter V of Vitruvius *De Architectura*, he recommends the use of white and hard stone to burn for lime to build the structural parts, whilst the most porous rock would be better for stucco for renderings (Morgan, 1914).

1.2.1 Lime mortars

Lime-based binders get their strength due to a series of chemical reactions given by the nature of the components and their interaction. The lime cycle plays the most important role and it consists of three main steps: a) calcination, b) hydration or slaking, and c) carbonation or hardening (Fig. 1.1) (ICCROM, 1981; Delatte, 2001; Elsen, 2006; Rodríguez-Navarro, 2009).

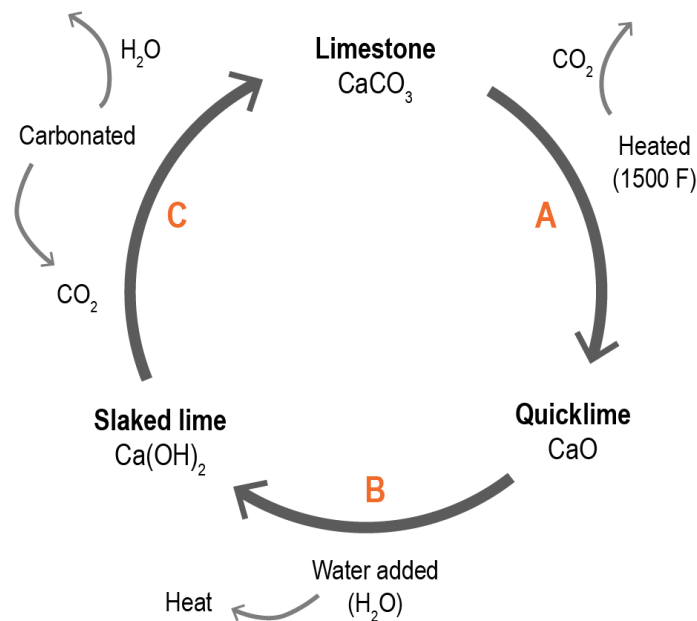
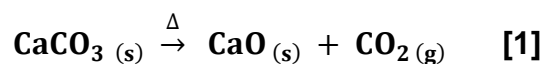


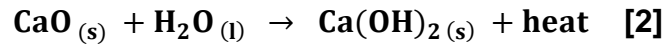
Figure 1.1. The lime cycle. A) Calcination, B) hydration and C) carbonation.

During calcination, the selected limestone is burned at high temperatures (up to 898°C) (Artioli, 2010) in order to decompose calcite (CaCO_3). It is an endothermic reaction which requires high energy consumption and the use of kilns. The product of this reaction is calcium oxide (CaO), known as quicklime, and carbon dioxide (CO_2) as byproduct, as shown in the equation [1].



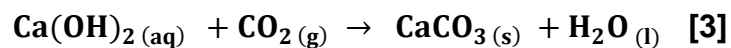
After calcination, the quicklime goes through a hydration process by the incorporation of water to yield calcium hydroxide (or Portlandite) known also as slaked or hydrated lime

[2]. This is an exothermic reaction and energy is released during this step in the form of heat:



During the hydration process two outcomes are possible: either a dry powdered precipitate is formed during the production of the calcium hydroxide if the stoichiometric amount of water is used; or a lime paste (lime putty) is created in cases where there is an excess of water added to the reaction (Rodríguez-Navarro, 2009; Artioli, 2010).

The last step of the lime cycle is carbonation, which consists of the hardening of the calcium hydroxide when it reacts with the atmospheric CO_2 to form calcium carbonate and water: [3]



With the hardening of calcium carbonate, all the elements of the mixture come together as a whole to create a hard and solid mixture (Rodríguez-Navarro, 2009) with a finely crystallized matrix of calcite (Elsen, 2006).

Some binder-related particles can be associated with the type of limestone used and the burning conditions, forming lime-lumps which, when underburned can give an insight on the raw material used, and when overburned they can be used to determine the maximum burning temperature used during calcination (Elsen, 2006).

The second most important components of lime-based mortars are the aggregates, which normally act as a filling to reduce the amount of binder. They can be either the most commonly used inorganic (or inert) such as sand, rocks and gravel (non-porous) or bricks and pottery (porous); or organic, such as charcoal from the burning process, or fibers to provide with tensile strength, and they can involve a mixture of aggregates depending on the application of the mortars. The study of the aggregates can provide us with information regarding their geological origin and can determine the potential raw materials sources used for the mortar's fabrication for the construction of the structures (Elsen, 2006). In his treatise *The ten books on Architecture*, Vitruvius recommends the use of clean pitsand freshly taken from the sandpits, river beds, gravel or sea sand in order to avoid weathering, and also warns about the use of beach sand and the associated problems, such as slow drying and surface spoiling. Vitruvius also indicates

the proportions of binder to aggregate ratios depending on the source of the sand as follows: “After slaking it, mix the mortar with 3 parts of pitsand and one of lime; for river or sea-sand, 2 parts of sand and one of lime. Using river or sea-sand, a third part of burnt brick pounded up and sifted can be added to make a better composition” (Book II, Chapter V, Vitruvius).

An occasional component of mortars are additives. They can be of organic origin (straw, hair, eggs), and mineral (or pozzolanic), and when they are combined with the hydrated lime, they form hydration cementitious products (Elsen, 2006). These pozzolanic additives can be of natural origin, as described by Vitruvius (Book II, Chapter VI), and be taken from volcanic pyroclastic rock; or man-made, from powdered ceramic materials, commonly from tiles and pottery (Elsen, 2006).

1.2.2 Mortars related to hydraulic structures

The mortars’ composition varies in function of the use of the structure in which they will be applied (Borsoi *et al*, 2019). Roman mortars related to water-bearing and hydraulic structures have a particular characteristic, which is the use of *opus signinum* coating. This type of waterproofing coating is obtained by mixing lime-based mortars with fine sand and a big percentage of *cocciopesto* (ceramic fragments or crushed pottery, used also as coating by itself, as in pavements) (Borsoi *et al*, 2019). Crushed ceramics have been used since early Hellenistic to early Byzantine times (Elsen, 2006) for structures related to water bearing facilities such as baths, canals and aqueducts, mainly to protect the walls from the moisture. The use of *opus signinum* in water facilities has been identified in the roman sites of *Pisões* (Borsoi *et al*, 2019), *Ammaia* (Cardoso *et al*, 2014), *Augusta Emerita* (Robador *et al*, 2010), *Conímbriga* (Velosa *et al*, 2007), *Tróia* (Silva *et al*, 2006), *Mérida* (Franquelo *et al*, 2008; Robador *et al*, 2013) and *Mértola* (Santos Silva *et al*, 2004) in the Iberian Peninsula, but it is widespread throughout the Mediterranean in Roman archaeological sites.

2 ARCHAEOLOGICAL CONTEXT

2.1 HISTORICAL BACKGROUND

Villa Horta da Torre (39°07'12.0"N 7°33'52.9"W) is an archaeological site, and its construction is dated to around the 3rd-4th century AD (Carneiro, 2017*b*). It's situated near Cabeço de Vide in the municipality of Fronteira (Portalegre District of Alto Alentejo), Portugal (Fig. 2.1.a).



Figure 2.1. a) Location of the Roman *villa* Horta da Torre in Portugal and b) relationship between *villa* Horta da Torre and the *via* XIV (dotted line), based on the routes proposed by André Carneiro in (Almeida *et al*, 2011). Base image taken from Google Earth Pro (12/2016).

The site might have been part of a series of settlements located along a main route likely to be travelled mostly for trading purposes, as part of the Romanization process of the territory during Roman Empire (Carneiro *et al*, 2019; Gonçalves *et al*, 1999; Stephens, 1891), together with other *villae* in the Lusitania region (Carneiro, 2017*a*).

This *villa* is located around 500 meters away from the *via* XIV (Carneiro, 2019*b*), one of the three Roman routes as proposed by Carneiro (in Almeida *et al*, 2011) (Fig. 2.1) connecting from east to west the provincial capital of Augusta Emerita (today's Spanish city of Mérida) with the coastal port of Felicitas Iulia Olisipo (today's Lisbon). This *via* was part of the Antonino's itinerary, and served as a network of socio-economical activation and exchange of ideas and cultures (Carneiro, 2019*a*; Morgado & Rocha, 2014). The *villa* Horta da Torre was linked to the main *via* for the ease of access with a private entrance road (*diverticulum*), which has been found "fossilized within the landscape" (Carneiro, 2014). Its purpose was to provide tranquility and safety to the owners of the *villa*. According to the list of features proposed by Carneiro (2019*a*) for the projection and

distribution of the classical Roman *villae*, the connection and proximity with the main road axis was typical, and the distances between the *villae* and the main road axis used to vary between 500 and 1000 meters (Carneiro, 2014).

Besides this relationship, Carneiro (2014) in his study highlights a set of characteristics that may have influenced on the placement and distribution of the *villae*, that go hand in hand with the pursuit of the “ideal landscape” (Carneiro, 2017a; Carneiro, 2014). These characteristics consisted of suitable land for olive, cereals and wine cultivation and production, named “Mediterranean Triade”. This landscape was characterized by its proximity to waterways that would be used for irrigation, and its topography needed to be appropriate for the buildings construction facing west or west-southwest to maximize the solar exposure, visibility, and favorable wind currents and protection (Carneiro, 2019a; Carneiro, 2014). The region of Alto Alentejo fulfilled all of these requirements appropriate for agriculture and also for *villae* establishment and therefore, small settlements were developed throughout the region along the proposed via XIV’s itinerary (Carneiro, 2014).

In literature, the concept of *villa* has earned different connotations and it is widely discussed by classical and contemporary authors. The classification of *villa* is given by its use, and it can be classified, according to Carneiro (2016), as *villa* as a space of *negotium*, which is determined by its functionality in terms of “agricultural and livestock production cannons of property” (Carneiro, 2016); or as *villa* as a space of *otium*, which consists of a set of spaces and environments where daily personal life habits take place.

The second type of *villa* was used not only as a private residence to display the identity of the *dominus* and his cultural knowledge of the world, but also as a political, social and economic statement reinforced by the personal relationships of the owner (Carneiro, 2017a; Carneiro, 2014).

The *villa* as a space of *otium* became a tool to show to the world the *dominus*’ power by the celebration of exclusive feasts and gatherings involving people from the same socio-economic status. These feasts would take place in opulently adorned rooms sometimes with colorful mosaics and water mirrors imitating nature to create astonishing atmospheres (Carneiro, 2014), such as in the case of the *villa* Horta da Torre.

For Romans, water was a precious resource, and their technology highlights their comprehension and also their proficiency for its collection, transportation and distribution of domestic and public character for recreational, health and economical purposes. These hydraulic labors would also serve to demonstrate the magnanimity of the power of the Emperors and their capability to perform such ostentatious works in form of dams

and cisterns for water contention and storage, aqueducts and channels for water distribution, wells for water extraction and tanks for domestic water supply, and their dominance over the natural elements (Cardoso *et al*, 1997).

In the *villa* Horta da Torre, water plays an important role, given the fact that the excavated buildings comprise of a set of structures intended to store and channel water through a series of spaces and areas, which would create the most extraordinary scenarios to display to a selected and privileged audience.

2.2 VILLA HORTA DA TORRE

2.2.1 Excavations

The buildings related to housing (or *pars urbana*) of *villa* Horta da Torre were first found in 1998 thanks to a project of relocation, identification and inspection of sites in the IPA – Crato extension, to map and assess the conservation state of its archaeological sites. Some fallen walls, a double apse and a tank were identified, but as it was located in a plowed field, it inevitably showed signs of partial destruction. The following year, an archaeological survey project was launched in the county of Fronteira leaded by André Carneiro, aiming to characterize of the site and identify the materials and structures found. In this survey new structures were identified. In 2003 emergency excavation works took place, and subsoil explorations were made. A set of water conducts and a stucco coated wall were identified. In 2004, the excavations continued under the project PNTA/2004 for the study of roman settlements in the county of Fronteira, together with excavations of Monte de São Pedro and Talha de Baixo (Direção-Geral do Património Cultural, 2019).

Scarce information can be found about archaeological excavations prompted in the site during the following years, but it is significant to highlight here that georadar and magnetometry prospections have been performed. These subsurface investigations had been done by Neves *et al* (2014) in 2012 based on previous explorations with the aim to identify new structures, confirm prior results and to orient future excavations (Carneiro, 2017c; Neves *et al*, 2014). During these investigations, part of the *pars urbana* was corroborated, and the fact that the *stibadium* (previously identified as “tower”) was surrounded by the double apse, allowed for the correlation of the structure with typical roman *villae* of the 4th – 5th century (Neves *et al*, 2014).

In 2014, georadar and magnetometric tests were performed once again to find plausible archaeological remains based on previous findings (Oliveira *et al*, 2015). The comparison between these two investigation techniques identified the existence of three areas, of which one was excavated and manifested the presence of a wall (Oliveira *et al*, 2015).

In 2018, the Fronteira Landscape Project in collaboration with Leiden University (NED) launched a third prospection by georadar in the site, and according to personal communication by André Carneiro, preliminary results point towards the existence of an unexcavated productive area (or *pars rustica*) extended towards the south of the *pars urbana* already excavated (Fig. 2.2). Excavations are being currently carried out, nevertheless, preliminary results of these excavations have not being published.

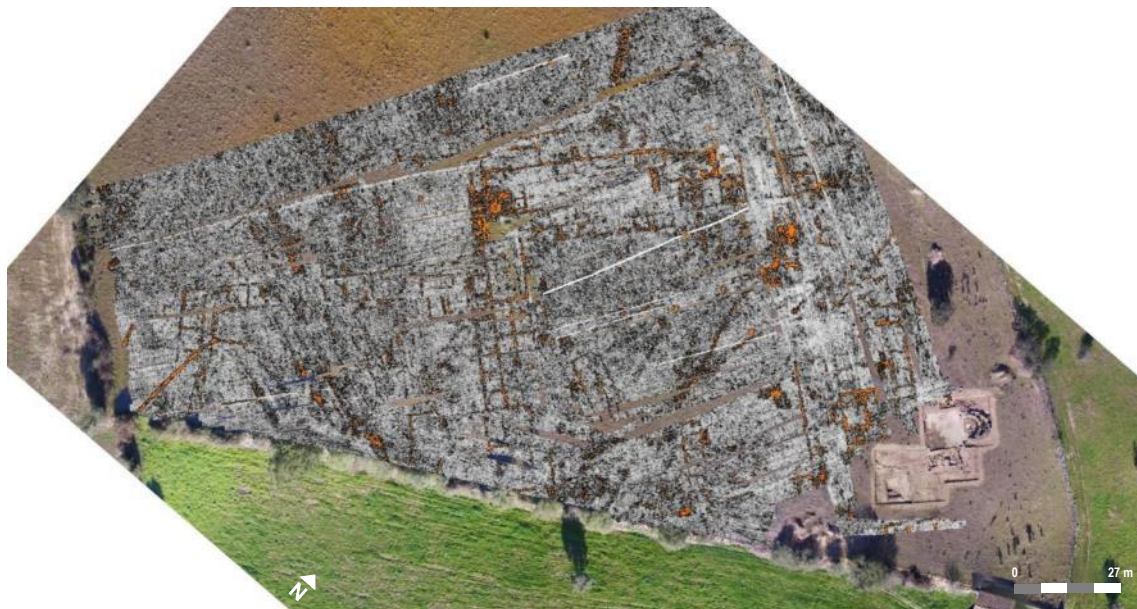


Figure 2.2. Preliminary results of the georadar prospection made in January 2018 by Lazaro Lagostena Barrios (Cadiz Univeristy), under the Fronteira Landscape Project (Universidade de Évora/Leiden University with funding from Prins Bernhard Cuulturfunds). André Carneiro's communication.

2.2.2 Configuration of the *villa*

After all the prospections and excavations carried out in *villa* Horta da Torre, a comprehensive overview of the site can be given by the relationship between its structures and their function. In this case, the excavated *pars urbana* shows a clear connection with water and its management, not only in a practical way to satisfy the individual consumption and cleanliness needed, but also for a whimsical and recreational purpose. To explain this, a description of the structures will be shown next.

In the first place, this *villa* has been characterized during the past years by the first three structures discovered, namely *stibadium* (Fig. 2.5.a), Mosque (Fig. 2.5.b) and Bath (Fig. 2.4.b and Fig. 2.3.g for its location with respect to the main area). Nevertheless, subsequent excavations revealed two more tanks (Figs. 2.3.d and 2.3.e) and a “Y” channel (Fig. 2.3.c) connected to the main area (*triclinium*) (Fig. 2.3.b) binding the prior elements and giving to this *villa* a whole new significance. A most recent feature partially revealed in the site but not published yet, consists of a tray-like structure suitable to be a water mirror. It is disposed surrounding what could have been an interior garden (personal communication from André Carneiro) (Fig. 2.3.f). Although the structure has not been fully excavated yet, it shows in the eastern corner a column base, which could’ve formed part of a gallery or colonnade (Fig. 2.4.a). From now on, this structure will be referred to as “garden water mirror”.



Figure 2.3. Location of water bearing structures: a) double apse tank, b) *triclinium* water mirror, c) “Y” channel, d) tank 1, e) tank 2, f) unexcavated garden with surrounding water mirror (dashed lines), g) tank 3 (Bath) located approximately 65 meters towards NW. Orange arrows show the location of the pictures of Figure 5. Floorplan of *villa* Horta da Torre taken by geodrone, 2017, given by André Carneiro.



Figure 2.4. a) Probable water mirror surrounding the “garden” and the base of a column, and b) area comprising the Bath’s structure (dashed line), showing colonization by trees. (Pictures taken by author, in March 12th, 2019).

Disregarding the *stibadium* and considering the double apse as a water containment structure, it can be suggested that this *pars urbana* was almost entirely devoted to the management, containment and exploitation of water, and the closeness of the individual structures to each other suggests that this was a sequential and integrated system.

The *stibadium* (Fig. 2.5.a) was amongst one of the first structures discovered and consisted of stone blocks coated with a *stucco* layer (Carneiro, 2017c). It was previously known as the “tower” and forms part of the *pars urbana*. Its main purpose was for recreation, in which the *dominus* and his guests would gather to celebrate ceremonial meals (Carneiro, 2014). This structure crowns the *triclinium* (Fig. 2.3.b), which occupies an area of approximately 90 m² (Carneiro, 2017b).

Some remains at the skirting of the walls imply that the *triclinium* used to bear marble slabs, but looter actions had lead to their loss (Carneiro, 2014; Carneiro, 2017b). On special occasions, the *triclinium* floor was meant to be flooded throughout a hidden door covered with tiles (Carneiro, 2017c), and it was located in the double apse behind the *stibadium*. It served as a contemplative feature for the display of power of the owner and his capability to perform such sophisticated engineering works.

The double apse, better know as the “Mosque” (Fig. 2.5.b), consists of a couple of half-mooned walls linked at both extremes, generating an interior area that would serve as a water containment unit. It was coated with a layer of *opus signinum* to perform as such, and the wall facing the *stibadium* was covered with mosaics (Carneiro, 2017b). The water would flow down the double apse wall by a brick duct system resembling a waterfall (Carneiro, 2017b), and once on the floor it would reflect the colorful *teselae* coating situated around the walls and the ceiling (Carneiro, 2014), producing a unique visual and acoustic atmosphere starred by water and light.

The Bath (Fig. 2.4.b) was a tank of 15x25 meters coated with *opus signinum*, and has gone through great damage due to land plowing works (Carneiro, 2019b). Two of its walls are still preserved standing (Fig. 2.5.c), whilst the remains of a third structure (supposedly a collapsed wall) are scattered and lay around the area. The central space nowadays hosts a contemporary concrete barn and a batch of trees providing shadow to the surroundings.

Little more is known about tank 1 after the excavation in 2002 (Fig. 2.5.e) besides the fact that it had an *opus signinum* coating. Tank 2 (Fig. 2.5.f) was identified in 2012 as a columned *peristylum* of an *impluvium* nourished by a fountain, which would have been surrounded by mural paintings (Carneiro, 2017b). The “Y” channel (Fig. 2.5.d) formed part of the discoveries of excavations carried out in 2015 (personal communication, Carneiro, 2019), and can be related to the water discharge at the southeastern extreme of the *triclinium* (Carneiro, 2017b).

Finally, the garden water mirror has been only partially displayed (Fig. 2.4.a), and it is necessary to carry out more excavations to be able to retrieve the possible answers we are looking for, such as its limits and possible functions within the site.

Close to the Bath, an important amount of various types of ceramic fragments for construction materials were found and dated without apparent interruption from the 1st century to mid 7th AD (Carneiro & De Sepúlveda, 2004). This shows a continuity in the occupancy throughout the centuries. Besides mortar stones, also *opus signinum* blocks were identified in the vicinity (Carneiro, 2017b).



Figure 2.5. a) *Stibadium*, b) Mosque, c) bath wall, d) “Y” channel, e) tank 1 and f) tank 2 or *peristylum*. (Pictures taken by author, in March 12th, 2019).

2.2.3 Reoccupation of the site

Around the middle of the 5th century, the *villa* Horta da Torre was abandoned by its original inhabitants (Carneiro *et al*, 2019; Carneiro, 2017*b*). Nevertheless, as a result of this abandonment and considering that the structures were still preserved in good conditions (disregarding the collapsed *impluvium*'s rooftop), the *villa* was reoccupied few years later by a *squatter* community from the middle until the end of the 6th century. This reoccupation contributed to the looting of the site by clearing out the walls from the marble slabs and perforating the *triclinium*'s floor to install a hut (*Longhouse*) made out of perishable materials such as wooden posts, and the *peristylum* was used to shelter animals and to dump rubbish (Carneiro, 2017*b*). No remains of the structures were found in the site due to the nature of the materials employed. However, the determination of this occupation was made by the signs of their actions towards the damage of the *villa*. This damage is extended to nowadays due to agriculture practices, non-authorized excavations, intrusions and treasure hunters (Carneiro *et al*, 2019; Carneiro, 2019*b*).

2.3 GEOLOGICAL CONTEXT

The municipality of Fronteira is located in the Ossa-Morena Zone, a major subdivision of Iberian Massif, which runs along the occidental half of the Peninsula (Fernández & Díaz, 2008). OMZ consists of metamorphic and igneous rocks with a major NW-SE trend. The area is crossed, almost perpendicularly to regional trend, by secondary water streams (Ribeira do Verdigão runs along the *villa*, located ~150 m away) flowing towards the SW.

The roman *villa* is built in a geological substrate consisting of schists, graywackes and black quartzites, from the Cambrian, extended in a 3 km radius accompanying the orientation NW-SE (Gonçalves & Peinador, 1973; Gonçalves *et al*, 1975) (Fig. 2.6). This unit is associated with some hyperalkaline granitic and syenitic orthognaiss, basic vulcanites and conglomerates, together with quartz veins and porphyritic granite. Further to the west within a 5-7 km radius, some hornblendic microtonalites and metadolerites dykes, holocenic sedimentary deposits, marly limestones, feldspatic sandstones and angular gravel with reddish and brownish clays are observed. The basic and ultrabasic intrusion Alter do Chão is total or partially serpentized and composed by igneous magmatic gabbros, pyroxenes, epidotes and serpentines, while surrounded by hornfels (quartzitic, pelitic and calcosilicate). It elongates and aligns with the variscan structure and originates a contact aureole in the regional limestone (sometimes recrystallized) and

dolomites enriched in silica. Around 4 km to the SW, the cambrian geological unit is crossed by a calc-alkaline to alkaline granite intrusion, ringed by metamorphic regional rocks (hornfels). From 8 km to the NE to SW until Horta da Torre, the water lines cross by a sequence of the parallel geological units of schists and graywackes, biotitic granitic orthogneisses and granitic and syenitic hyperalkaline orthogneiss conglomerates and arkoses, the above mentioned intrusion of Alter do Chão surrounded by hornfels, crystalline limestones (with recrystallizations) and dolomites, and finally the Cambrian unit composed by shists, quartzites, graywackes and conglomerates in which the *villa* Horta da Torre is located. A major N-S fault cuts the igneous and metamorphic lithologies and passes ~ 500 m to the east of the site, originating the Sulfúrea *thermae* (Cabeço de Vide) (Carneiro, 2019a).

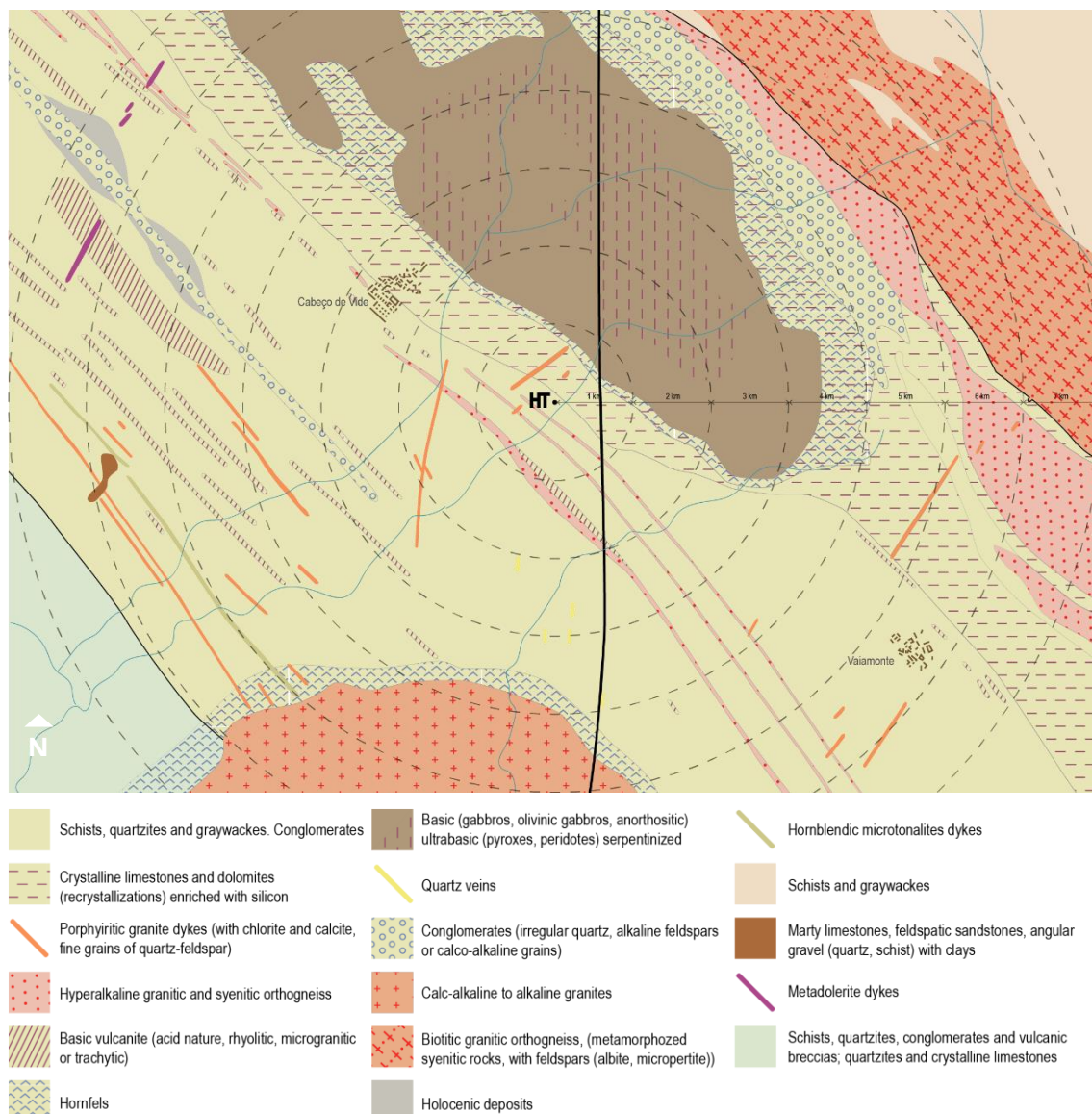


Figure 2.6. Geological scheme from Sousel (32-D) and Portalegre (32-B) geological maps, scale of 1/50000 (Gonçalves & Peinador, 1973; Gonçalves *et al*, 1975), in a 7km radius from the *villa* Horta da Torre. The vertical line depicts a fault across the geological units.

3 SAMPLES AND METHODOLOGY

3.1 ANALYTICAL TECHNIQUES AND METHODS

Mortar analysis entails the performance of invasive and destructive techniques to assess a proper and accurate characterization. Non-invasive techniques as *in situ* visual inspection for a broad first examination or portable X-Ray Fluorescence analysis can provide us with information regarding the main characteristics of the mortars (type, aggregates, binder) and their elemental composition. Non-destructive and minor destructive testing techniques, namely Double Punch Tests (DPT) for tensile strength, and Helix Pull-Out Test (HPT) and Windsor Probe for compressive strength analysis (Pelà *et al*, 2017), can be performed for the analysis of their mechanical properties; such as imaging techniques like Hyperspectral Imaging (HSI) for the evaluation of sand/lime ratios (Eriksson, 2018), have been performed in mortar analysis. These techniques are used to obtain a first assessment for the classification of the samples and their mechanical and broad elemental properties. Therefore, it is assumed that sample taking will be required to achieve a complete and more accurate physical, chemical and mineralogical characterization.

The characterization of the mortars related to the hydraulic system of the *villa* Horta da Torre, was performed by a multi-analytical approach. The assessment of their characteristics was first executed by visual examination and microscopic observations through stereoscopic and petrographic microscopes, as well as Variable Pressure Scanning Electron Microscopy coupled to Energy Dispersive X-ray Spectrometry (VP-SEM-EDS), which besides giving us a high resolution image of the texture and the chemical composition of each sample, was used to acquire elemental composition mappings in the selected areas as an image, and point and linear analysis in the form of spectra. Powder X-Ray Diffraction (XRD) was used to gather information about the crystalline phases present in the powdered samples, which complemented the previous microscopic and elemental composition results. A complementary experimental procedure was performed to identify the clay minerals present in the samples through Glycolation and heat treatments.

Thermogravimetric analysis (TGA-DTG) in combination with acid attack and granulometric analysis will be used to determine the proportion of carbonates, of soluble fraction and of aggregates of each sample, respectively (Jedrzejewska, 2014).

Each technique is described further in this chapter, as is the specific sample preparation needed to implement each analysis, the expected resulting information to be obtained and the specific experimental conditions used for each analysis.

3.1.1 Visual inspection

Visual examination must be, amongst all the other analytical techniques employed, the first step to perform the analysis and characterization of historic mortars (Stuart, 2007; Artioli, 2010). For this purpose, macroscopic observations with an unaided eye might be of use to make a broad description of the samples regarding their general features such as thickness, color, lithological characteristics of aggregates and distribution, weathering and/or degradation products, amongst others; nevertheless, sampling is mandatory for a representative chemical and mineralogical characterization of mortars. Different lightning setups and conditions can also reveal information about textures, cracks and distortion in plane if located in distinct angles of incidence (Groot *et al*, 1999; Stuart, 2007), and can provide us with some insights for their morphological characterization. These preliminary results would be helpful to group the samples and to preset the basis for the assumptions regarding their chemical and mineralogical constitution (Artioli, 2010).

3.1.2 Optical Microscopy (OM)

Microscopic examination is used to magnify objects (from 2 to 2000x times with resolutions up to 0.2-0.5 μm depending on the instrumentation (Stuart, 2007)) that allow us to gather information about the morphological characteristics and structure of a sample. It is most frequently used in the area of mineralogy and petrography to carry out investigations of rocks and their forming minerals, and can be performed in centimeter-sized portions of material (Artioli, 2010). Nevertheless, these techniques are broadly used for a wide range of materials such as metals, ceramics, paintings, etc. (Stuart, 2007).

The main properties analyzed in mortars by means of optical microscopy involve, as recalled by Artioli (2010), the mineral phase identification and textural associations; the characterization of the comprising grains (size, shape and distribution) and inclusions; cleavage, twin boundaries, and cracks (Middendorf *et al*, 2005a). For archaeological

purposes, OM can be useful to establish the provenance of the raw materials based on the mineralogical content of the samples and matching the fingerprint of the minerals found with the geological signature; as well as the manufacturing processes and amongst others, the preliminary interpretations of the type of binder used; and to determine the presence of degradation processes due to external factors such as weathering (Elsen, 2006; Stuart, 2007).

In optical microscopy, the premise is that visible light interacts with the specimen by passing through thin sections (of around 20-30 μm thickness) of the specimens (in transmitted-light or polarized-light modes), resulting in a range of color absorptions and pleochroism of the sample through plane-polarized light (PPL), and showing interference colors and birefringence by using cross-polarizers of light (XPL) (Artioli, 2010).

By means of Polarized light microscopy, anisotropic materials can be distinguished due to their specific optical properties in terms of their crystallographic axes and the characteristic interference colors obtained by the splitted incident light rays through the sample, which show various refractive indices according to the vibrational plane coordinates (Middendorf *et al*, 2005a; Stuart, 2007).

3.1.3 X-Ray Diffraction (XRD)

X-ray Diffraction (XRD) is used in the study of mortars to identify the mineralogical phases of crystalline structures to assess the qualitative mineralogical composition of the global and fine (binder enriched) fractions of mortar samples to identify the type of binder (lime, gypsum) and aggregates (siliceous, calcareous, ceramic) present in the mortar (Middendorf *et al*, 2005a). This is done by analyzing the characteristic “orientation texture, crystallite size distribution, and lattice micro-strain effects of the crystalline compounds” (Artioli, 2010), and therefore makes a semi-quantification of the mineralogical composition of the specimens based on the relative intensities given by the diffraction patterns. Powder X-ray Diffraction can only contribute to a bulk analysis of the carefully homogenized powders, therefore information about the interrelationships of the structure and the spatial distribution of the mortar’s components have to be corroborated by petrographic observations (Groot *et al*, 1999; Middendorf *et al*, 2005a) to confirm the assumptions given by the crystal phases of the diffraction patterns. X-ray Diffraction is given by the strike of x-rays towards a crystalline solid, in which “two waves reach the crystal at an angle θ and are diffracted at the same angle by adjacent layers. When the first wave strikes the top layer and the second wave strikes the next layer the

waves are in phase” (Stuart, 2007) (Fig. 3.1), and is explained by the Bragg’s Law equation [4]:

$$n\lambda = 2d \sin \theta \quad [4]$$

In which **n** is an integer number, λ is the wavelength of the incoming radiation in Å, **d** represents the interplanar spacing between atoms as shown in Figure 3.1 given in Å, and θ represents half the diffraction angle between the incident and diffracted monochromatic X-ray beams (Stuart, 2007; Artioli, 2010).

The diffractogram obtained will be the result of the sum of diffracted X-rays in function to the angle of scattering angle while the detector, which is mounted on a movable platform, rotates at a constant speed from 0-90° measured in 2θ , depending on the particular requirements of the analysis; the intensity of the diffracted peaks will be plotted in the diffractogram and the resulting profile will represent a characteristic pattern of a specific crystalline phase or phases, which will be compared with a XRD file in database for their identification (Stuart, 2007; Artioli, 2010). A schematic layout of an XRD diffractometer is shown in Figure 3.2.

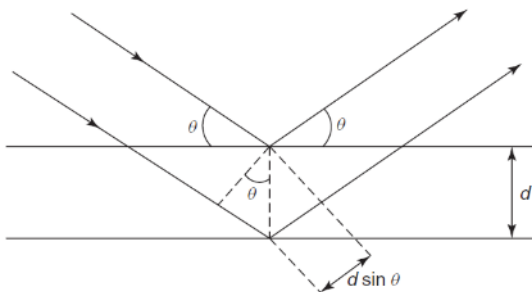


Figure 3.1. Schematic representation of the interference process by waves produced by the ordered arrangement of atoms in a crystal (Stuart, 2007)

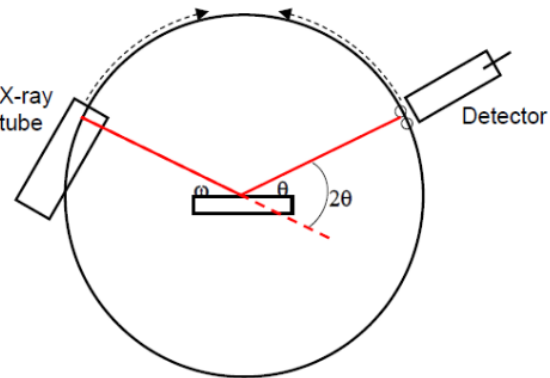


Figure 3.2. Schematic diagram of a XRD diffractometer setup (Stuart, 2007)

A disadvantage of powder XRD comes with the nature of the sample required as a powder, in which the sum of the patterns of the crystalline phases present in the sample may overlap in the diffractogram, thus their individual characterization may represent a complex task (Stuart, 2007). Therefore, the careful homogenization of the powder is required to achieve the best results, so does the qualified personnel for the interpretation of the results for a proper match with the profiles’ database.

3.1.4 Thermogravimetric analysis (TGA-DTG)

By means of Thermogravimetric analysis, it is possible to identify characteristic patterns of the weight losses of the materials caused by physical or chemical changes. The mass losses were tracked throughout the heating program by placing the sample in a crucible inside a furnace in a sensitive balance under a controlled temperature program in an inert atmosphere (N₂). In this process, the First Derivative Thermogravimetric curve (DTG) with respect to temperature, allows to plot the most representative changes within the sample during the heating process, in which the peaks will indicate the maximum mass losses due to the characteristic physical or chemical decomposition of the distinct materials in function of temperature (Middendorf *et al*, 2005a; Stuart, 2007; Földvári, 2011).

The mass change within the sampled material during the heating is recorded in a thermogram and it is used to make a relative quantification of the carbonate fraction of the mortars and to estimate the ratios of their composition and therefore determine the technologies employed in their manufacture. The data obtain from the soluble fraction results from acid dissolution, and the data of the aggregates composition obtained by means of granulometric analysis will complement the information given by TGA to achieve a complete characterization.

For mortars studies, it is expected to obtain a main weight loss between the range of temperature between 600 - 900°C confirming the decomposition of calcium carbonate (CaCO₃) forming calcium oxide (CaO) and carbon dioxide (CO₂), which is indicative of a calcitic composition of the lime-based binder; however, weight losses at lower temperatures can be shown in the ranges of 75-100°C for the dehydration of the sample (Middendorf *et al*, 2005a).

The calculation of the carbonate content in terms of percentage of calcite, is normally made by the following equation [5]:

$$\text{CaCO}_3\% = [P_{(\text{CO}_2)} \cdot M_{(\text{CaCO}_3)}] / M_{(\text{CO}_2)} \quad [5]$$

In which $P_{(\text{CO}_2)}$ stands by the percentage of mass loss between 600-900°C, that corresponds to the decomposition of CaCO₃, $M_{(\text{CaCO}_3)}$ represents the molar mass of calcium carbonate (100.082 gmol⁻¹), and $M_{(\text{CO}_2)}$ the molar mass of carbon dioxide (44.02 gmol⁻¹) (Borsoi *et al*, 2019).

3.1.5 Variable Pressure Scanning Electron Microscopy (VP-SEM-EDS)

Variable Pressure Scanning Electron Microscopy coupled to Energy Dispersive X-ray Spectroscopy (VP-SEM-EDS) is the microscopic technique that can show us a higher magnification image up to x100,000 times (Stuart, 2007), with higher resolution and wider depth of focus, compared to optical microscopy, owing to the use of accelerated electrons (between 102–104 eV, 0.123–0.012 nm wavelength) under vacuum (high or low) instead of light (Stuart, 2007; Artioli, 2010). VP-SEM-EDS is able to plot three-dimensional images with detailed morphological attributes of the material analyzed (Middendorf *et al*, 2005a; Stuart, 2007). When using an EDS detector, it is possible to determine the qualitative composition of the chemical elements in the sample by SEM, by recording at each point the intensity of the characteristic X-rays of specific elements in a spectra and tables, and map their distribution on the sample's surface (Middendorf *et al*, 2005a; Stuart, 2007).

A scanning electron microscope consists of an electron source (comprising a tungsten filament, a Wehnelt cylinder and an anode) which produces a beam of electrons under vacuum by the application of a current that emits and accelerates them through the anode towards a specific area of the surface of the sample in a raster scan, interacting with the atoms of the surface (Stuart, 2007; Artioli, 2010). This interaction produces different kinds of signals collected and amplified by a detector positioned above the sample (Stuart, 2007; Artioli, 2010), and are used for different purposes.

The back-scattered electrons (BSE) are the result of the elastic scatter by the sample after the electron beam strikes the sample, retaining an insignificant lower energy than that of the beam, and they are of use for the detection of the contrast of areas with varied chemical structures to determine the topography of the surface and their elemental distribution throughout the sample's surface (Stuart, 2007; Artioli, 2010); secondary electrons (SE) are low energy electrons (<50 eV) emitted from the sample's surface producing an inelastic collision followed by an ionization process, and they yield images that demonstrate their features and morphologies (Stuart, 2007; Artioli, 2010); X-rays are produced due to the ionization processes and are detected by an EDS, which allows the identification of chemical elements (Stuart, 2007; Artioli, 2010) and the production of an elemental distribution map of the selected raster area (Artioli, 2010).

In mortar studies, VP-SEM-EDS allows us to identify the binder and aggregates composition with different types of data collection, such as: elemental mappings of the composition of localized areas in thin and cross-sections; or through point, multipoint or

line analysis focused either on lime lumps to obtain more detailed information of the raw binder, in ceramics to analyze their composition and possible reactions in the contact surfaces, or for the identification of trace minerals to determine lithic provenances. Also, the BSE images are useful to provide us with information of the textural features of the mortars.

3.1.6 Acid attack and Granulometric analysis

The dissolution of mortars in acid is used to provide us with information of the ratio of soluble fraction and insoluble siliceous residual aggregates present in the mortars, assuming that the soluble fraction, representing the binder, will be the one composed by carbonates, and the aggregates will remain intact after the chemical process of dissolution in acid (Middendorf *et al*, 2005b). The resulting insoluble residue is used to make a quantification of the composition of the different grain fractions, as well as to carry out a morphological characterization of each type under a stereoscopic microscope.

The method developed by Hanna Jedrzejewska (Jedrzejewska, 2014) for the definition of the basic aspects to understand the technology used for the historical lime mortars production resides in three properties that can be determined by acid attack (by using hydrochloric acid for dissolution) together with Thermogravimetric analysis. These properties are the proportion of the “soluble” amount of sample in acid (without CO₂ formation), the amount of sand (the insoluble fraction in acid), and the proportion of carbonates (given by the percentage of calcium carbonate determined by means of TGA-DTG) (Jedrzejewska, 2014; Borsoi *et al*, 2019). The soluble fraction will be given in terms of percentage and determined by the equation [6] (Borsoi *et al*, 2019):

$$\text{Soluble Fraction} = 100 - \Sigma(\text{Insoluble Residue} + \text{Carbonates}) \quad [6]$$

According to Middendorf *et al* (2005b), it is recommended that mineralogical and petrographic microscopic analysis are performed on the samples before chemical analysis to have an idea whether or not the aggregates may dissolve with acid or if the binder possesses hydraulic characteristics to achieve the desired separation of elements.

The resultant insoluble residues are used further on to obtain the grading curve of the aggregates to determine the predominant grain fraction present on each sample, and this, together with the binder to aggregate ratio, will conform an important step for the characterization and reproduction of the historical mortar (Middendorf *et al*, 2005b).

3.2 SAMPLING

Twelve samples were collected in total, with a hammer and chisel (Figs. 3.3 and 3.4), ten of them from structures directly related to water management structures, comprehending a double apse (HHT-1), two water mirrors located in the main room (HHT-2) and surrounding the private garden to the south of the building (HHT-8 and HHT-9), the inner coatings of three tanks of varied dimensions (HHT-4, HHT-5, HHT-10 and HHT-12), a fallen structure in the tank 3 considered as a wall (HHT-11), and a canal fed by the main room (HHT-3), procuring to conserve the orientation of the layer in direct contact with water. Some samples were divided into an upper and lower layer due to their physical and morphological characteristics and compositions (HHT-10 and HHT-11) due to their specific purpose; two more samples (PHHT-6, PHHT-7) were collected from the interior of the Tank 2, lying loose, in which one of them showed a chromatic layer (red and blue with a white stripe in between), whilst the other one despite having certain similarities, did not show at first a chromatic layer until the cleaning process, in which a red leaf-like figure was shown.



Figure 3.3. Illustrative pictures of the sampling: a) HHT-1 (double apse), b) HHT-8 (garden's water mirror) and c) HHT-11 (tank 3).

After collection, the samples were deposited in plastic bags and labelled, later cleaned with brushes, a chisel and scalpel to remove dirt, dust and biological colonization such as mold, lichens and insects. The samples were left in the oven overnight to dry at 40

°C. The process was repeated twice to guarantee a sufficiently clean surface. The samples were documented using a High Dynamic Range camera with a resolution of 12 MP after cleaning to perform a first visual inspection of each sample.

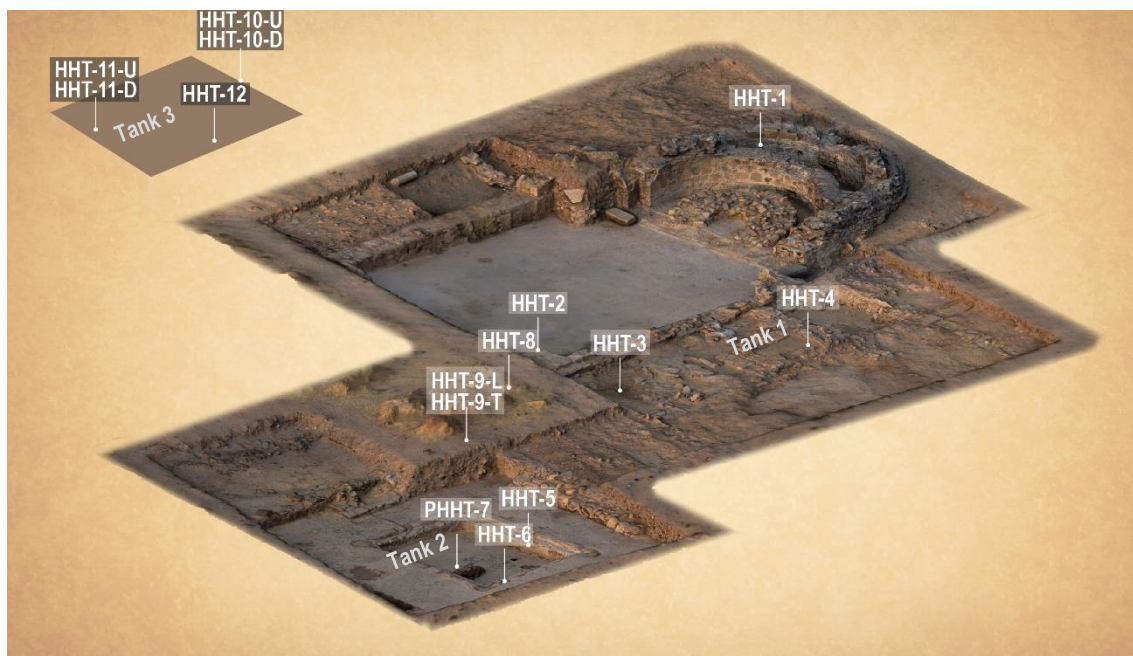


Figure 3.4. Scheme showing the location of the samples in *villa Horta da Torre*. Base photogrammetric survey image taken from Carneiro (2017b), authorship of Carlos Carpetudo. The location of Tank 3 is schematic and out of scale.

Once the samples were cleaned and dried, a set of different sample preparation procedures were carried out in order to suit each different technique requirements to be performed for their characterization, and they will be individually described in the following section 3.3.

3.3 SAMPLE PREPARATION

The following diagram (Fig. 3.5) shows the different samples prepared for each one of the analytical techniques carried out in this project. Each type of sample in the diagram is linked to the technique which it was used for and/or to a secondary sample preparation, and the numbers underneath indicate the corresponding section explaining the sample preparation procedure and the analytical technique performed.

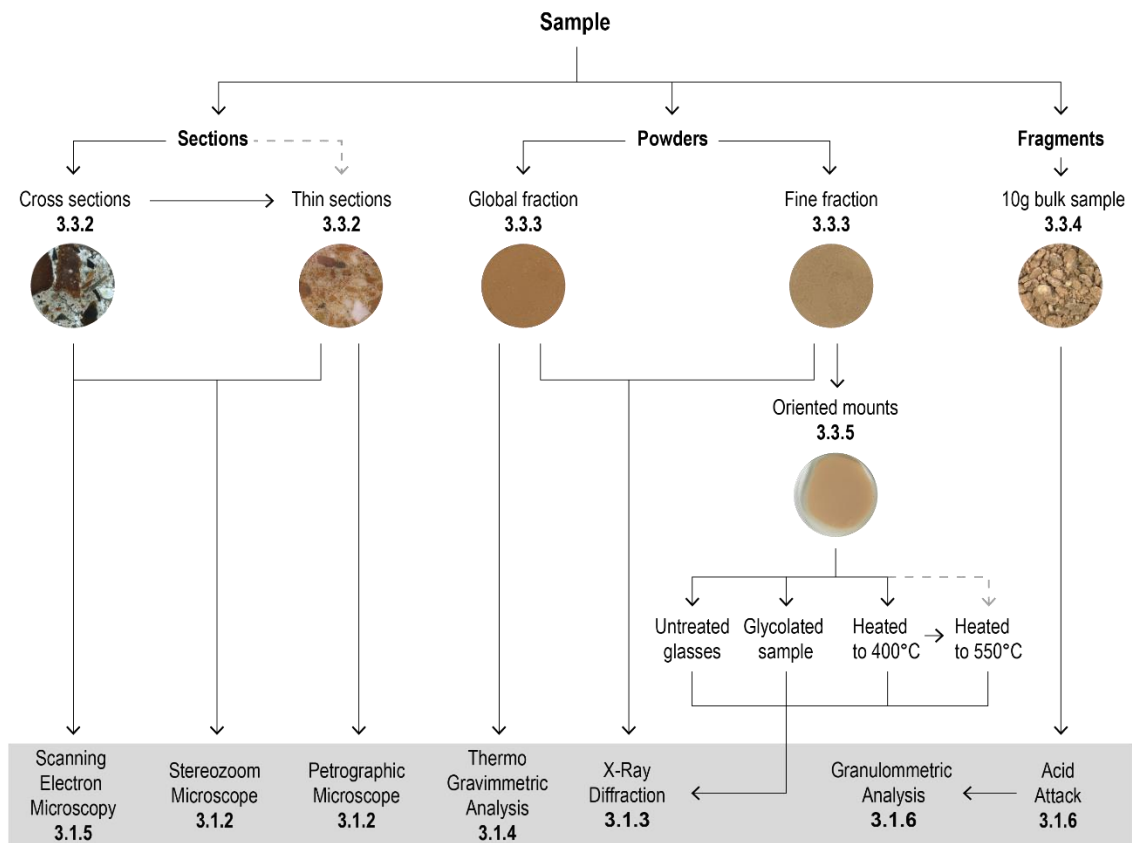


Figure 3.5. Sample preparation diagram.

3.3.1 Cleaning for visual inspection

For a first visual examination, the sample preparation consisted in the surface cleaning described above. As the samples were exposed to the elements, some mud, moss and insects had to be meticulously removed with a brush and scalpel and then dried in the oven overnight at 40°C. The cleaning process was repeated twice for every fraction of each specimen.

The samples were documented after both cleaning processes for their description, and photographed to preserve the orientations in contact with water.

3.3.2 Sample preparation for Optical Microscopy and SEM-EDS – Cross and thin sections

For Optical and Scanning Electron Microscopy analysis, thin sections were prepared from cross sections (Fig. 3.6) of the samples for visual inspection by Stereoscopic, Petrographic and Scanning Electron Microscope, using the TS-Method developed by

Struers. For this purpose, the cross section of the stratigraphy of each sample was obtained by cutting them with Discoplan-TS diamond cut-off wheel (Struers) and documented to preserve the right orientation, letting them dry overnight in the oven at 40 °C (Appendix 1). The cross sections were placed facing the bottom in circular mounting plastic cups from 2 to 4 cm diameter depending on the sample's size, and embedded in a mixture of 25 parts of EpoFix Resin (Struers) and 3 parts EpoFix Hardener (Struers) by weight. The cross sections embedded in resin were left to dry for at least 12 hours at room temperature and afterwards cut in the Discoplan-TS to fit the dimensions of the glass Standard Slides for thin sections by Struers. Subsequently, the cross sections were polished by hand in P #220 and P #600 SiC Paper to totally expose the surface of the mortar and finally polished with P #1000 silicon carbide powder to reach a perfectly flat and smooth surface. Afterwards, the cross sections were mounted in the glass slide with a SystemAbele press using a mixture of 2 g of EpoFix Resin and 0.9 g of EpoFix Hardener, and left to dry overnight in a hot plate. The Discoplan-TS was then used to cut the cross sections and polish them with the cup wheel to reach a thickness between 20-30 µm, according to (Middendorf *et al*, 2005a) and later in a RotoPol-35 (Struers) with a Cast Iron Disc in 0.5 liters of solution of Glicerine 1:2 parts of water with 45 grams of P #1000 silicon carbide powder, until the samples reached a thickness of 1,020 mm, showing a first order Birefringence color in the Michel-Levy chart. Finally, the thin sections were polished by hand in P #2400 and P #4000 SiC Paper for 2 minutes and left for 3 minutes to rinse in an Ultrasonic Cleaner USC-T (VWR) (Appendix 2). More detailed information about the mineralogical specimens preparation for microscopic examination using the TS-Method, can be found in the online official manual by Struers¹.

No further preparation nor graphite coating of the samples was required to perform SEM analysis in the thin sections, nevertheless, the resulting cross sections after the thin section elaboration were used to perform SEM analysis. For this purpose, the cross sections were consolidated with a mixture of 25 parts of EpoFix Resin (Struers) and 3 parts EpoFix Hardener (Struers) by weight, and left to dry overnight at room temperature. After, the cross sections were polished by hand in P #600 P #1000 and P #2400 SiC Paper until the surface of the mortar was exposed. Lastly, the cross sections were put for 3 minutes to rinse in an Ultrasonic Cleaner USC-T (VWR) and then dried at room temperature.

¹ Struers manual for mineralogical specimens preparation by the TS-Method: https://www.als.com.tr/?wpfb_dl=135

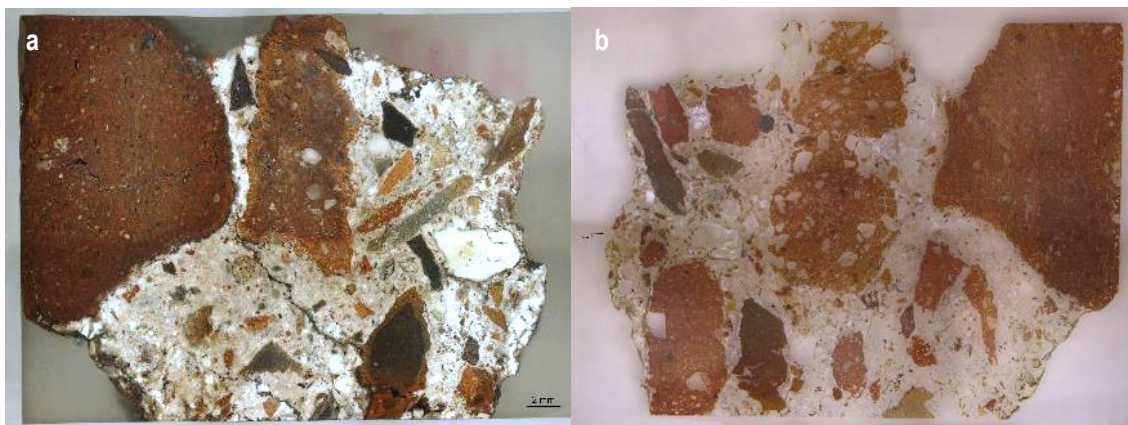


Figure 3.6. Representative result of a a) thin section obtained from a b) cross section of the sample HHT-3.

3.3.3 Sample preparation for X-Ray Diffraction and Thermogravimetric Analysis – Powders (GF+FF)

Powder XRD was implemented for the mineralogical characterization of the mortars in their global and binder enriched fractions. For this purpose, two different sampling processes will be carried out for both fractions. For the bulk analysis, the global fraction (GF) was obtained by separating approximately 10 g of the sample using a hammer and chisel. Later, the fragments previously separated were ground by hand in an agate mortar and pestle in order to disaggregate them in finer fractions, and they were ground in a PM 100 agate mill machine (Retsch) for 10 minutes at 500 rpm (with 3 balls of < 1 cm Ø) to obtain a fine powder. In cases where it was needed, the process was repeated in order to dispose of all the big fragments, such as ceramic and quartz grains, to obtain a homogeneous powder. Between 25-30 mg of the global fraction powder were used to perform Thermogravimetric analysis.

In the process of obtaining the binder enriched fraction (fine fraction), it is important to not to break apart the aggregates, thus, each sample was gently disaggregated using a rubber hammer. Afterwards, the disaggregated fractions were collected and sieved with a stainless steel test sieve of 63 microns of aperture by Retsch in order to obtain an amount of 0.5-2 mL (depending on the density of the powder) and used to perform the powder XRD analysis.

The samples HHT-10 and HHT-11 were divided in both their characteristic layers for these analyzes (HHT-10-U and HHT-10-D, and HHT-11-U and HHT-11-D), due to their different stratigraphic composition.

3.3.4 Sample preparation for clay minerals identification

The identification of clay minerals required the preparation of oriented mineral specimens, which allows for the distinction between different layer types of mineral groups. In these oriented samples, as cited in Lugwisha (2011), “clay particles tend to align themselves in one direction”, which makes the identification by means of X-ray Diffraction more accurate. For this analysis, the samples were prepared using the fine fraction powder (FF), as it is the binder enriched portion of the sample with higher amount of clay minerals, which was obtained as described in chapter 3.3.3.

Approximately 0.25 g of the fine fraction powder were added into a test tube together with approximately 10 mL of distilled water; the mixture was manually stirred for 1.5 minutes until reaching a homogeneous composition; the solution was left to sit for 30 seconds to collect a mildly diluted solution from the surface of the test tube with a Pasteur pipet; subsequently, the collected solution was carefully released and spread in a glass holder and left for 48 hours to dry at room temperature. The samples were prepared in duplicates in order to undergo two different treatments: Ethylene glycol and Heat treatment.

XRD was performed in both sets of glasses when air dried before treatments, as well as after each glycol and both heat treatment analysis under the experimental conditions explained in the following section 3.4.2.

Two sets of glass holders were prepared from each sample to perform the experimental procedure from USGS for clay minerals identification (USGS, n.d.). The samples were subjected to two different processes, Ethylene Glycol vapor impregnation and heat treatments, for this, both sets of glasses with the air-dried samples were analyzed by means X-ray Diffraction to obtain their initial diffraction patterns and then proceed with the Glycolation and heating treatments. The parameters used for XRD analysis of clay minerals are the same as the ones described in Section 3.4.2 on experimental conditions of Powder XRD.

For ethylene glycol vapor treatment, one set of glass holders containing the prepared samples was located in a desiccator shelf of a desiccator containing about 1 cm depth of ethylene glycol at the base and then hermetically closed. The desiccator containing the glasses was then put in an oven at 60°C for at least 16 hours for impregnation (as recommended by the USGS manual and Mosser-Ruck *et al* (2005). After this, the samples were taken out and analyzed by means of X-ray Diffraction using the same experimental conditions used for Powder XRD analysis described above. The second

set of glasses was used to carry out the heat treatment. It was divided in two: the first heat treatment was carried out in a Nabertherm P 330 with a first step of 20 minutes long in which the furnace will reach from room temperature to 400°C, and then stay at 400°C for 40 minutes (USGS recommends half an hour but longer periods of time won't affect the results according to their protocol). After the heating process, the samples were left to cool down with the furnace's door closed to prevent rehydration for more or less 1 hour and then taken one by one out of the furnace to the X-ray Diffractometer to be analyzed (under the same parameters as for Glycolated samples and Powder XRD). The second heat treatment was performed in the same glasses heated at 400°C, and this time the furnace reached a maximum temperature of 550°C at the end of the first step of 20 minutes, and remained at 550°C for 40 minutes more. The glasses were left to cool down and then analyzed as the previous set of samples by means of X-ray Diffraction.

According to the process for clay minerals identification following the flow diagram of USGS, the resulting diffractograms of one of the air-dried samples, from the glycolated sample and from the samples heated at 400°C and 550°C should be put together overlapping. The recognition of the clay minerals will be given by the shift of their characteristic peaks in the d-count setup of the DIFFRACT.SUIT EVA software, shown in terms of angstroms (Å), and compared with the Flow diagram of Appendix 3.

3.3.5 Sample preparation for Acid attack and Granulometric analysis – Fractions

For acid attack analysis, all the samples were analyzed; in particular, samples HHT-10 and HHT-11 were analyzed on their different stratigraphic layers, as required due to their different composition. They were divided into two: upper (-U) and lower (-D) layer, in which the upper layer is considered to be in direct contact with water, whilst the lower layer is not. The stratigraphic layers of samples HHT-10-U and HHT-10-D were separated with a Discoplan-TS Diamond disk, and afterwards they were left to dry overnight in the oven at 40°C; then a scalpel and tweezers were used to make a finer separation and to avoid contamination from the adjacent layer. The cleaning process was performed with soft brushes and a scalpel to remove contamination.

The sample preparation for chemical analysis consisted of carefully grinding each sample with a rubber hammer to disintegrate it in smaller fractions, then two sets of 10 g of the sample were taken, ensuring that the selection was representative of the composition and contained a homogeneous mixture of the different fractions of the sample (Middendorf *et al*, 2005b). The initial weight of each sample was recorded

(Appendix 4) prior to the dissolution in acid for comparison with the final result after the filtration and drying processes.

3.4 EXPERIMENTAL CONDITIONS

3.4.1 Experimental conditions for Optical microscopy (OM)

Optical observations were made by means of a Leica M205 C Stereoscopic Microscope and recorded with a Leica DFC295 digital camera, whereas petrographic analysis was performed on a Leica DM2500 P Modular Polarization Microscope, and recorded with a Leica MC170 HD digital camera.

3.4.2 Experimental conditions for X-Ray Diffraction (XRD)

Both global and fine fraction powders were analyzed by means of X-Ray Diffraction on a Bruker D8 Discover X-Ray Diffractometer using a CuK α source working at 40 kV and 40 mA. The diffractograms were recorded in the range 3°-75° 2Theta every 0,05° per step with a step time of 1 second per increment. The DIFFRAC.SUITE EVA software was used to identify the mineral phases with the Powder Diffraction Files of the International Centre for Diffraction Data -2. Standard polymer sample holders were used to contain the powdered samples (\approx 1 g depending on the sample's density). For the semi-quantification of the crystalline phases on each sample, the I/I_0 (in which I stands by the integrated intensity per unit length of diffraction line, and I_0 is the intensity of the incident beam (Lugwisha, 2011) ratio of integrated intensities ("Reference Intensity Ratio" as cited on Hubbard *et al* (1976)) was used.

3.4.3 Experimental conditions for Thermogravimetric analysis (TGA-DTG)

The global fraction powder of the samples was analyzed in a Simultaneous Thermal Analyzer STA 449 F3 Jupiter (NETZSCH), under inert atmosphere of Nitrogen (Air Liquide Alpagaz compressed N₂) with a flow rate of 70 mL/min. The heating program was set to start at 40°C and then increase it at a constant rate of 10°C/min until reaching 1000°C.

3.4.4 Experimental conditions for Variable Pressure Scanning Electron Microscopy coupled to Energy Dispersive X-ray Spectrometry (VP-SEM-EDS)

A Hitachi S-3700N (Hitachi High Technologies, Berlin, Germany) Scanning Electron Microscope coupled with a Bruker XFlash 5010 (Bruker Corp, Billerica, Mass. USA) Silicon Drift Defector (SDD) Energy Dispersive X-ray Spectrometer was used to perform the micro-analysis of the samples. The analysis was performed under variable pressure, operated with an accelerating voltage of 20 kV and chamber pressure of 40 Pa. The SDD was operated on an energy scale of 0-20 keV, with a resolution of 129 eV at Mn K α , and it was used to obtain the chemical analysis and the EDS elemental data, acquired by point microanalyses in the form of elemental distribution maps with an Esprit 1.9 software. The SEM images were captured in backscattering electron (BSE) mode.

3.4.5 Experimental conditions for Acid attack and Granulometric analysis

For the acid dissolution of mortars, 120 mL of an aqueous solution of hydrochloric acid 1:3 was added to a 250 mL beaker containing the prepared sample giving time for the reaction to take place. Immediately after, the beaker was left in a hot plate for 10 minutes after it reached the boiling point while stirring. The resulting mixture was left to cool down to reach room temperature to be filtered afterwards under vacuum with a Bucker funnel and filter paper (Whatman) and washed at least two times with distilled water; then the filtered residues were left in the oven to dry overnight at around 60 °C. The already dried residues were weighed and recorded (Appendix 4) to compare against the initial weight of the sample and determine the final soluble-insoluble ratio on each sample.

The resultant insoluble residue was then used to perform the Granulometric analysis with stainless steel test sieves by Retsch (Germany) with 4, 2, 1, 0.5, 0.25, 0.125 and 0.063 mm mesh apertures. Each individual set of grain fraction obtained was weighed and recorded (Appendix 4) in terms of weight and percentage in function of the total amount of the insoluble fraction. An average value of both tests per sample was determined and graphed. A minimum amount of sample was lost during the sieving process, nevertheless, a third test had to be done for sample HHT-5 due to the significant weight loss during the sieving process. The results of sample HHT-5-HCl1 were omitted and substituted by the third test (HHT-5-HCl3) for a better representation and accuracy.

4 RESULTS

4.1 VISUAL INSPECTION

During the visual inspection of the samples with an unaided eye, certain similarities and differences among the samples were identified, and allowed to formulate preliminary assessments. The mortars obtained from the coating layer of the tanks (HHT-1, HHT-4, HHT-5) show very similar and homogeneous composition with small ceramic aggregates, overall thickness from 1 to 3 cm, and orange-pinkish binder color with the presence of some crushed ceramics. Sample HHT-10 showed the same composition of the previous group described, but only in the upper stratigraphic layer and with an inconsistent and smaller thickness throughout the sample (up to 15 mm). The composition of the adjacent layer of sample HHT-10 together with the sample HHT-12 presents a homogeneous light colored binder and siliceous aggregates. No ceramic fragments were spotted in neither both mortars.

The sample HHT-11 from the tank 3 was separated in two different layers, in which the upper layer displayed a more heterogeneous composition, a mixture of crushed ceramics and a small amount of big ceramic aggregates up to 8 mm; whereas the lower layer exposes an orange-pinkish binder color, and a clear predominance of big ceramic fragments greater than 12 mm.

The samples HHT-2, HHT-8 and HHT-9 collected from the floors present ceramic aggregates in high proportions and crushed ceramics within the binder, and display a more orange-pinkish color. The aggregates' dimensions varied from 2 mm up to 20 mm. The sample HHT-3 (from the channel) also exhibits big ceramic aggregates but a lighter binder color.

Samples PHHT-6 and PHHT-7 show similar characteristics in thicknesses (20-25 mm), binder composition and color (light brown). The main characteristic of both samples is their chromatic layer in the surface, in which the sample PHHT-6 showed a feathered-like figure in red color, and the surface of the sample PHHT-7 is divided in 3 main colored areas: a 6 cm red and a 5 cm blue sections divided by a 1 cm thick white line. A blue/white 3 cm long feathered-like figure in red area was also observed.

4.2 OPTICAL MICROSCOPY (OM)

4.2.1 Stereozoom microscope

Some observations made during the preliminary assessment of the samples were confirmed by the analysis of the cross polished sections under stereo microscope (Tab. 4.3), and additional information regarding the physical characteristics of the binder and aggregates was obtained with the examination of the thin sections and documented in Appendix 2. The main types of aggregates found in the samples were ceramic fragments and siliceous grains, which vary in size and proportion throughout the samples (Tab. 4.1). It was also possible to identify cracks in the binder in most of the samples (except for sample PHHT-6) (Tab. 4.2.f), and also around the ceramic aggregates, and in some cases also across the ceramic fragments and the binder.

Table 4.1. Results obtained from the microscopic observations of cross and thin sections of the samples. %= approximate percentage of aggregate within the binder matrix, CC= crushed ceramics.

Sample	Binder color	Ceramic aggregates		Quartz aggregates			Additives
		Size (mm)	%	Size (mm)	%	Roundness	
HHT-1	Orange	0.5-5	30	1-2	10	Subangular - poorly rounded	CC
HHT-2	Orange	2-15	50	1-1.5	3	Poorly rounded	CC
HHT-3	Light orange	2-15	40	0.5-2.5	20	Poorly rounded	CC
HHT-4	Orange	0.5-5	30	1-1.5	5	Subangular - poorly rounded	CC
HHT-5	Orange	0.5-5	30	1-5	15	Poorly rounded	CC
PHHT-6	Light brown	-	-	0.5-6	40	Subangular - poorly rounded	-
PHHT-7	Light brown	-	-	0.5-5	40	Subangular - poorly rounded	-
HHT-8	Orange	2-15	50	0.5-2	3	Subangular - poorly rounded	CC
HHT-9	Orange	2-15	50	0.5-3	10	Subangular - poorly rounded	CC
HHT-10-U	Orange	0.5-5	30	0.5-2	5	Subangular - poorly rounded	CC
HHT-10-D	White	-	-	0.5-2	40	Subangular - poorly rounded	-
HHT-11-U	Orange	2-10	20	0.5-2	20	Subangular - poorly rounded	CC
HHT-11-D	Orange	2-15	60	0.5-2	5	Subangular - poorly rounded	CC
HHT-12	White	-	-	0.5-3	30	Subangular - poorly rounded	-

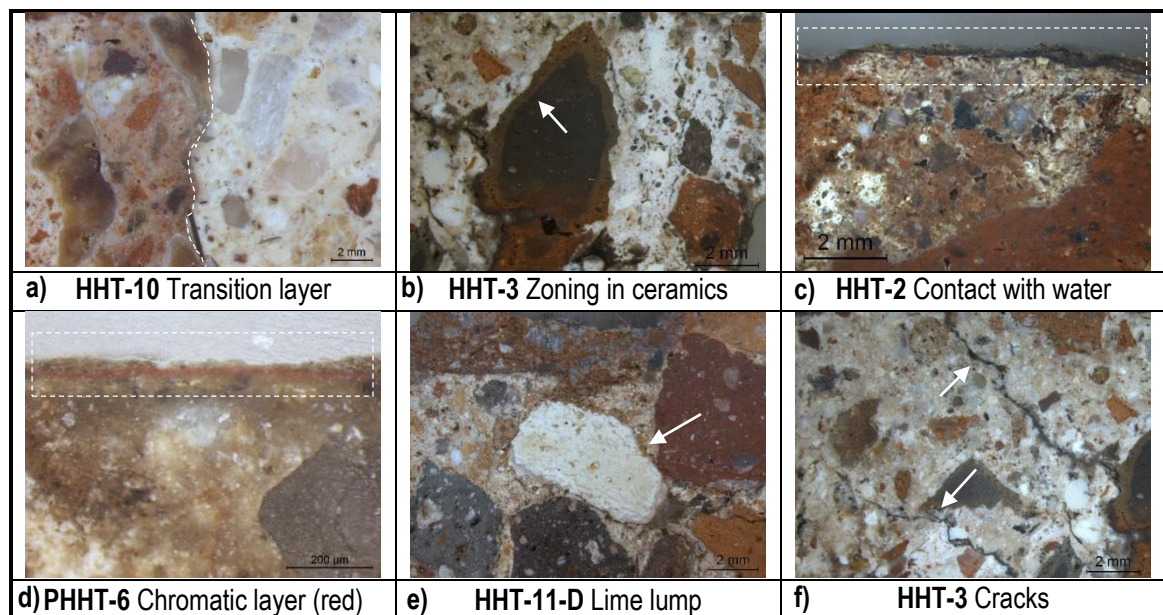
Samples HHT-1, HHT-4, HHT-5 and the upper layer of the sample HHT-10 (U) show a homogeneous composition, with small ceramic fragments (0.5-5 mm) comprising around 30% of the mortars, some crushed ceramics and an orange-ish binder color. Subangular and poorly rounded siliceous aggregates were also observed within the binder (around 10%). Cracks were observed across the sections and around the ceramic aggregates.

Samples PHHT-6 and PHHT-7 demonstrate a chromatic layer (Tab. 4.2.d) and a high proportion of sub-angular and poorly rounded and sorted siliceous aggregates (between 30 to 40%), which vary from 1 to 6 mm, and a few amount of brown-yellow inclusions and some micaceous aggregates (1-4 mm) were found. No coarse aggregates were seen in the finishing layer (*intonaco*) of both samples. Cracks were only noticeable in sample PHHT-7. The binder showed a light brown color and some small black inclusions.

The lower layer of sample HHT-10 (D) and the sample HHT-12 present a similar light beige-colored binder. Sample HHT-10-D displays a subtle change in the aggregates composition dividing the sample in two parts: the first half (in contact with sample HHT-10-U) contains about 30% of moderately sorted sub-angular and poorly rounded siliceous aggregates (from 0.5 to 2 mm), whereas the other half of the sample shows the same matrix as in sample HHT-12 with about 30% of poorly sorted siliceous aggregates from 1 to 4 mm from sub-angular to poorly rounded.

Some lime lumps, zoning surrounding the ceramics (noticeable due to lighter or darker color than the overall composition of the fragment) and a fine layer above the surface that was in direct contact with water were spotted in the samples (Tabs. 4.2.e,b,c).

Table 4.2. Particularities of representative samples observed under stereo microscope.



The ceramic fragments displayed in the cross sections of the mortars related to the hydraulic system were analyzed for comparison under stereo microscope. Eight types of ceramics (A-H) were distinguished and classified by their composition, color, size, porosity and inclusions (Tab. 4.4).

Table 4.3. Identification and description of the samples by visual inspection and microscopic observations of cross and thin sections.

Sample	Structure	Color	Strength	Aggregates	Thickness	Description	Cross section
HHT-1	Double apse coating	Light pink / Orange	Brittle	> 2 mm ceramic pieces Sub-angular-poorly rounded	1-2 cm	Cracks in binder. Ceramic aggregates from 1-5 mm with variated colors and shapes, crushed ceramics. Some sub-angular and sub-rounded aggregates.	
HHT-2	Water mirror floor	White / light pink	Strong	> 1 cm ceramic pieces, some > 1 mm Poorly rounded	1-3 cm	Big ceramic fragments, from 6 to 20 mm long. Few cracks distinguishable. Crushed ceramics and sub-rounded aggregates present.	
HHT-3	“Y” Channel coating	White	Strong	Heterogeneous ceramic aggregates between <1mm and 1.3cm Sub-rounded Lime lumps	~4 cm	Big ceramic aggregates present, from 7 to 14 mm long, different colors, compositions and temper. Some small ceramic fragments are embedded in the binder, such as sub-rounded aggregates. Some lime lumps.	
HHT-4	Tank 1 (detached)	Light pink / Orange	Strong	1-4 mm ceramic fragments, some black aggregates Sub-angular – poorly-rounded	3 cm	More or less homogeneous mixture of ceramic fragments and binder, from 1 to 4 mm long. Crushed fragments within binder with no visible cracks. Sub-angular and sub-rounded aggregates.	
HHT-5	Tank 2 coating	Light pink	Mildly strong	Powdered ceramics, and 1-4 mm ceramic fragments and some 3 mm poorly rounded siliceous grains	2.5 cm	Presence of medium sized ceramic fragments, from 0,5 to 8 mm, different colors and structure. Binder shows presence of lime lumps and crushed ceramics and from well-rounded to sub-rounded aggregates.	
PHHT-6	Mural painting (detached)	Light brown	Brittle	Aggregates smaller than 1mm, siliceous grains, micas	2 cm	Presence of 4 mm long aggregates. Presence of a small chromatic layer (red). Angular and sub-angular aggregates of 1-4 mm long. Dark aggregates of 1 mm long.	

Table 4.3 (continuation)

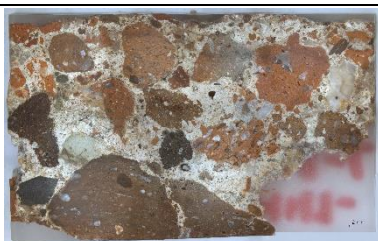

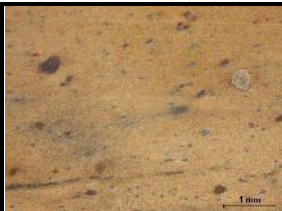
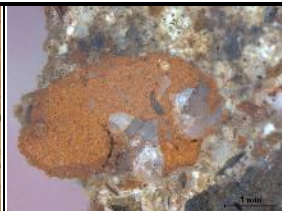
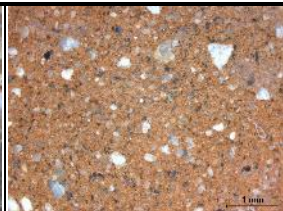
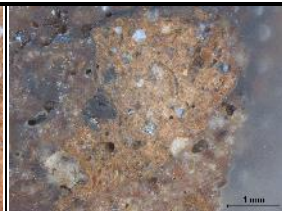
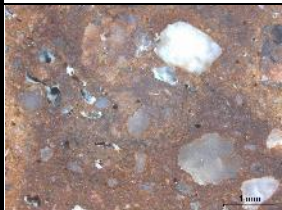
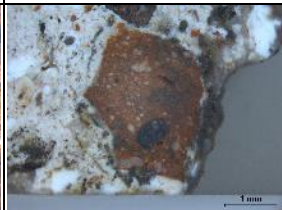
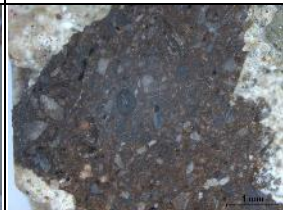

PHHT-7	Mural painting (detached)	Light brown	Brittle	Contains some 1-4 mm ceramic fragments and some 3 mm siliceous grains	2.5 cm	Blue chromatic layer. Sub-rounded and sub-angular aggregates smaller than 3 mm. Some darker aggregates (1-2 mm) are visible.	
HHT-8	Garden water mirror floor	Light pink	Strong	Ceramic aggregates of around 1mm and 1cm big Sub-rounded Lime lumps	1.5 cm	Ceramic aggregates from 1-10 mm long, different colors and compositions. Presence of crushed ceramics in binder and sub-rounded aggregates. Lime lumps visible	
HHT-9	Garden water mirror floor	Light pink	Strong	Upper part with ceramic fragments of 1-10mm, lower part with ceramic fragments up to 2cm in big proportions	1-4 cm	Big ceramic aggregates from 2-10 mm, different colors and compositions, some burnt ceramics. Presence of some crushed ceramics and sub-angular aggregates up to 2 mm long.	
HHT-10	Tank 3 coating	Light pink-orange / White	Strong	HHT-10-U 0.1-1cm ceramic aggregates with sub-angular siliceous grains and HHT-10-D around 2mm siliceous grains	U= 0.5-1.5cm D= 3-8cm	Presence of ceramic fragments up to 2 mm in the upper layer, so does crushed ceramics and small sub-angular aggregates. Down layer shows dark aggregates up to 1 mm and sub-angular well sorted aggregates up to 2 mm.	
HHT-11	Tank 3 coating	Light pink / Light pink	Mildly strong	Mixture of fine ceramic grains at the top layer up to 5mm, upper layer with 1.5cm. Angular - sub-angular aggregates ~1mm and lime lumps	2-8 cm	Ceramic aggregates up to 8mm in upper layer. Crushed ceramics embedded in the binder and presence of sub-angular siliceous aggregates up to 2 mm. Main composition out of ceramic fragments up to 12 mm, varied colors and compositions. Presence of some burnt ceramics. Crushed ceramics in the binder and some sub-angular aggregates.	
HHT-12	Tank 3 wall	White	Brittle	Presence of some sub-angular siliceous grains of 1-3mm. Lime lumps	~3-4 cm	Presence of some elongated dark aggregates up to 1 mm long. A lime lump present in one side. Some sub-angular aggregates present within the binder	

Table 4.4. Types of ceramics found in cross sections of the samples from *villa* Horta da Torre.

			
Type A Compact, fine grained, light colored, small dark inclusions	Type B Fine grained, compact, small siliceous inclusions, poorly sorted	Type C Coarse grained, high proportion of inclusions, porous, well sorted	Type D Coarse grained, small to medium inclusions, highly porous, poorly sorted
			
Type E Medium to big siliceous inclusions ~1 mm, compact, poorly sorted	Type F Brown and porous, compact, some dark-colored inclusions	Type G Dark gray, very fine grained, compact, small inclusions	Type H Light gray, medium to big inclusions, fine grained, porous

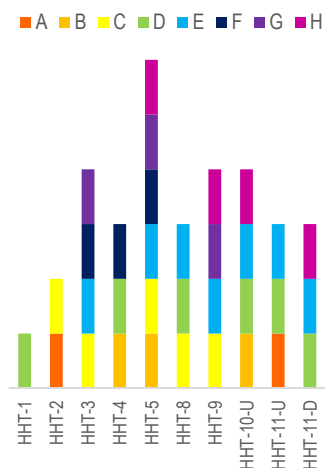
The frequency of the different types of ceramic fragments within the mortar was recorded (Tab. 4.5), and it was possible to determine that types A, B, F and G were found only in three samples and H in four, whereas types C, D and E were present in a bigger amount. Types A, C and E consist of big fragments, which vary from 5 to 20 mm, while the other types of ceramic aggregates were found as small fragments < 5 mm. No apparent *terra sigillata* fragments were identified, despite being present in mortars from the *stibadium* (pc. Carneiro, 2019). In most of the cases, samples with big fragments, contain at least two types, and additionally at least one more type of small grained ceramics (Fig. 4.1).

Table 4.5. Distribution of frequency of ceramic fragment types found in samples of hydraulic mortars.

Sample	Type of ceramic							
	A	B	C	D	E	F	G	H
HHT-1				++				
HHT-2	+		+					
HHT-3			+		+	+	+	
HHT-4		+		+++		+		
HHT-5		+++	+		++	+	++	+
HHT-8			++	+++	++			
HHT-9			++		++		++	++
HHT-10-U		+		+	+			+
HHT-11-U	++			++	++			
HHT-11-D				++++	++			+++

Most frequent +++++ +++ ++ + Least frequent

Figure 4.1. Types of ceramics found in each sample.



4.2.2 Petrographic microscope

By means of petrography, several minerals were recognized (Barker, 2014). It is remarkable that quartz was present in all the samples as the main mineral, and its grain roundness ranges from subangular to poorly rounded, from fine (<0,5 mm) to coarse grains (~3 mm) (Tab. 4.6). Although quartz grains have been mainly observed as single grains, it is present as part of lithic fragments such as quartzite, or associated with feldspars as granitic grains. Single minerals were observed within the binder, including some alkali feldspars (orthoclase and microcline), plagioclase feldspars (albite), amphiboles (mainly hornblende in samples HHT-1, HHT-2, HHT-4, HHT-5, HHT-8, HHT-9), micas (muscovite and biotite), pyroxenes (in samples HHT-1, HHT-4 and HHT-5) and possibly olivine (Tab. 4.7). Lime lumps were also observed in the binder in all the samples. Cracks surrounding the ceramic fragments were visible, as well as cracks across the binder and the voids. Samples HHT-1, HHT-2, HHT-3, HHT-8, HHT-9 and HHT-10 show a different composition in the outer layers, which apparently was in contact with water, and display a dark-greenish color, or a thin and fine-grained layer (Tab. 4.6.c).

Table 4.6. Representative petrographic images of the general composition of mortars.

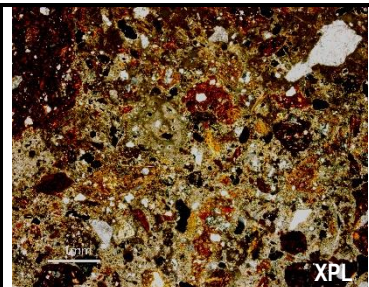
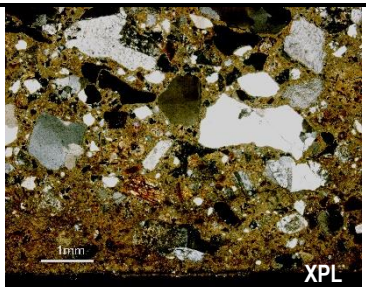
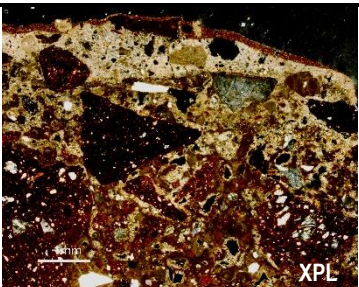
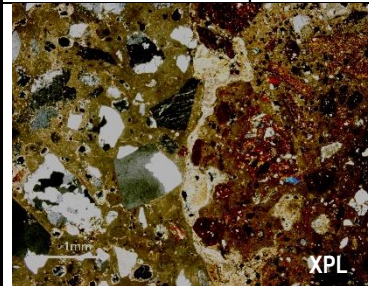
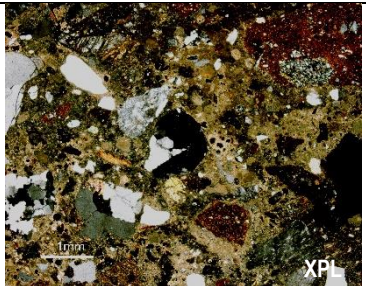
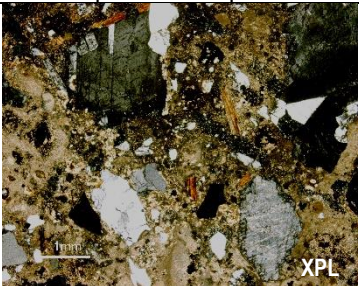
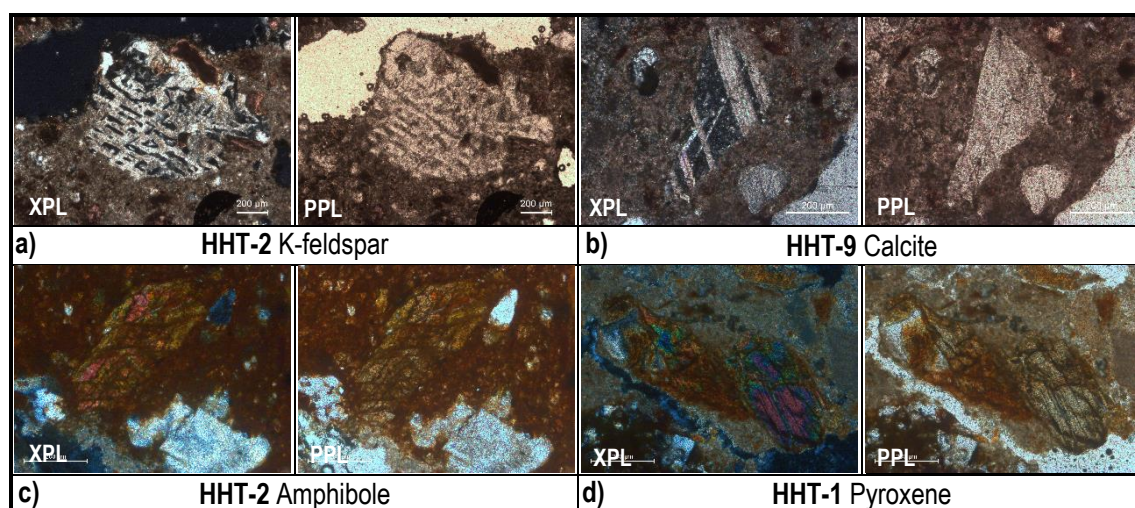
		
a) HHT-4 General distribution. Quartz and ceramic aggregates. Presence of some amphiboles, micas and feldspars.	b) PHHT-7 Quartz grains aggregates. Chromatic layer at the bottom. Alkali and plagioclase feldspars and micas.	c) HHT-8 Contact with water layer on top. Predominance of ceramic aggregates and quartz. Feldspars and amphiboles.
		
d) HHT-10 Transition between layers. Quartz and quartzite aggregates (left) and ceramics (right). Amphiboles, micas and plagioclases present.	e) HHT-11-U Quartz, quartzite and ceramic aggregates. Amphiboles, plagioclases and feldspars. Some lime lumps present.	f) HHT-12 Predominance of quartz aggregates. Some micas and feldspars present.

Table 4.7. Characteristic isolated minerals within the binder and ceramics.



4.3 X-RAY DIFFRACTION (XRD)

4.3.1 Powder X-ray Diffraction (Powder XRD)

Tables 4.8 and 4.9 illustrate the semi-quantified data of the crystalline phases present in the global and fine fraction powders of the samples.

The results of the global fractions indicate predominance of quartz and its presence as major compound in almost all the samples (Figs. 4.2.a and 4.2.c), the only outlier is sample HHT-12, which shows the same proportion of calcite and quartz as predominant phases. In the case of fine fraction powder analysis, calcite was identified as the predominant component in samples HHT-1, HHT-2, HHT-4, HHT-9, HHT-10-U, HHT-10-D, HHT-11-D and HHT-12 (Appendix 5). Samples PHHT-6, PHHT-7 and HHT-11-U show the same proportion of quartz and calcite as predominant mineral phases (Fig. 4.2.d); and samples HHT-3, HHT-5 and HHT-8 demonstrate predominance of quartz over calcite. Nevertheless, samples HHT-3 and HHT-8 show an increase of calcite proportions in respect with their homologous global fraction; whilst sample HHT-5 did not display any enrichment in calcitic composition in the fine fraction.

Abundant proportions of K-feldspars (orthoclase and microcline), micas (biotite and muscovite) and amphiboles (hornblende) were obtained from powder XRD analysis in the global fraction of the samples. Na-plagioclases (albite) was found in major proportions, whereas some phyllosilicates and accessory minerals such as aragonite, chlorite, clinocllore and hematite, were found only in minor or trace amounts. Cowlesite

was only present in sample HHT-1 as major phase compound, whereas fluorapophyllite was detected in trace amounts in only two samples (HHT-4 and PHHT-7).

In the fine fraction analysis, K-feldspars were spotted as major crystalline phases. Aragonite, albite, micas, amphiboles, clinocllore and fluorapophyllite phases were present in minor or trace amounts; and clinocllore and hematite only in trace proportions. Some oddities were observed: cowlesite was only present in samples HHT-1 and HHT-5 in abundant and major amounts; sample HHT-10-D demonstrated a rather high predominance of albite crystal phase; and sample PHHT-7 proved an enrichment of aragonite, possibly due to dissolution and re-crystallization processes of the calcitic binder (Borsoi et al, 2019).

For the identification of the specific micaceous minerals present in the samples, it was necessary to perform complementary analytical techniques, such as petrography.

Table 4.8. Mineralogical composition of the global fraction powders of mortars assessed by XRD.

SAMPLE	FRACTION	QUARTZ	CALCITE	ARAGONITE	K FELDSPARS	ALBITE	MICAS	AMPHIBOLES	CHLORITE	FLUORAPOPHYLLITE	CLINOCHLORE	HEMATITE	COWLESITE	ETTRINGITE
HHT-1	GF	+++	++	-	+	+	+	++	-	-	Tr	Tr	++	?
HHT-2	GF	++++	+	-	++	+	+++	+	+	-	-	Tr	-	?
HHT-3	GF	++++	+	-	++	+	++	+	+	-	Tr	Tr	-	?
HHT-4	GF	+++	++	-	+	+	+	+++	+	Tr	Tr	Tr	-	?
HHT-5	GF	++++	++	-	+	+	+	+	+	-	Tr	-	-	?
PHHT-6	GF	++++	+	+	+++	+	++	-	Tr	Tr	Tr	-	-	-
PHHT-7	GF	++++	+	+	++	+	++	-	+	-	Tr	-	-	-
HHT-8	GF	++++	++	-	++	+	++	++	-	-	-	Tr	-	?
HHT-9	GF	++++	++	Tr	++	+	+	+	-	-	-	Tr	-	?
HHT-10-U	GF	++++	+++	Tr	+	+	++	+	-	-	-	Tr	-	?
HHT-10-D	GF	++++	+++	Tr	++	+	+	-	-	-	-	-	-	-
HHT-11-U	GF	++++	+++	-	++	++	+	+	-	-	Tr	Tr	-	?
HHT-11-D	GF	++++	+	Tr	+++	++	+	+	-	-	-	Tr	-	?
HHT-12	GF	++++	++++	-	+	+	+	-	-	-	Tr	-	-	-

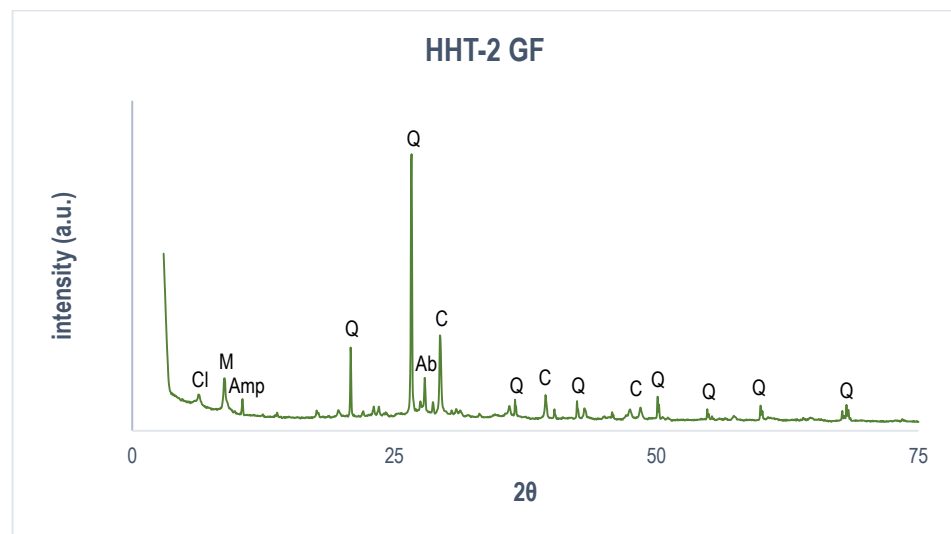
++++ Predominant, +++ abundant, ++ major, + minor, Tr trace, - undetected, ? doubts in presence.

Table 4.9. Mineralogical composition of the fine fractions of mortars assessed by XRD.

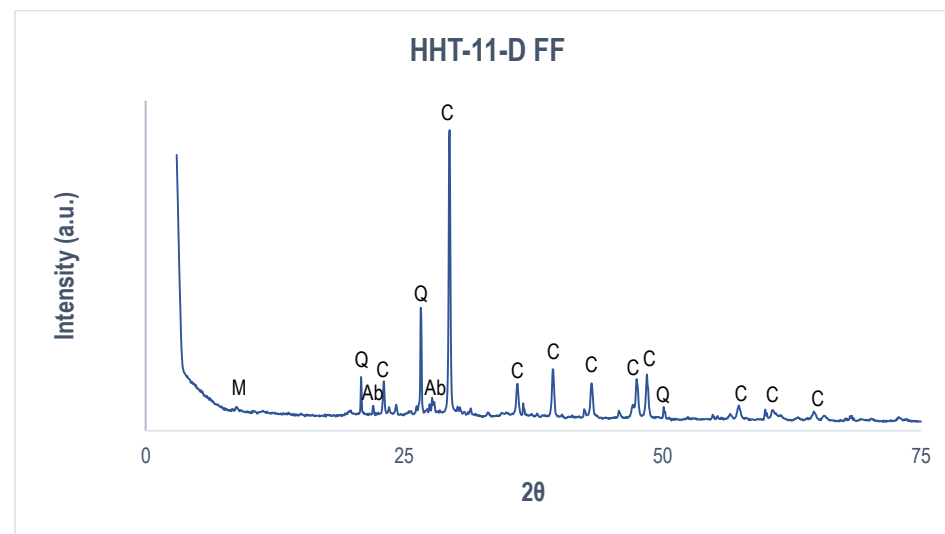
SAMPLE	FRACTION	QUARTZ	CALCITE	ARAGONITE	K FELDSPARS	ALBITE	MICAS	AMPHIBOLES	CHLORITE	FLUORAPOPHYLLITE	CLINOCHLORE	HEMATITE	COWLESITE	ETTRINGITE
HHT-1	FF	++	++++	-	-	+	+	+	-	-	Tr	-	++	-
HHT-2	FF	+++	++++	-	++	+	+	+	-	-	Tr	Tr	-	-
HHT-3	FF	++++	+++	-	+	++	+	-	+	-	-	Tr	-	?
HHT-4	FF	+++	++++	-	+	+	+	+	+	+	Tr	Tr	-	?
HHT-5	FF	++	+	-	+	+	+	+	-	+	Tr	-	+++	?
PHHT-6	FF	+++	+++	+	++	+	+	-	Tr	Tr	Tr	-	-	-
PHHT-7	FF	+++	+++	+++	++	+	+	-	+	Tr	Tr	-	-	-
HHT-8	FF	++++	+++	Tr	++	+	+	+	-	Tr	-	Tr	-	?
HHT-9	FF	++	++++	+	++	+	+	-	-	-	Tr	Tr	-	-
HHT-10-U	FF	+++	++++	-	+	+	+	Tr	-	-	-	Tr	-	?
HHT-10-D	FF	+	++++	-	+	++++	Tr	Tr	-	+	-	-	-	-
HHT-11-U	FF	++++	++++	+	+	+	+	Tr	-	-	-	Tr	-	?
HHT-11-D	FF	+++	++++	+	+	+	Tr	Tr	-	-	-	Tr	-	?
HHT-12	FF	++	++++	+	-	+	+	-	-	Tr	-	Tr	-	-

++++ Predominant, +++ abundant, ++ major, + minor, **Tr** trace, - undetected, ? doubts in presence.

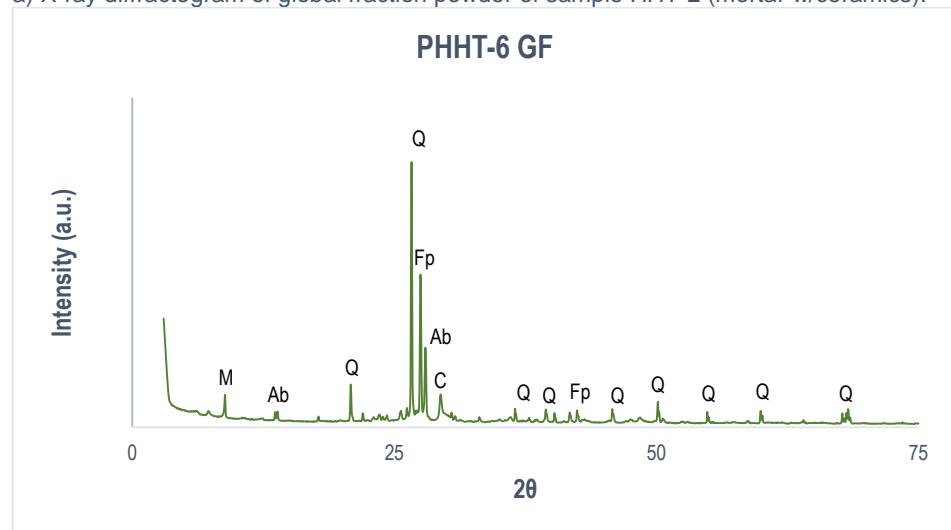
Figure 4.2. Representative X-ray diffractograms of analysis performed in GF and FF powders of mortars from the hydraulic structures and mortars with chromatic layers (Appendix 5).



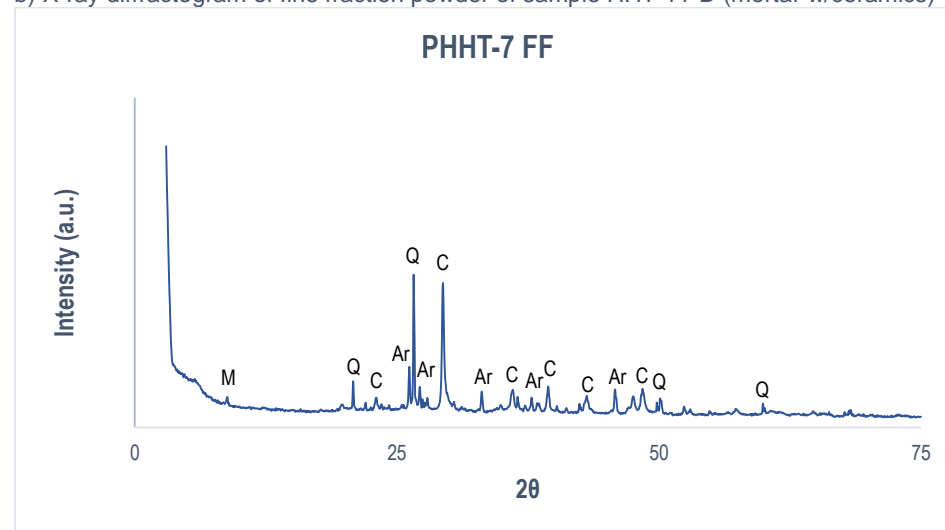
a) X-ray diffractogram of global fraction powder of sample HHT-2 (mortar w/ceramics).



b) X-ray diffractogram of fine fraction powder of sample HHT-11-D (mortar w/ceramics)



c) X-ray diffractogram of global fraction powder of sample PHHT-6 (chromatic layer).



d) X-ray diffractogram of fine fraction powder of sample PHHT-7 (chromatic layer).

*Q= quartz, C= calcite, M= micas, Cl= clinochlore, Amp= amphiboles, Ab= albite, Fp= K feldspars, Ar= aragonite, Cw= cowlesite, Fl= fluorapophyllite

4.3.2 X-ray Diffraction in oriented mounts

For clay minerals identification, oriented glass mounts of the fine fraction powder were analyzed after glycol and heat treatments to determine their behavior between the range 3 to 25 2θ angle (29-10 Å). For the interpretation of clay minerals identification, only one out of both diffractograms of the untreated oriented mounts was used for comparison against the glycol and thermal treatment. For samples HHT-9, HHT-10-U, HHT-11-U and HHT-12, the diffractogram of the untreated sample before glycolation was used, and for the rest of the samples, the diffractogram of the untreated sample for thermal treatments.

Sample 12 didn't show evident presence of clay minerals. For the rest of the samples, three different clay minerals were identified (Appendix 7). In all the samples (excluding sample HHT-12), peaks at $\sim 10\text{\AA}$ and no change during glycol and heat treatments were observed (Fig. 4.3), and according to the behavior of the treatments interpreted with the USGS clay minerals identification flow diagram (Appendix 3), it demonstrates the presence of illite (and/or mica), muscovitic as various polymorphs. Besides, samples HHT-1, HHT-4 and HHT-5 showed peaks at $\sim 14\text{\AA}$ with shifts to $\sim 17\text{\AA}$ after glycol treatment, and then back to $\sim 14\text{\AA}$ after the first heat treatment at 400°C with no change after the second heat treatment at 550°C (Fig. 4.4). This relates to the presence of montmorillonite or another member of the smectite group (Barton & Karathanasis, 2002; Schulze, 2005; Huggett, 2015; Mukasa-Tebandeke *et al*, 2015). Additionally, samples HHT-5, HHT-8 and HHT-10-D displayed a third clay mineral at $\sim 7\text{\AA}$, with no change after glycol treatment and destruction of the peaks after both thermal treatments, which is indicative of kaolinite, chlorite, dickite and nacrite (Warshaw *et al*, 1960) (Fig. 4.4).

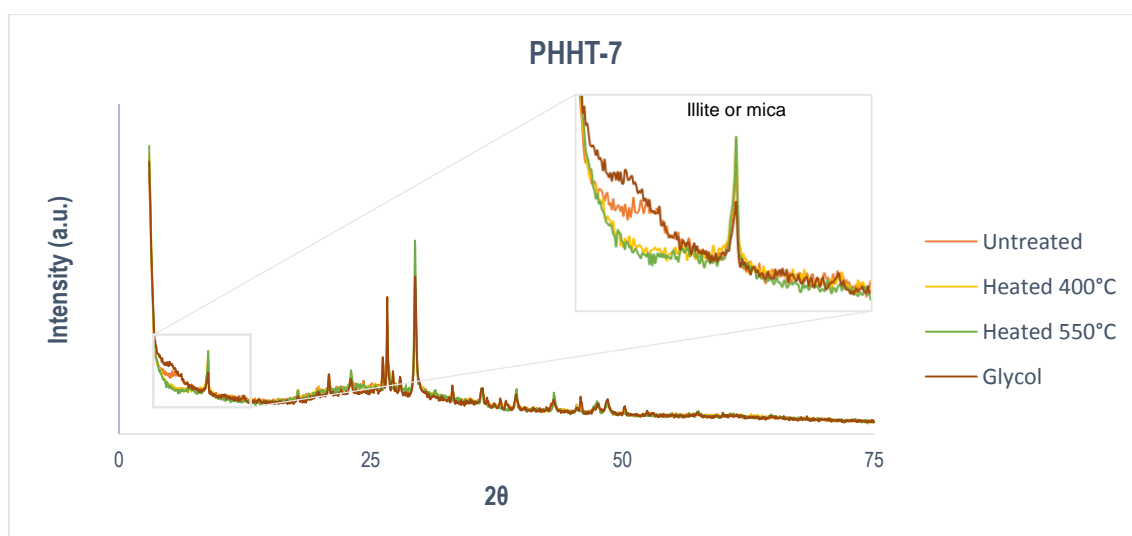


Figure 4.3. Representative diffractograms of clay minerals identification of sample with chromatic layer.

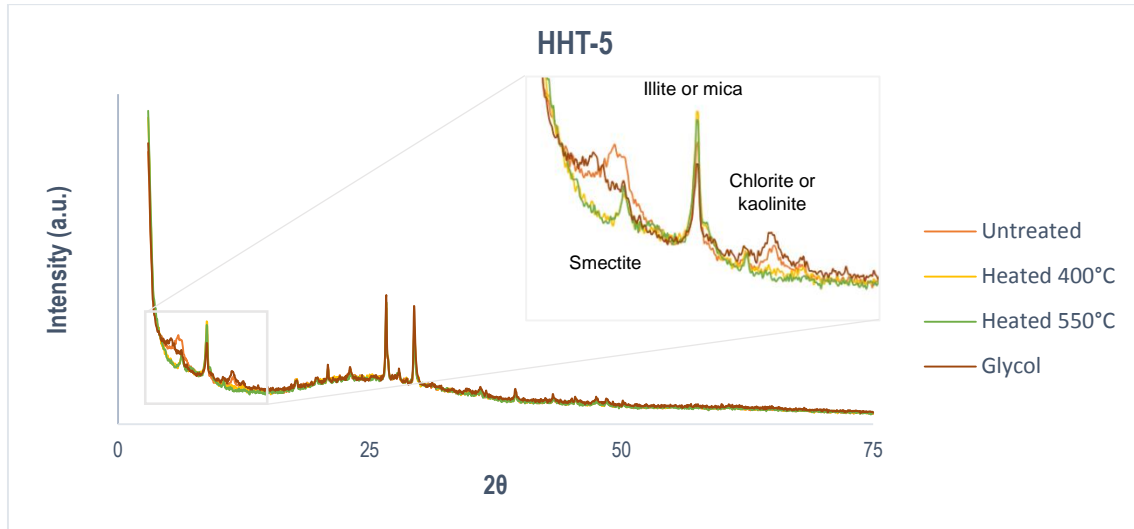


Figure 4.4. Representative diffractogram of clay mineral identification of mortars related to hydraulic structures.

4.4 THERMOGRAVIMETRIC ANALYSIS (TGA)

The results from Thermogravimetric analysis carried out in the global fraction powders of the samples, displayed the percentages of the most significant mass losses during the heating program. The losses between 200-600 °C correspond to the structurally bound water, and the CO₂ to H₂O ratio in relation to the CO₂ percentage can be of use to calculate the inverted hydraulicity index of the sample (Moropoulou, 2005). The greater mass losses were given within the temperature range of 600 to 800 °C, with losses varying between 4.65 and 14.76 % with respect to the total amount of material analyzed (Tab. 4.10). This corresponds to the characteristic mass loss range for the decomposition of calcium carbonate (CaCO₃) to calcium oxide (CaO). The percentage of calcium carbonate was calculated with the equation [5]:

$$\text{CaCO}_3 \% = [P_{(\text{CO}_2)} \cdot M_{(\text{CaCO}_3)}] / M_{(\text{CO}_2)} \quad [5]$$

in which $P_{(\text{CO}_2)}$ represents the mass loss in the temperature range 600-800 °C, $M_{(\text{CaCO}_3)}$ is the molar mass of calcite (100.082 g·mol⁻¹) and $M_{(\text{CO}_2)}$ the molar mass of carbon dioxide (44.02 g·mol⁻¹).

The percentage of calcium carbonate was calculated in function of the greater mass losses recorded by TGA (Appendix 6), leading to a maximum percentage of CaCO₃ of 33.6% and a minimum of 10.6% (Fig. 4.5). These percentages were used to calculate the estimated binder to aggregate ratios used for the elaboration of each mortar,

assuming that the amount CaCO_3 present in the sample represents the binder composition, and the rest of the mass comprises the aggregates. The resulting ratios confirmed the use of a wide range of ratios, from 1:2 (Fig. 4.6.a) to 1:9 (Fig. 4.6.c) in hydraulic mortars; whereas for mortars with a chromatic layer (PHHT-6 and PHHT-7) the ratio was calculated at around 1:3 and 1:4 (Fig. 4.6.b).

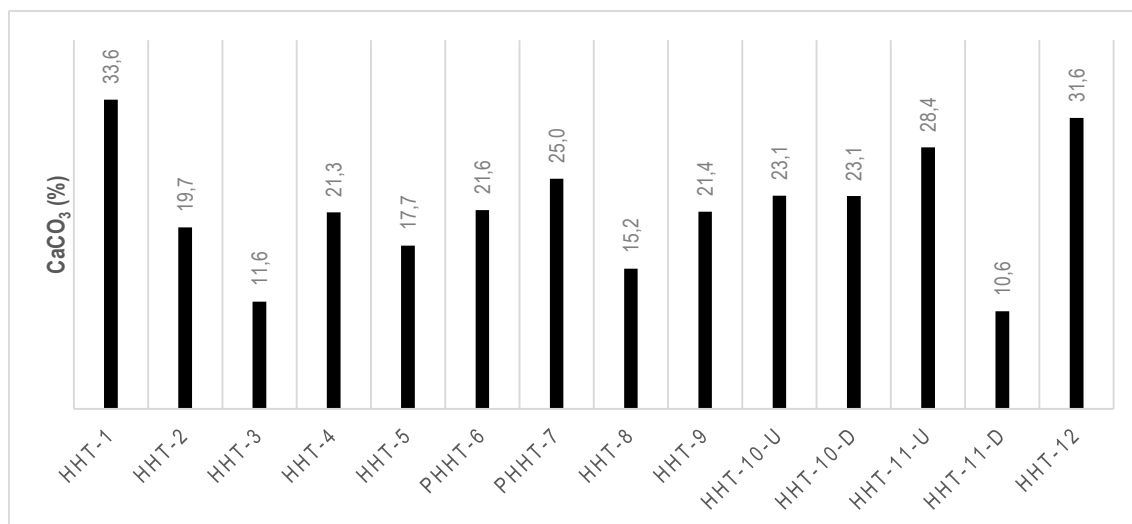


Figure 4.5. Percentage of calculated CaCO_3 percentage in samples from *villa* Horta da Torre.

Table 4.10. TGA results. Record of the greater mass loss percentages during structurally bound water loss, decomposition of CO_2 , CaCO_3 percentage and estimated binder to aggregate ratio.

Sample	Mass loss (%) between 200-600°C ¹	Mass loss (%) between 600-800°C ¹	CaCO_3 (%) ²	Binder to aggregate ratio ³
HHT-1	3.00	14.76	33.6	"1:2"
HHT-2	2.28	8.66	19.7	"1:4"
HHT-3	1.57	5.12	11.6	"1:8"
HHT-4	3.02	9.37	21.3	"1:4"
HHT-5	2.18	7.79	17.7	"1:5"
PHHT-6	1.67	9.49	21.6	"1:4"
PHHT-7	2.29	10.98	25.0	"1:3"
HHT-8	2.77	6.69	15.2	"1:6"
HHT-9	1.39	9.41	21.4	"1:4"
HHT-10-U	2.95	10.17	23.1	"1:3"
HHT-10-D	1.95	10.15	23.1	"1:3"
HHT-11-U	1.94	12.48	28.4	"1:3"
HHT-11-D	1.72	4.65	10.6	"1:9"
HHT-12	2.97	13.88	31.6	"1:2"

¹ Obtained from thermograms (Appendix 6)

² Calculated with the equation for CaCO_3 percentage estimation [5]

³ Obtained in function of the CaCO_3 (%) present and the total amount of analyzed sample

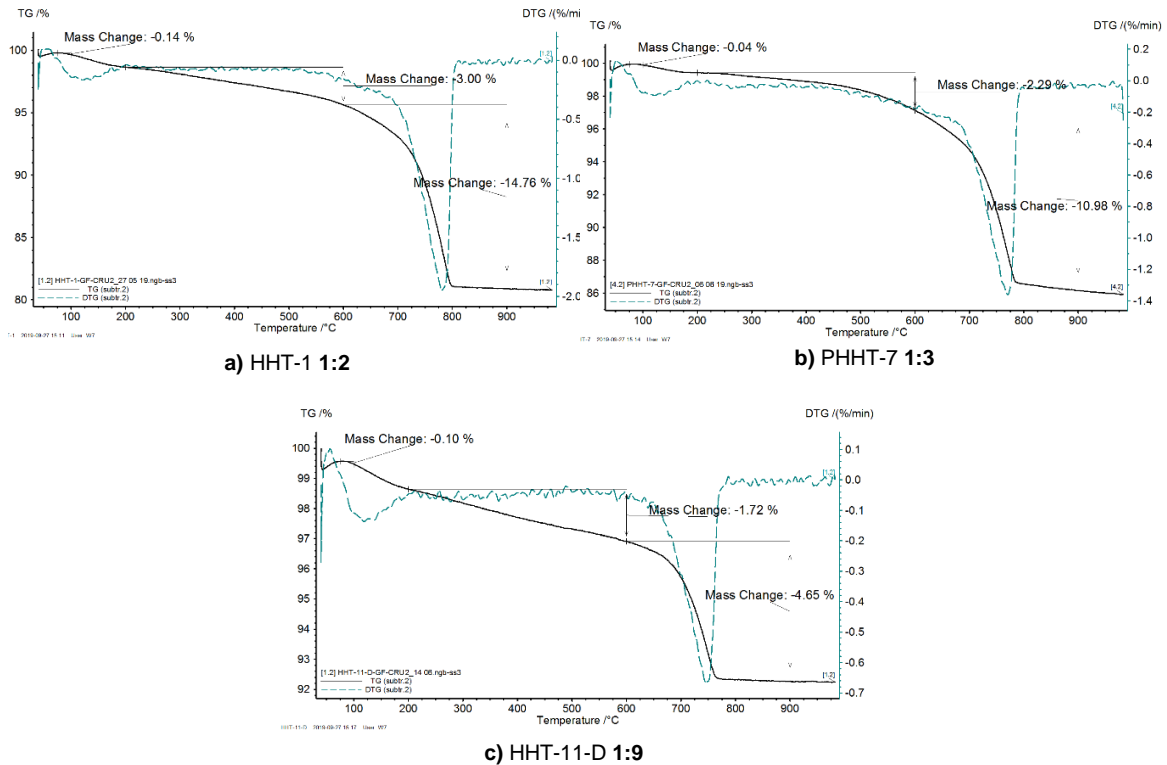


Figure 4.6. Representative thermograms depicting the different binder to aggregate ratios present in the samples (Appendix 6).

4.5 VARIABLE PRESSURE SCANNING ELECTRON MICROSCOPY COUPLED TO ENERGY DISPERSIVE X-RAY SPECTROSCOPY (VP-SEM-EDS)

Information about the chemical composition and textural relationship of the aggregates and binder was provided by VP-SEM-EDS. Elemental mappings of representative areas were obtained to provide information regarding binder-aggregates compositions in all the samples.

The samples obtained from the hydraulic structures show a homogeneous and continuous binder enriched in Ca. In Figure 4.7, a map of a representative sample of a mortar related to the hydraulic structures with a surface in direct contact with water can be observed (HHT-1), and indicates the presence of ceramic fragments and siliceous aggregates. A lime lump can be observed (Fig. 4.7.b) and a point analysis was performed (Fig. 4.10) to assess the pure lime composition. The results demonstrate that the lime was mainly composed by Ca, C and O. Figure 4.7.c shows the distribution of Mg, and it is directly related to the distribution of the ceramic grains, and Figure 4.7.d shows that K and Na were associated to Al and Si. The upper layer (water contact surface) pointed at

with arrows in Figure 4.7.a shows an enrichment in Si, Mg and Al. Additionally, the elemental map performed in sample HHT-2 displays a similar elemental distribution and mineralogical composition than the rest of the samples with ceramic fragments, although, it manifests an enrichment in P in the layer in contact with water (Fig. 4.8).

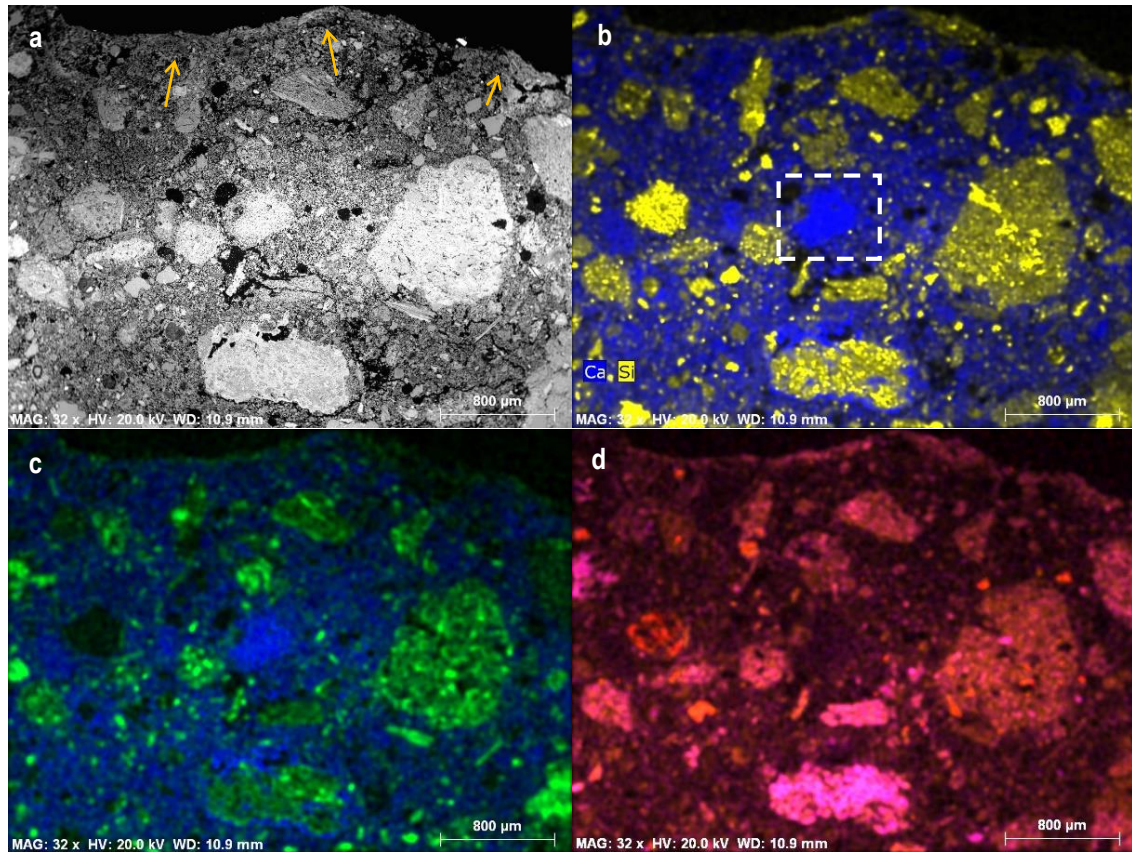


Figure 4.7. Representative elemental map of sample HHT-1 (hydraulic mortar). a) BSE image and arrows pointing at the surface in contact with water, b) ceramic and siliceous aggregates in a calcium enriched binder, with a lime lump enclosed in the dotted area, c) Mg and Ca elemental map, Mg related to ceramic aggregates, d) K and Na feldspars. Blue=Ca, yellow=Si, green=Mg, pink=K, orange=Al, red=Na.

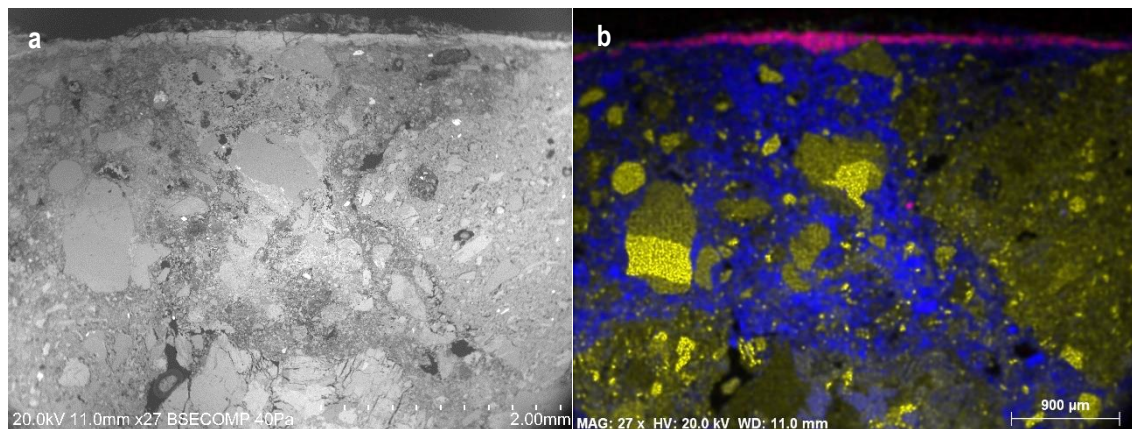


Figure 4.8. Elemental map of sample HHT-2 with P enrichment in the contact surface. a) BSE image and b) P, Ca and Si elemental map, P present in a fine layer in the top. Blue=Ca, yellow=Si, pink=P.

Elemental maps of the samples PHHT-6 and PHHT-7 (the ones containing a chromatic layer) were performed. Figure 4.9 depicts the representative results of sample PHHT-6. The maps demonstrate that the chromatic layer is enriched in Fe and it is in between two bedding layers: the underneath layer displays a Ca enrichment, whereas the upper layer shows enrichment of Si, Mg and Al. An aggregate of calcite was also found (Fig.4.9).

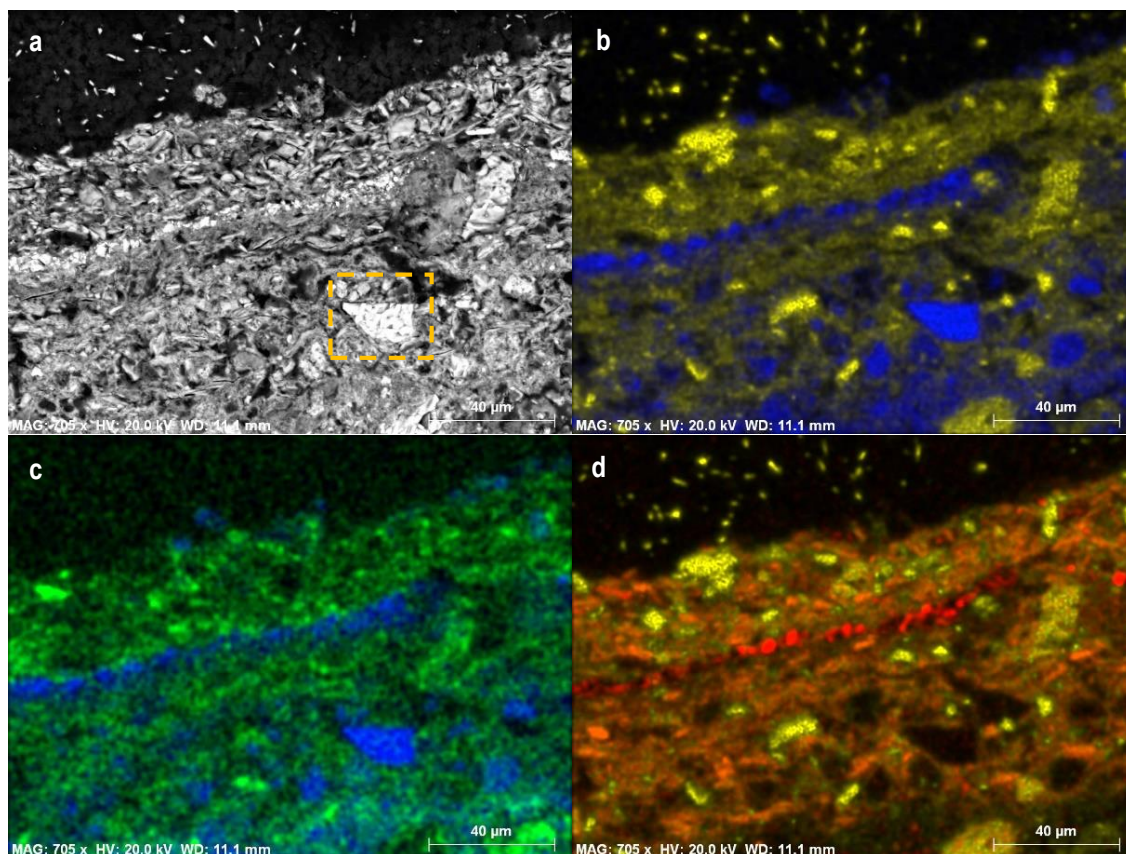


Figure 4.9. General elemental composition of sample PHHT-6 (mortar with a red chromatic layer). a) BSE image and recrystallization of calcite, b) relation between Si and Ca, c) Mg related to Si and Al, d) Fe enrichment in red chromatic layer. Blue=Ca, yellow=Si, green=Mg, orange=Al, red=Fe.

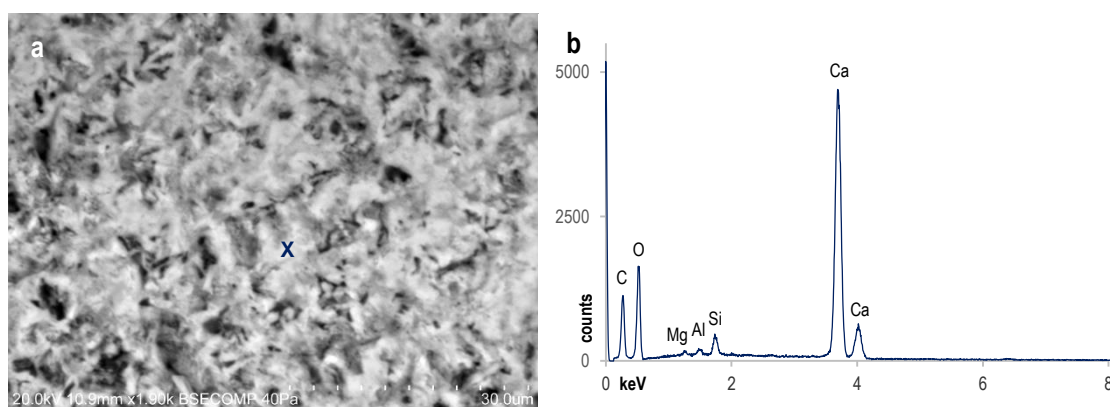


Figure 4.10. Representative point analysis of a lime lump performed in sample HHT-1. a) BSE image of lime lump in Figure 4.7.b, and b) point analysis spectrum of the spot marked in a.

Signs of zoning were seen around some ceramic fragments in samples HHT-3, HHT-5 and HHT-9, and were displayed as different shades of gray in the BSE image (Fig. 4.11.a). The crack developed along the side of the ceramic fragment and the zoning area in sample HHT-3, show enrichment of carbon (Fig. 4.11.b). Besides that, a calcium enriched area can be observed at the right limit of the ceramic aggregate (marked analyzed spot in Fig. 4.11.b) and was compared against the binder matrix composition in the cross section of the same sample in Figure 4.12.

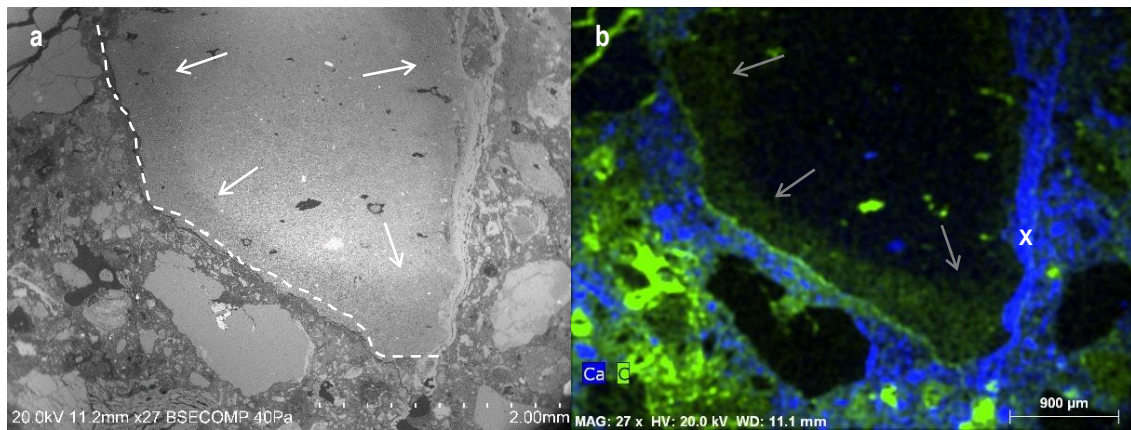


Figure 4.11. Zoning around ceramic aggregate in thin section of sample HHT-3. a) BSE image, arrows point at zoning area, and dashed line indicates crack along the limit of the fragment. b) Elemental mapping of Ca and C, showing an enrichment of C along the crack and in zoned area of the ceramic, and an enrichment of Ca, in which "x" indicates the location of the point analysis of the binder (Fig. 4.12).

The results of this comparison between the composition of binder next to the ceramic in the thin section and the binder matrix of the cross section from the sample HHT-3 (Fig. 4.12) show a rather similar composition, except for a slight increase in Al and Si and a decrease in Ca in the binder next to the ceramic.

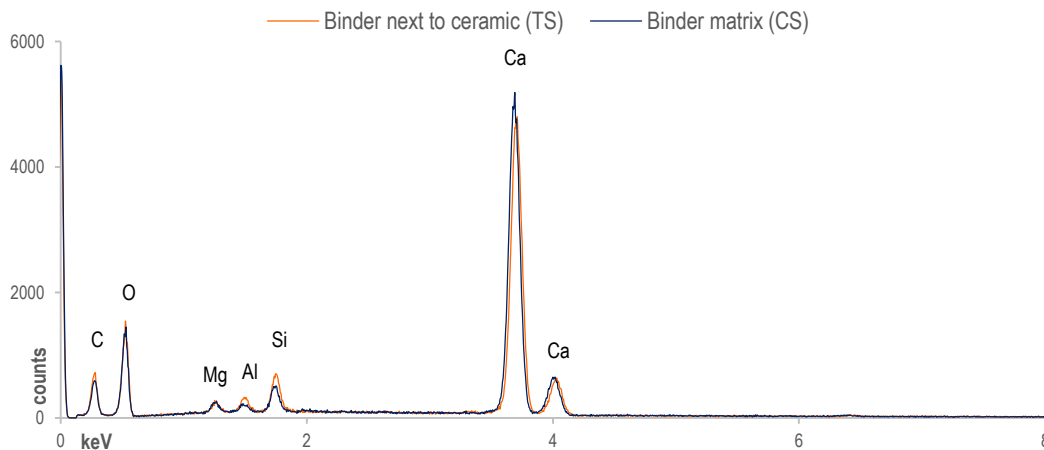


Figure 4.12. Comparison between binder composition next to ceramic in thin section (TS) from sample HHT-3 (marked in Figure 4.11.b) and binder matrix of cross section (CS) of the same sample.

Regarding the ceramic aggregates, MultiPoint analyses were performed to assess their chemical composition. Representative results indicated a fairly homogeneous composition throughout the fragments analyzed, in which Si was the dominant element present followed by Al, and Mg, K, Ca and Fe found in minor quantities (Fig. 4.13). A comparative analysis between different types of ceramics was carried out by means of MultiPoint analysis. A yellowish ceramic from the thin section of sample HHT-4 and a reddish ceramic from sample HHT-9 were examined, and the resulting spectra were plotted in Figure 4.14. Results suggest a similar chemical composition but a slight variation in Na, Mg, Si, K, Ca and Fe quantification.

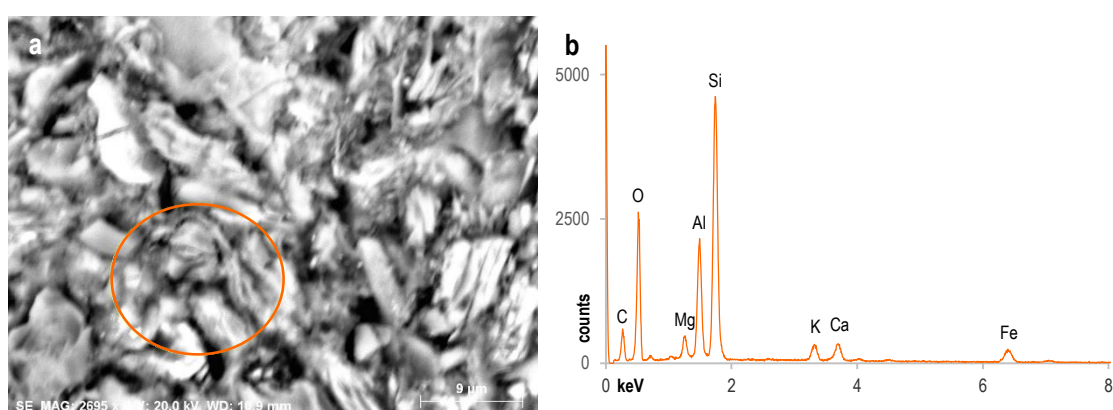


Figure 4.13. Representative multipoint analysis of a ceramic fragment performed in sample HHT-1. a) BSE image, b) spectrum of the area marked in a.

The ceramic fragment with a yellowish tone, mentioned before, displays higher amounts of Na, Si, K and Ca, whereas the reddish fragment was higher in Mg and Fe (Fig. 4.14).

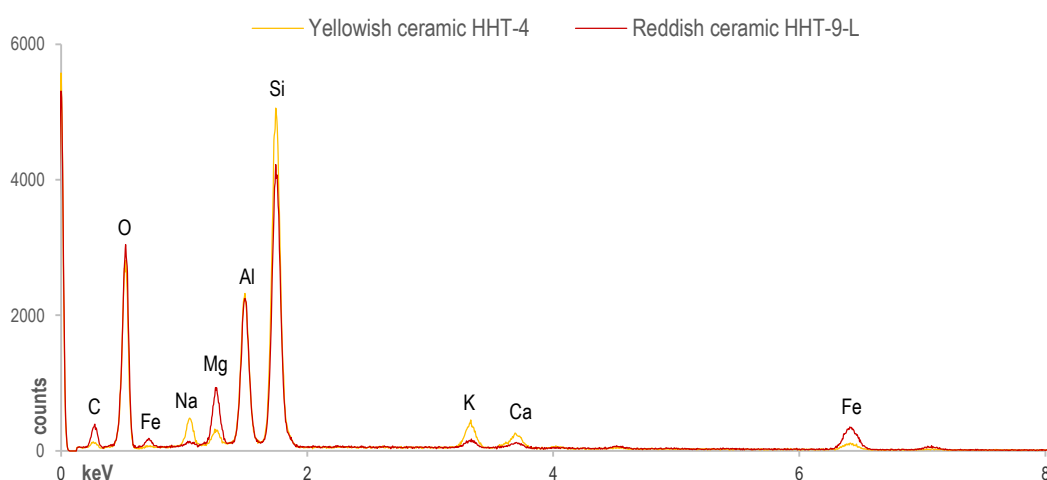


Figure 4.14. Comparison between yellowish (HHT-4) and reddish (HHT-9) ceramic fragments' composition.

The behavior of the elemental composition during the transition between ceramic aggregates and binder was examined by means of line analysis in the mortars. A representative analysis from the cross section of sample HHT-3, shown in Figure 4.15, provides us with valuable information about variations in texture and composition of the sample. Cracks surrounding the ceramic grains are manifested by the decrease in counts in the limits of the fragments. A slight decline of Si and Al can be observed in the binder area with a higher intensity in the right boundary. A contrasting behavior related to Mg and Ca was demonstrated, and both slightly increase intensities in the binder range.

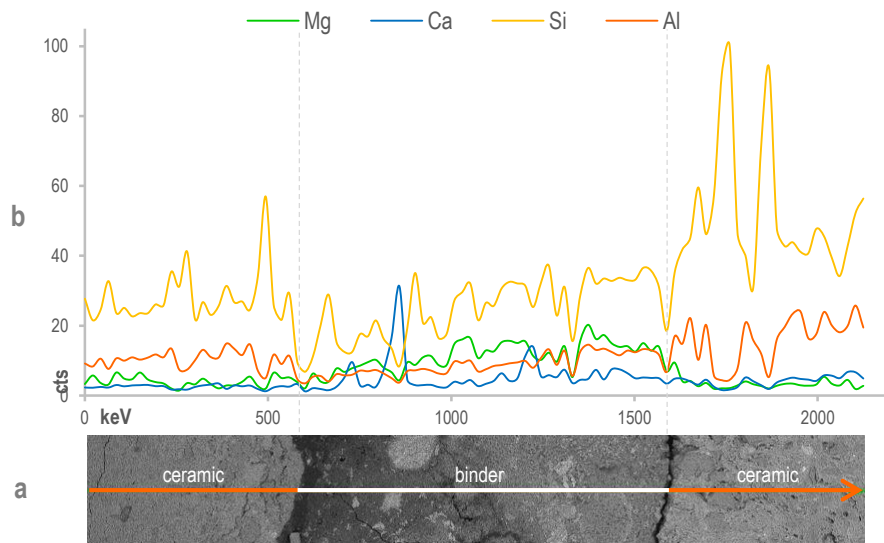


Figure 4.15. Line analysis of the elemental composition of the ceramic-binder-ceramic transition in cross section of sample HHT-3. a) BSE image and b) spectra.

Amphiboles were found in the samples with ceramic aggregates as isolated minerals in the binder (Tab 4.7.c), and point analyses were performed to examine their elemental composition. Figure 4.16 displays the representative results of the composition of an amphibole (sample HHT-2) enriched in Mg, Ca and Al. The characteristic cleavage of amphiboles at 124° and 56° can be seen in the fractures of the crystal in the Figure 4.16.a.

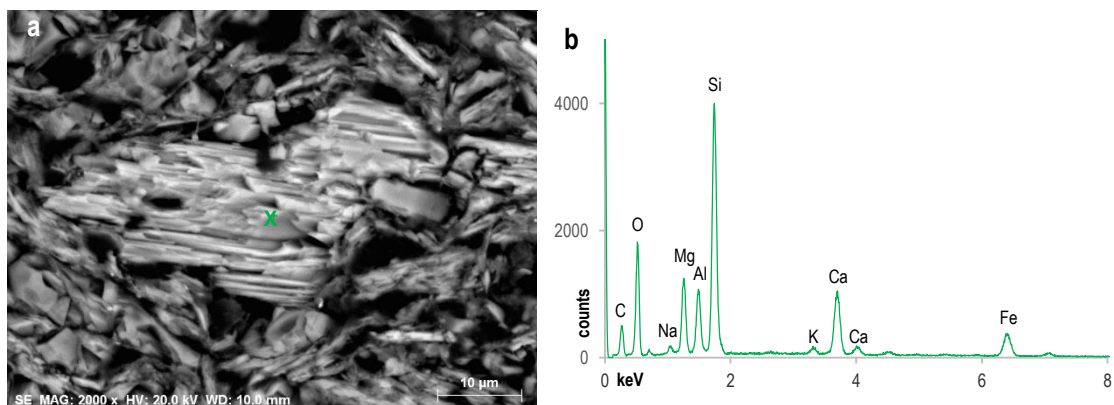


Figure 4.16. Representative point analysis of an amphibole performed in sample HHT-2 (Tab. 4.7.c). a) BSE image of amphibole, b) point analysis spectrum of the spot marked in a.

Some pyroxenes were encountered in trace amounts within the binder (Tab. 4.7.d), and their presence was confirmed by means of VP-SEM-EDS. Point analyses were performed to determine their elemental composition, and representative results from a pyroxene enriched in Mg and Ca in the sample HHT-1 are shown in Figure 4.17. The well-illustrated cleavage at $\sim 90^\circ$ BSE image (Fig. 4.17.a), as well as the lack of aluminum, displays it as a typical pyroxene and differentiates it from an amphibole.

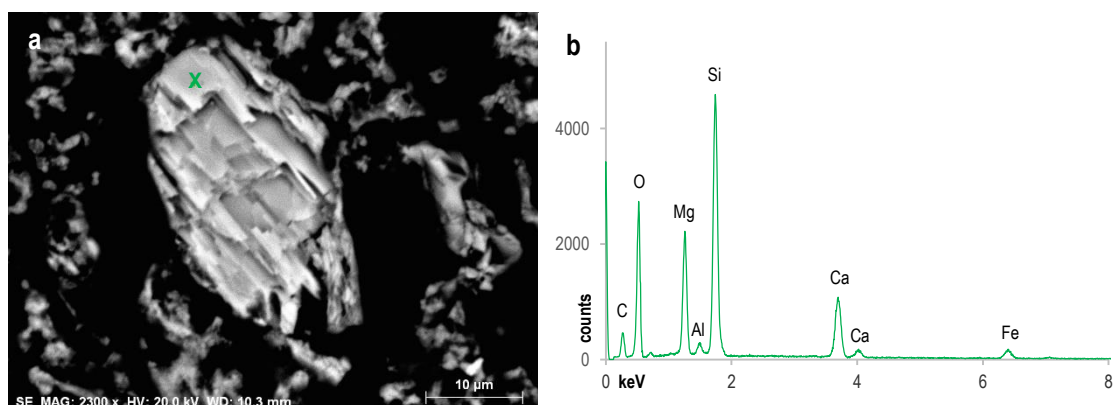


Figure 4.17. Representative point analysis of a pyroxene performed in sample HHT-1 (Tab. 4.7.d). a) BSE image of pyroxene, b) point analysis spectrum of the spot marked in a.

Alkali feldspars in the forms of orthoclase and microcline were detected in all the samples (Tab. 4.7.a). A peculiarity observed in a great amount of the orthoclases found was the intergrowth of quartz in the feldspar crystals which resulted in a graphic texture, and it is revealed by the Si (yellow v shapes) and K (pink) elemental maps in a representative feldspar crystal from a sample HHT-2 in Figure 4.18.b.

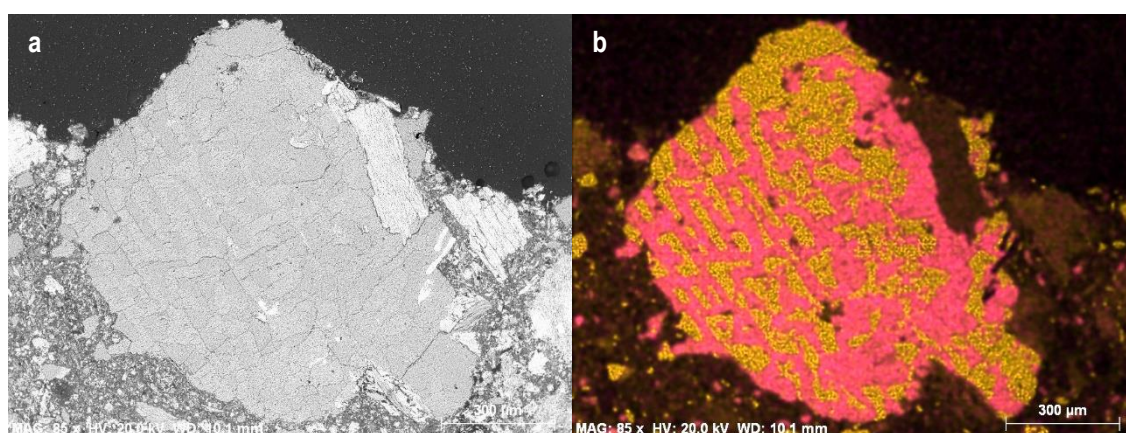


Figure 4.18. Representative elemental map of a K-feldspar with graphic texture performed in sample HHT-2 (Tab. 4.7.a). a) BSE image and b) Si (yellow) and K (pink) elemental maps.

A constant proportion in minor amounts of albite was detected by XRD throughout the samples, and a point analysis was performed in a representative crystal from the sample HHT-5 to determine its composition. The spectrum shows an enrichment of Na, Al and Si, which confirms the presence of albite (Fig. 4.19). The small amount of Ca detected confirms it is plagioclase feldspar (possibly oligoclase).

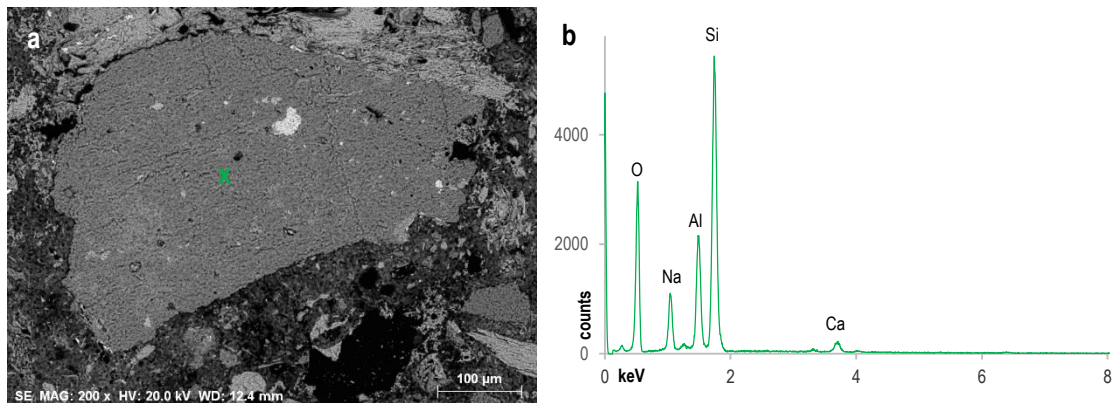


Figure 4.19. Representative point analysis of a Na plagioclase (albite) performed in sample HHT-5. a) BSE image of plagioclase grain, b) point analysis spectrum of the spot marked in a.

4.6 ACID ATTACK AND GRANULOMETRIC ANALYSIS

Acid attack analysis was performed in duplicates of the samples to determine the soluble and insoluble fractions present (Appendix 4). The soluble fraction was used to determine the proportion of calcitic binder and for comparison against other techniques such as TGA-DTG. The mean values of the soluble fractions showed percentages ranging from 22.8 to 48.4%, whereas of the insoluble vary from 51.6 to 77.4% (Fig. 4.20).

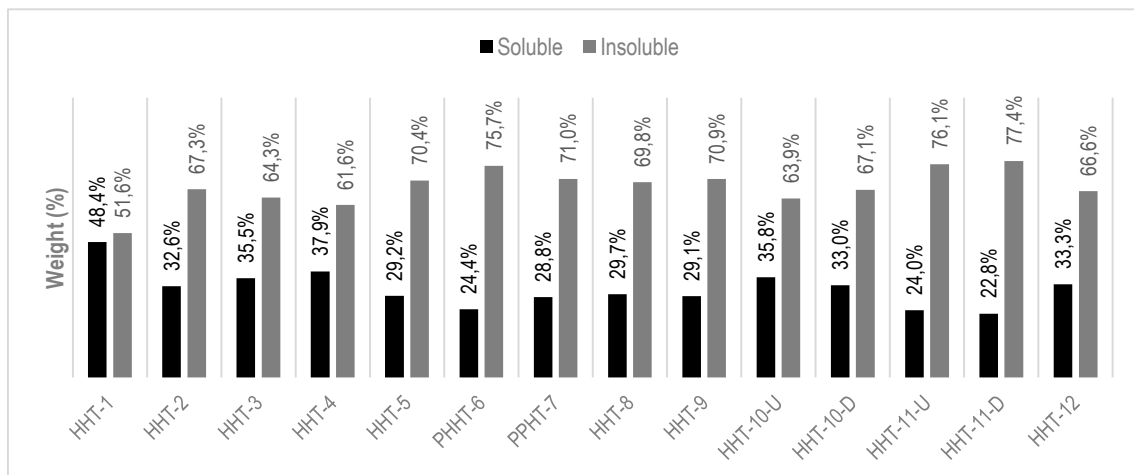


Figure 4.20. Mean values obtained from the soluble and insoluble fractions of mortars after acid dissolution.

The resulting insoluble fractions were left in an oven to dry at ~55°C, and after sieved in mesh sizes from 4 to 1/16 mm to sort the aggregates between fine gravel (above 4mm) and silt and clays (under 1/16 mm) textural groups (Wentworth, 1922).

The samples' tests HHT-1-HCI1, PHHT-7-HCI2 and HHT-12-HCI1 did not show fractions greater than 4 mm. The duplicate test did show greater fractions, indicating that they were present in the sample. Thus, the absence/lack of greater fractions can be explained either by the fact that the greater fractions were not collected during the sample preparation, or that the bigger fragments collected were mainly carbonates and were dissolved during the dissolution in acid.

The mean values of the particle size tests were calculated and plotted in Figure 4.21. Most of the samples indicate the predominance of fractions greater than 4 mm, categorized as fine gravel textural group (according to Wentworth (1922)). The second most predominant fractions correspond to very coarse sand (2-1 mm). Only one sample (HHT-10-U) demonstrates the predominance of very fine gravel (4-2 mm). In terms of the less abundant fractions, the samples show three main groups: fine gravel (greater than 4 mm), medium sand (0,5 – 0,25) and silts and clays (under 0,063 mm). Sample HHT-11-D presents less abundance of fine sand (0,25 – 0,125 mm).

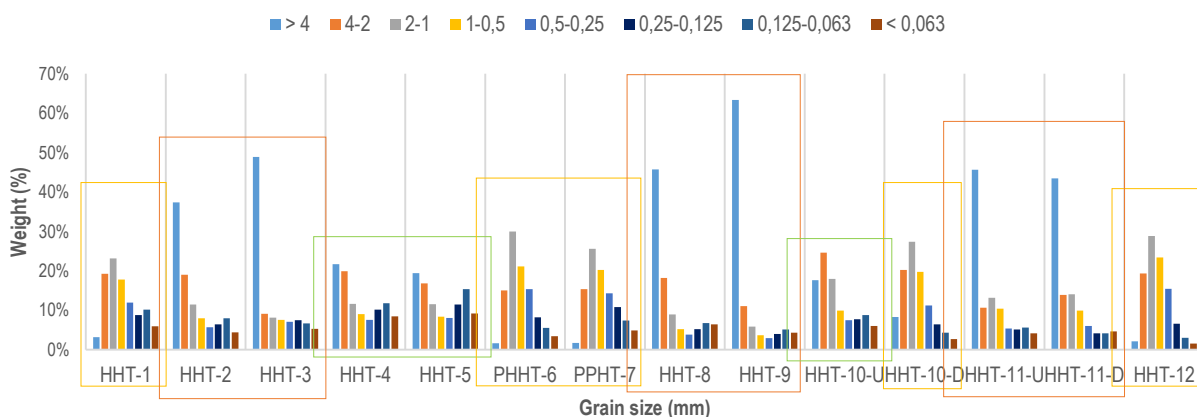


Figure 4.21. Particle size distribution of samples using the mean values. The rectangles indicate a similar distribution pattern.

The mean values of the insoluble residues were analyzed with the statistics software GRADISTAT developed by S. Blott (2010)² to determine: 1) sieving error derived from the sieving process, 2) mode, showing the predominant fractions, 3) sorting, and 4) physical description of the specific textural group they belong to (Tab. 4.11). The software uses the Udden (1914) and Wentworth (1922) particle size and textural group

² Obtained from <http://www.kpal.co.uk/gradistat.html>.

description, and provided a triangular gravel:mud:sand diagram, identifying the samples within the correspondent textural group (Fig. 4.22).

Table 4.11. Results from GRADISTAT based on Udden (1914) and Wentworth's (1922) classifications.

Sample	Sieving error	Mode	Sorting	Textural group
HHT-1	1.3%	Unimodal	Very Poorly Sorted	Gravelly Sand
HHT-2	2.2%	Unimodal	Poorly Sorted	Sandy Gravel
HHT-3	-0.5%	Unimodal	Poorly Sorted	Muddy Sandy Gravel
HHT-4	0.0%	Unimodal	Very Poorly Sorted	Muddy Sandy Gravel
HHT-5	1.1%	Unimodal	Very Poorly Sorted	Muddy Sandy Gravel
PHHT-6	0.8%	Unimodal	Poorly Sorted	Gravelly Sand
PPHT-7	0.8%	Unimodal	Poorly Sorted	Gravelly Sand
HHT-8	0.7%	Unimodal	Poorly Sorted	Muddy Sandy Gravel
HHT-9	0.5%	Unimodal	Moderately Sorted	Muddy Sandy Gravel
HHT-10-U	0.3%	Unimodal	Poorly Sorted	Muddy Sandy Gravel
HHT-10-D	0.5%	Unimodal	Poorly Sorted	Gravelly Sand
HHT-11-U	0.1%	Unimodal	Poorly Sorted	Sandy Gravel
HHT-11-D	4.2%	Unimodal	Poorly Sorted	Muddy Sandy Gravel
HHT-12	0.2%	Unimodal	Poorly Sorted	Gravelly Sand

The results from GRADISTAT determine a unimodal mode for the samples of mortars with crushed ceramics, and assign a unimodal character to those without ceramics and with chromatic layer. The mortars with ceramics were located in the muddy sandy gravel and sandy gravel textural groups (Fig. 4.22), whilst the other belong to a gravelly sand textural group. Moreover, it was also indicated that the sorting type ranges between very poorly sorted and moderately sorted.

After the granulometric analysis, the insoluble fractions were observed under the stereo microscope to analyze the different aggregates in the samples. Two main types of residues were found in accordance to the results of the statistics: the first group (and most abundant) was the one related to the mortars with ceramics. This group shows a high amount of ceramic fragments in different shades of orange to gray, and fractions greater than 0.5 mm, and some powdered ceramics in the smaller fractions. Some poorly rounded 'milky' quartz grains were observed from 4 to 1/4 mm (Tab. 4.12). The second group was related to the samples without ceramic fragments and with a chromatic layer. The predominant insoluble fraction consists of sub-angular to poorly rounded quartz from pinkish to whitish color (Tab. 4.13). Some precipitates are observed due to lack of acid dissolution of the carbonates. In samples PHHT-6 and PHHT-7, some micas are present.

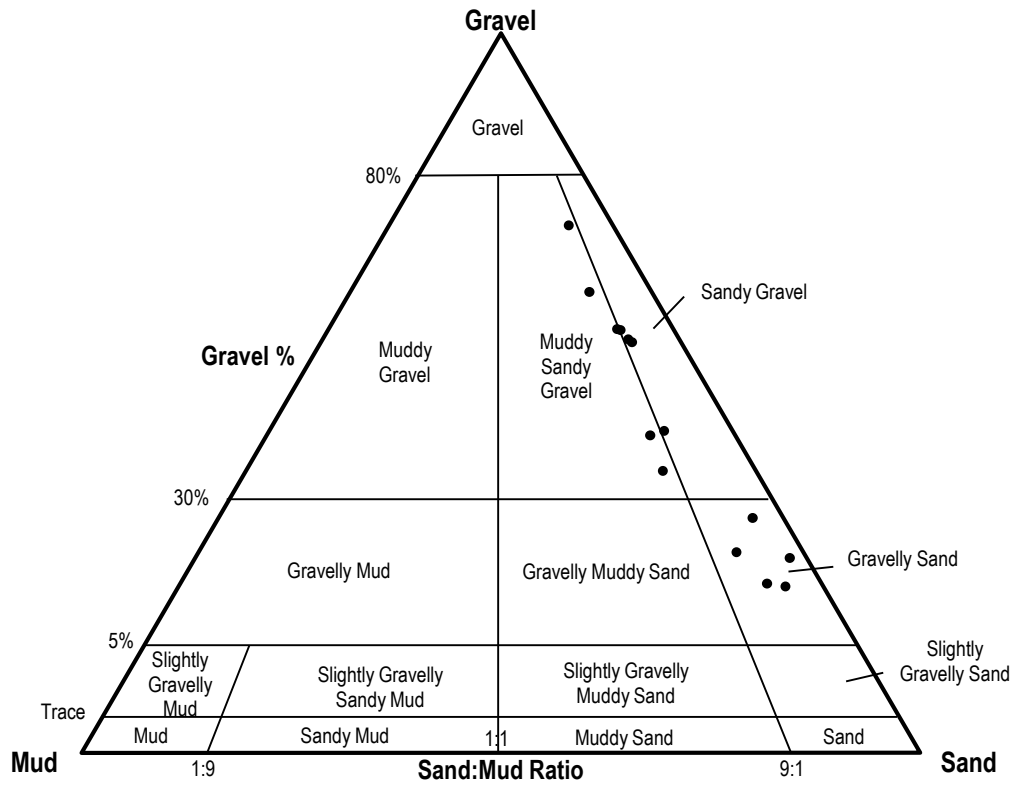










Figure 4.22. Gravel:mud:sand diagram from GRADISTAT.

Table 4.12. Representative grain fraction results of samples related to hydraulic mortars (HHT-3 test HCl2) taken from Appendix 8.

> 4mm	4-2 mm	2-1 mm
1-0.5 mm	0.5-0.25 mm	0.25-0.125 mm
0.125-0.063 mm	< 0.063 mm	

Table 4.13. Representative grain fraction results of mortar with chromatic layer (HHT-6 test HCl2) taken from Appendix 8.

		
> 4mm	4-2 mm	2-1 mm
		
1-0.5 mm	0.5-0.25 mm	0.25-0.125 mm
		
0.125-0.063 mm	< 0.063 mm	

5 DISCUSSION

The mortars obtained from the hydraulic structures of the *villa* Horta da Torre were analyzed through a multianalytical approach, and results regarding the separate components of the mortars, namely binder, aggregates and additives, and the outcomes of their interaction were obtained and confirmed by supporting techniques. Two additional samples of mortars not related to the hydraulic structures were also analyzed under the same conditions and compared to the mortars with ceramics.

The analyses performed on these samples provided information to assess the differences and similarities among the mortars related to their specific functions, namely walls, floors and mortars with a chromatic layer; and the correlation between them. Additionally, the evidence provided was discussed to assess the possible raw materials used and to formulate a hypothesis for their provenance as well as the production technologies of their manufacture process. The gathered information was discussed in order to understand whether or not ancient recipes from old roman treatises were followed in the manufacture process, or if the traditional formulae were changed and adapted either to suit a specific need or due to the availability of resources.

According to the location of the samples, their macro characteristics and their purpose (as mortars from the hydraulic structures or mortars with a chromatic layer), the samples were preliminary divided in three main groups: 1) the group comprising of samples HHT-1, HHT-4, HHT-5, HHT-10 (U+D), HHT-11 (U+D) and HHT-12, which served as wall coatings and adjacent internal layer, and are subdivided in two: a) samples with ceramic fragments and b) without ceramics; 2) the group of samples coming from the floors (HHT-2, HHT-3, HHT-8 and HHT-9); 3) and the group of samples containing a chromatic layer (PHHT-6 and PHHT-7) (Tab. 5.1).

Table 5.1. Subdivision of samples by groups used for the discussion of results.

Group 1		Group 2	Group 3
Walls		Floors	Chromatic layer
a) With ceramics	b) Without ceramics		
<ul style="list-style-type: none"> • HHT-1 • HHT-4 • HHT-5 • HHT-10-U • HHT-11-U * • HHT-11-D * 	<ul style="list-style-type: none"> • HHT-10-D • HHT-12 	<ul style="list-style-type: none"> • HHT-2 • HHT-3 • HHT-8 • HHT-9 	<ul style="list-style-type: none"> • PHHT-6 • PHHT-7

* Indicates the samples taken from a fallen structure.

5.1 RAW MATERIALS

5.1.1 Binder

Based on the results of OM, XRD, SEM and TGA, it was possible to determine that in general, the mortars are composed of a calcitic aerial binder. The predominant composition of calcite crystal phase was identified in the binder-enriched fractions in all the samples by means of powder XRD analysis. Nevertheless, the sample HHT-5 did not show an enrichment of calcite in comparison to the global fraction, having quartz as predominant phase. Additionally, sample PHHT-7 demonstrated an important amount of aragonite, a polymorph of calcite, which according to Borsoi *et al* (2019), can be attributed to the process of dissolution and re-crystallization of the calcitic binder.

Results from TGA indicate the greatest mass losses between 600-800 °C in the samples, corresponding to the characteristic range for thermal decomposition of calcite. This is consistent with the results obtained by XRD that indicate a predominance of calcite in the binder-enriched fractions. The DTG curves peaked between 750-790 °C, corresponding to a carbonate with low crystallinity, whereas well-crystallized variations peak at around 895 °C, given that the temperature of decomposition of the minerals varies in function of their crystallinity (Földvári, 2011).

The presence of some impurities within the binder is observable in the elemental maps by the increase of Mg, Al and Si (augmented in samples HHT-4 and HHT-10-D) due to the influence of various silicates. This is also confirmed by the XRD analysis of the oriented mounts for the identification of clay minerals, indicated by the presence of illite/mica in all the samples, swelling clays from the smectite group (probably montmorillonite) in some samples of the walls of group 1a and chlorite/kaolinite in some walls and floors (groups 1a, 1b and 2). Additionally, the presence of micas, feldspars, plagioclases, amphiboles and pyroxenes was also confirmed by SEM and OM.

The lime lumps observed in all the samples were analyzed by point analysis in VP-SEM-EDS to determine the purity of the limestone used for the lime manufacture and compare them against the set of samples (Bakolas *et al*, 1995; Elsen, 2006). Results indicate the generalized and abundant presence of Ca, C and O, which is interpreted as calcium carbonate (CaCO_3) and thus, a calcitic aerial lime (Fig. 5.1). This confirms previous assumptions made by XRD and TGA analysis.

The remains of small and angular calcitic grains of recrystallized limestone were visible in the samples by SEM and OM, which is consistent with their use as raw material, and

present in the vicinity of *villa* Horta da Torre. Resulting from of the above mentioned set of techniques, it can be suggested that masons used recrystallized limestone with some impurities, that probably resisted the calcination process during the lime production, agreeing with the decomposition temperatures of CaCO_3 obtained in TGA, the powder XRD results and SEM observations.

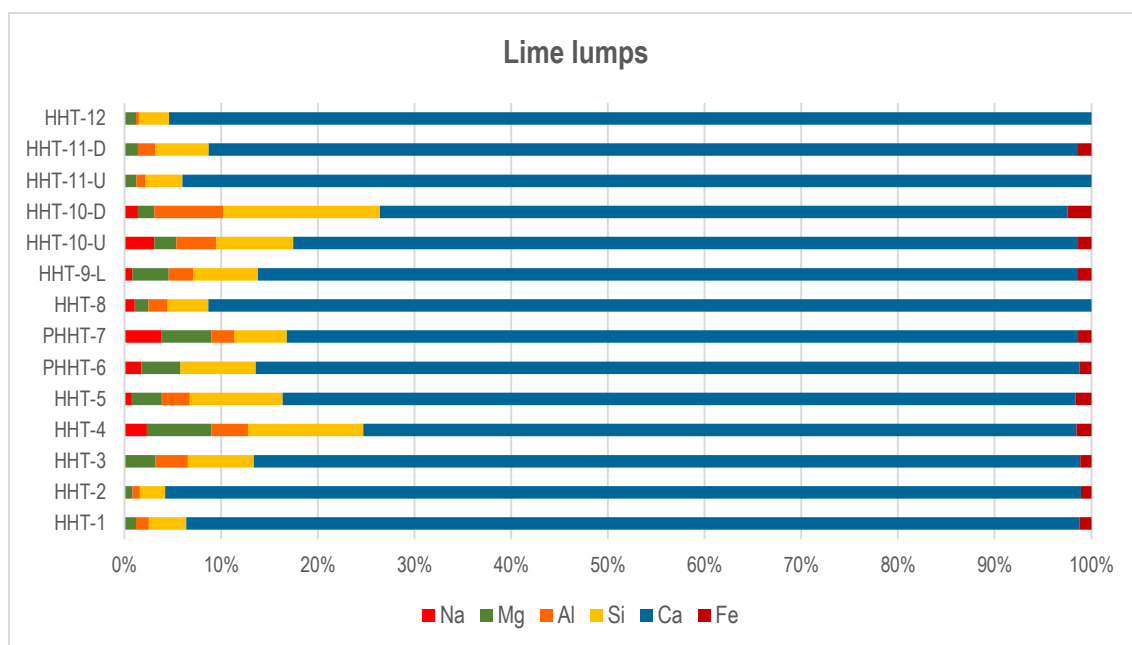


Figure 5.1. Comparison between lime lumps composition present in the samples given by point analysis in EDS.

Regarding the color of the binder and according to the microscopic observations captured in Table 4.1, the samples with a more orange-ish or light orange color are those with the presence of crushed ceramics (*cocciopesto*) as additives, and it is inferred that the pigmentation might be given by their addition to the mixture (relating the presence of hematite to the samples with ceramics of the groups 1a and 2). They also might confer to the mortars a pozzolanic character with the aim of waterproofing the coating, such as the one described by Vitruvius (Book II, Chapter VI), replacing the natural pozzolanic material of volcanic ash with powdered tiles or pottery. Nevertheless, no significant chemical and mineralogical variations were detected in the binder due to pozzolanic reactions (Fig. 4.12), such as reported in Pavía & Caro (2008). Although the high values of the soluble fraction can be attributed to neoformation products derived from pozzolanic reactions (Cardoso *et al*, 2014), these amorphous mineralogical phases are not detected by XRD, but are evident when compared with the percentage of CaCO_3 in the samples by means of TGA.

5.1.2 Aggregates

In terms of aggregates and their composition, and based on the results of the techniques employed, mortars with predominance of ceramic fragments and mortars without ceramics but with a predominance of quartz sand, were identified. The samples with ceramics are those corresponding to the layers in contact with water (groups 1a and 2), and the presence of these aggregates grants them a hydraulic character, whereas the samples lacking ceramics were those with a chromatic layer (group 3), and the preparatory mortars of the walls adjacent to the layer with ceramics (group 1b).

The presence of quartz sand from sub-angular to poorly rounded grains was verified by several techniques in all the samples, making it a common aggregate amongst them, regardless of the presence or absence of ceramic fragments. Some observations regarding the percentage of the aggregates within the samples were made during microscopic analysis of the cross sections (Tab. 4.3), and the approximate percentage of ceramic fragments and quartz sand aggregates was established to make a comparison within each sample. A relationship between both types of aggregates was observed, and it was determined that the samples with a greater amount of ceramics, have a smaller percentage of quartz sand. According to stereozoom and petrographic observations, the average amount of quartz aggregates present in the samples without ceramics is relatively close to the percentage of the sum of the ceramic and quartz aggregates of the samples with ceramics. It can be suggested that regardless of the type of aggregate, more or less the same proportion was used for mortars related to the hydraulic structures as for those with chromatic layers and adjacent internal mortars of the walls. This assumption was confirmed by the resulting insoluble residue after the acid dissolution of the bulk samples (Fig. 4.20), in which the same proportion of insoluble residue is maintained throughout the samples (except for sample HHT-1, which demonstrate almost the same amount of soluble fraction and insoluble residue).

The stereozoom observations of the insoluble residue and their grain size distribution (Appendix 8) allowed for the recognition of three patterns of particle size distribution (Fig. 4.21). The first pattern is recognized in the samples from the groups 1a and 3, which are the samples with chromatic layers (PHHT-6 and PHHT-7) and without ceramics (HHT-10-D and HHT-12); additionally, the sample HHT-1 from group 1a also presents the same pattern, although it was taken from the coating layer of the double apse. This pattern is characterized by the predominance of very coarse sand and smaller fractions (<2mm), composed mainly of granitic aggregates, quartz, K-feldspars, micas (mainly biotite), sandstone, and a low percentage of fragments greater than 4 mm. These

samples were also described as “unimodal” and belonging to the “gravelly sand” textural group according to the Wentworth’s classification (Wentworth, 1922). Nevertheless, regardless of the grain size distribution, sample HHT-1 shows a different composition and is categorized as unimodal. It is predominated by ceramic fragments, sandstones and powdered ceramics, whereas quartz grains, micas and feldspars are seen in smaller proportions and in smaller grain sizes (<1mm). A predominant quartz mineral phase, and K-feldspars, albite, and micas in minor amounts in the global fractions (GF) of the samples were confirmed by powder XRD analysis. The particle size distribution of the aggregates of sample HHT-1 can be related to the thickness of the coating layer employed in the double apse, which was about 10-20 mm, not allowing for the presence of big aggregates within the mixture due to practical purposes.

The second pattern observed by granulometric analysis and stereozoom is present in the group 2 of samples from the floors (HHT-2, HHT-3, HHT-8 and HHT-9), and in the samples HHT-11-U and HHT-11-D from the fallen structure of the tank 3 (group 1a). These samples show a clear predominance of ceramic grains greater than 4 mm, and a granitic mineralogy, with a small percentage of quartz (transparent and milky), micas and alkaline feldspar grains in the fractions below 4 mm. It can be suggested that the increase of ceramic fragments in these samples is related to the purpose of the mortars, which needed to be very well waterproofed and with greater hydraulicity to perform as such. Some doubts regarding the samples of the group 1a of the fallen structure (HHT-11-U and HHT-11-D) were developed due to their composition and aggregates. If compared with the other samples of the standing walls of the tank 3, they seem mismatched in terms of aggregates composition, although they show very similar characteristics with the mortars sampled from the floors (group 2). The predominance of quartz as main mineral phase was verified by means of powder XRD analysis in the GF, followed by micas and K-feldspars in major amounts, and calcite, albite, amphiboles and chlorite in minor proportions.

The third distribution pattern is recognized in the samples of the walls of group 1a (HHT-4, HHT-5 and HHT-10-U). This set of samples contains the most homogeneous composition, and is slightly predominated by >2 mm grains. The bigger fractions are conformed by ceramics with different colors (as shown in the cross sections in Tab. 4.3), quartz and some sandstones, and the smaller fractions show a mixture of ceramics, quartz, feldspars and sandstones. The presence of K-feldspars, Na-plagioclase and micas was confirmed by means of powder XRD performed in the global fractions of the samples, and are present in minor amounts whilst amphiboles in major proportions. Quartz was detected as the predominant crystal phase by means of XRD and K-

feldspars, albite, micas and amphiboles in minor abundance. Additionally, the presence of K-feldspars (orthoclase and microcline), albite, micas (biotite) and amphiboles (hornblende) was confirmed by means of petrography. Some pyroxenes and olivine were observed in the petrographic microscope and the presence of pyroxenes was confirmed by means of SEM.

Amphiboles and hematite crystal phases were only detected in trace or minor amounts by XRD in the samples containing ceramic fragments. According to Ion *et al.* (2016), the presence of hematite could be associated with the red pigmentation of the ceramics. In the case of the ceramics with a dark color, it was determined by VP-SEM-EDS that they have very similar elemental compositions to the reddish ceramics, and the color might only be given by the oxidation-reduction reaction of the iron oxides during the firing. Nevertheless, the comparison between a yellowish and a reddish ceramic fragment performed (Fig. 4.14) shows some variations in Na, Si, K and Fe composition, associating the increase of Fe to the reddish characteristic color.

The “zoning” identified around the ceramic fragments exhibit color and textural variations through OM (Tab. 4.2), and it was verified by means of VP-SEM-EDS (Fig. 4.11.a). The elemental map of the zoned areas displayed a C enrichment in the outermost part of the fragment, probably influenced by the resin used during the impregnation that filled the existing gaps within the cracks and the limits of the ceramic fragment (Fig. 4.11.b). Point analyses were performed in the outer and innermost parts the ceramic fragments to compare their elemental composition. No changes besides the C enrichment were observed, suggesting that no pozzolanic reactions are occurring. This is consistent with the results obtained from the comparison of the elemental composition of the binder adjacent to the zoned fragment and a regular binder.

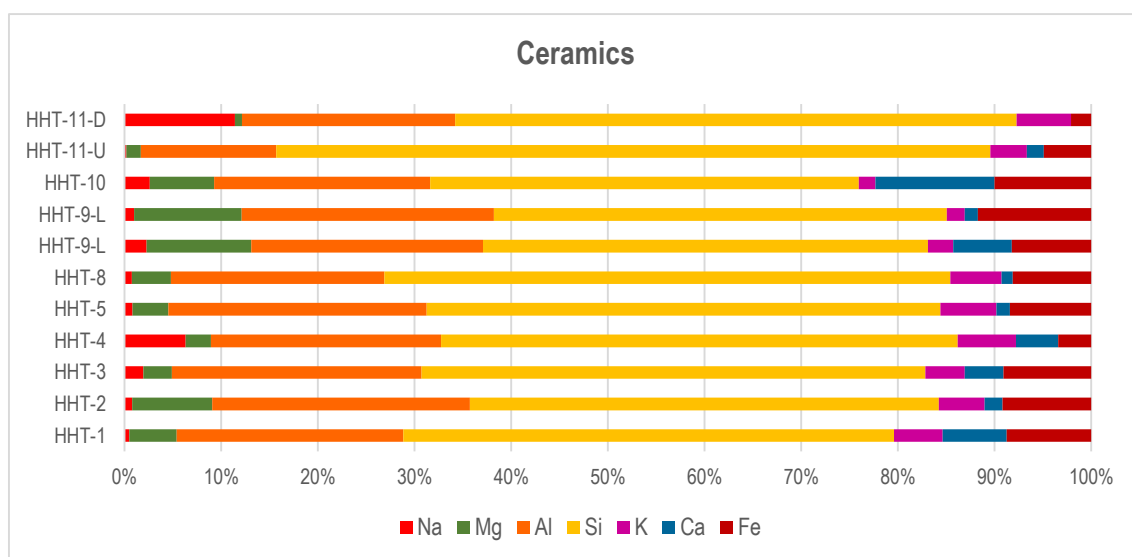


Figure 5.2. Comparison between ceramics composition of the samples by multipoint analysis in EDS.

As a result of the elemental analyses performed by VP-SEM-EDS in the different types of ceramics, it could be implied that most of the fragments have quite a similar composition with slight variations in Na, Mg, Ca and Fe amounts, probably due to the influence of the accessory minerals embedded in the grains (Fig. 5.2).

5.2 PROVENANCE

For the provenance analysis of this set of samples, the mineralogical data obtained was considered within the geological context of the *villa* Horta da Torre and its surroundings, as well as with the recommendations given by Vitruvius regarding the selection and sources of the raw materials used for binder and aggregates.

Based on the previously discussed binder composition results, that indicate the use of a calcitic aerial lime for the binder preparation, it is assumed that a sedimentary rock such as limestone was used. The binder shows impurities in the matrix, supported by the results obtained from powder XRD analysis in the binder-enriched fraction, petrography and VP-SEM-EDS. This can be attributed to the presence of some phyllosilicates, and it is reflected in the variations of Na, Mg, Al, Fe and Si percentages in the elemental composition of lime lumps (Fig. 5.1). It can be suggested that the limestone was very likely to have been quarried from the geological unit located in the vicinity in a <1km radius, which consists of crystalline limestones with some recrystallizations (Fig. 2.6). Furthermore, some fairly angular grains of calcite were also identified within the binder of some samples from the floors (group 2) and with a chromatic layer (group 3) by petrography (Tab. 4.7.b) and SEM (Fig. 4.9), which agrees with the identification as recrystallized limestone.

In terms of aggregates, Vitruvius recommends in his treatise (Book II, Chapter IV) the use of sand freshly taken from sandpits, river-beds, gravel or sea as aggregates. Nevertheless, Vitruvius discards river sand for the fabrication of *signinum* due to its thinness (Morgan, 1914). In all the samples, quartz was identified by most of the analytical techniques as the major compound related to the aggregates, either as quartz sand or ceramic fragments.

The quartz grains in all the samples range from sub-angular to poorly rounded, which implies a fairly local provenance and a reduced transportation from the geological source. A big proportion of alkali feldspars with a sub-angular shape were also identified in the samples. They display a graphic texture, given by the intergrowth of quartz (Fig. 4.18.b). Some sub-angular and poorly rounded grains of microclines, Na-plagioclase and

micas (muscovite and biotite) were also identified in most of the samples by means of petrography and validated by XRD. It can be assumed that all these minerals have a granitic character, and they could have come from a medium to short distance, probably from the weathering of the calc-alkaline to alkaline granitic intrusion which outcrops around 4 km to the south-west of the site.

Some isolated iron-magnesium minerals such as pyroxenes, amphiboles and olivine were identified in trace amounts within the binder of the samples related to the hydraulic structures. As these minerals are rather easily weathered, their preservation might indicate a fairly close geological provenance. It might suggest that these aggregates could be related to the Alter do Chão ultrabasic intrusion of igneous mafic gabbros, which outcrops between 1-3 km to the NE. Besides the binder, these minerals are also present in higher amounts within the matrix of the ceramics. Their occurrence in some of the ceramic fragments could also indicate a local production, consistent with the concentration of ceramics for construction found in the neighboring areas of the buildings (Carneiro, 2019b). Previous studies indicated the presence of imported fine ceramics, but their use for construction purposes is not referred to in literature (Carneiro, 2019b). It is not clear if the existence of these isolated iron-magnesium minerals within the binder is directly related to the presence of ceramics in the samples, and if they are a consequence of the detachment during the mixing of the raw materials in the mortar preparation.

Some samples show the presence of poorly rounded grains (HHT-11-D), but also rather elongated and rectangular (HHT-2) within the ceramic fragments. It can be suggested that for the production of the ceramics, potters might have taken either materials coming from the shists occurrence located 7 km to the NE of the site and probably transported by the waterlines, or most probably from the immediate surrounding vicinity of the *villa*.

5.3 PRODUCTION TECHNOLOGY

It is assumed that roman masons should have followed certain guidelines for the construction of their sites, and fortunately recipes from roman treatises have been preserved until today, giving an idea of the selection of materials, the technological knowledge and building practices of the time, making possible the comparison of the composition of the conserved structures against these recommendations.

Two main features were studied for the assessment of the production technologies of the mortars. The Jedrzejewska method (2014) was employed to define the binder to

aggregate ratios based on the soluble and insoluble fractions obtained after acid dissolution and the proportion of carbonates determined by TGA analysis (Jedrzejewska, 2014). The second analyzed feature was the hydraulicity of the mortars based on the mass losses in the samples from the structurally bound water and the carbon dioxide calculated from the TGA results.

As it was mentioned previously in the chapter 1.2.1, Vitruvius suggests in his treatise different binder to aggregate proportions based on the types of sand used. In the case of using pit sand, three parts should be added together with one of lime; two parts of sand and one of lime in the case of river or sea-sand, and for a “better composition”, a third part of sieved powdered brick can be added (Book II, Chapter V, Vitruvius). Additionally, he recommends the aging of the slaked lime to obtain a better mixture.

The results from the dissolution in acid and TGA were analyzed and plotted in Table 5.2, in which the aggregates and binder percentages were calculated to obtain the binder to aggregate ratios employed in the samples from the *villa*. The ratios obtained demonstrated huge differences amongst the samples, from the “ideal proportions” proposed by Vitruvius (1:3) and lower (1:2), up to 1:9 ratios.

No discernable pattern could be identified by the comparison of the binder to aggregate ratios obtained by this method and although results were inconclusive, some assumptions could be made. The samples with the lowest 1:2 ratios (HHT-1 and HHT-12) demonstrated similarities regarding their grain size distribution, though sample HHT-1 was obtained from a waterproof coating mortar from the double apse and contains ceramic fragments and powder, whilst sample HHT-12 was not in contact with water and does not contain ceramics. The samples with the highest ratios (HHT-3 with 1:8, HHT-8 1:6 and HHT-11-D 1:9 ratios) contain the smallest binder percentage and have the same particle size distribution, with predominance of big ceramic fragments. Sample HHT-3 was collected from the floor of the “Y” channel, sample HHT-8 from the garden water mirror floor and sample HHT-11-D from the lower layer of a fallen structure of the tank 3. The rest of the samples show binder to aggregate ratios ranging from 1:3 to 1:5, and they do not share very common characteristics regarding their physical and mineralogical composition, particle size distribution nor function.

The high ratios obtained can be the result of the increased percentage of crushed ceramic additives added to the mixture of the binder and counted as part of the insoluble fraction. Nevertheless, this explanation could only be applicable to the samples related to the hydraulic structures from the groups 1a and 2. The inaccuracy of the proportions of aggregates added to the mixture can also be due to the inaccessibility to traditional recipes and a construction based on empiric and intuitive knowledge and a “trial and

error” practice or the result of an inexperienced laborer. The remoteness of this rural environment might have influenced in the lack of qualified masons, who were most likely to live in the bigger cities. There, the construction methods would have been more faithful to the traditional recipes given in roman treatises, and as an example, it was demonstrated in previous works from the roman site of Pisões that the Vitruvian rules for mortars were followed, and brick fragments were also included to increase the water retention and form pozzolanic products (Borsoi *et al*, 2019).

Table 5.2. Sample composition (mass %) and binder to aggregate ratio.

Sample	Aggregate		Total aggregates %	Binder	Binder to aggregate ratio ⁴
	Soluble fraction % ¹	Insoluble residue % ²		Carbonates % ³	
HHT-1	14.8	51.6	66.4	33.6	"1:2"
HHT-2	13.0	67.3	80.3	19.7	"1:4"
HHT-3	24.1	64.3	88.4	11.6	"1:8"
HHT-4	17.1	61.6	78.7	21.3	"1:4"
HHT-5	11.9	70.4	82.3	17.7	"1:5"
PHHT-6	2.7	75.7	78.4	21.6	"1:4"
PPHT-7	4.0	71.0	75.0	25.0	"1:3"
HHT-8	15.0	69.8	84.8	15.2	"1:6"
HHT-9	7.7	70.9	78.6	21.4	"1:4"
HHT-10-U	13.0	63.9	76.9	23.1	"1:3"
HHT-10-D	9.8	67.1	76.9	23.1	"1:3"
HHT-11-U	-4.6*	76.2	71.6	28.4	"1:3"
HHT-11-D	12.0	77.4	89.4	10.6	"1:9"
HHT-12	1.8	66.6	68.4	31.6	"1:2"

¹ Soluble fraction = 100 - Σ (insoluble residue + carbonates)

² Insoluble residue in hydrochloric acid

³ Calculated from CaCO₃ content (by TGA analysis)

⁴ Binder (considered to be the carbonate fraction) and aggregate (sand + soluble fraction)

* The negative value can be due to the heterogeneity of the samples obtained for both analyses.

The hydraulicity of the mortars was calculated with the CO₂ to structurally bound water ratio in relation to CO₂ (obtained with the percentage of weight loss by means of TGA) (Tab. 5.3). The hydraulicity of different types of mortars has been studied (Moropoulou *et al*, 2005), and it was determined that the “inverse trend of hydraulicity of mortars is being augmented exponentially with CO₂”, in which the lower the ratio is, the higher the hydraulicity.

Results suggest that there are two discernable assemblages of samples according to their hydraulicity index (HI) (Tab. 5.3) and the relationship between CO₂ to structurally

bound water ratio in versus the CO₂ mass losses (Fig. 5.3). The samples with the lowest CO₂% mass losses and a lower HI index (Fig. 5.3, pink), correspond to samples of the group 1a (HHT-4, HHT-5, HHT-10U and HHT-11-D) and the floors (group 2, except sample HHT-9). They display the highest binder to aggregate ratios ranging from 1:3 to 1:9, and have a similar particle size distribution dominated by ceramic fragments greater than 2mm. This set of samples hold the highest hydraulicity character, which is compatible with the fact that it is a necessary intrinsic characteristic for mortars that are employed for flooring purposes and contention walls in the hydraulic structures. These results are in agreement with the results obtained for the granulometric evaluation of the mortars of the roman site of *Pisões* (Borsoi *et al*, 2019).

The other identified cluster (Fig. 5.3, purple), includes all the samples without ceramic aggregates (groups 1b and 3 of walls and chromatic layer), and samples HHT-9 and HHT-11-U from the floor of the water mirror and a fallen structure (with ceramics). These samples have a higher HI index and therefore, lower hydraulicity. The samples absent of ceramics and the sample HHT-1 (with ceramics) share the same particle size distribution group dominated by quartz sand between 2-1 mm. They also share the lowest binder to aggregate ratios (1:2 and 1:4), and have a relatively high CO₂/H₂O ratio due to the increased CO₂%. In the other hand, the samples HHT-9 and HHT-11-U (from the water mirror (group 2) and the fallen structure of tank 3 (group 1a)) show a low HI index, but their low binder to aggregate ratios (1:3 and 1:4) directly related to their high CO₂% and their low percentage of structurally bound water, locate them far away from the other samples with ceramic aggregates in the chart, discarding a direct correlation with the samples related to the hydraulic structures of the first two groups with lower CO₂/H₂O ratios. Although their hydraulicity differs in comparison to the first cluster, they share common aggregates distribution, dominated by ceramic fragments above 4mm.

It can be concluded that most of the samples related to the hydraulic structures demonstrate very similar characteristics in terms of aggregates composition, particle size distribution, binder to aggregate ratios and hydraulicity, although some exceptions were found. The same is applied to the samples without any hydraulic character.

It is important to draw attention to the additional factor of the presence of lime lumps in the samples, given that they can be partly attributed to the manufacturing technologies (Bakolas *et al*, 1995; Elsen 2006). Two hypotheses mentioned in Bakolas *et al* (1995) lead to the assumption that lime lumps can be present due to their preexistence in the mixture as slaked lime during the production, and they were not properly mixed with the inert; or that the lime was used right after the slaking without the 2-years aging period (as recommended by Vitruvius), which prevented the growth of portlandite crystals. This,

together with a lack of water, it became difficult to mix lime and inert (Bakolas *et al*, 1995), stimulating the formation of cracks due to shrinkage while hardening.

Table 5.3. Weight loss percentages of structurally bound water in the temperature range 200-600 °C, and CO₂ (600-900 °C) taken from Appendix 6 to calculate their ratio and the hydraulicity index (HI) of the mortars.

Sample	H ₂ O %	CO ₂ %	CO ₂ /H ₂ O	HI
HHT-1	3.00	14.8	4.9	3.0
HHT-2	2.28	8.7	3.8	2.3
HHT-3	1.57	5.1	3.3	1.6
HHT-4	3.02	9.4	3.1	3.0
HHT-5	2.18	7.8	3.6	2.2
PHHT-6	1.67	9.5	5.7	1.7
PHHT-7	2.29	11.0	4.8	2.3
HHT-8	2.77	6.7	2.4	2.8
HHT-9	1.39	9.4	6.8	1.4
HHT-10-U	2.95	10.2	3.4	3.0
HHT-10-D	1.95	10.2	5.2	2.0
HHT-11-U	1.94	12.5	6.4	1.9
HHT-11-D	1.72	4.7	2.7	1.7
HHT-12	2.97	13.9	4.7	3.0

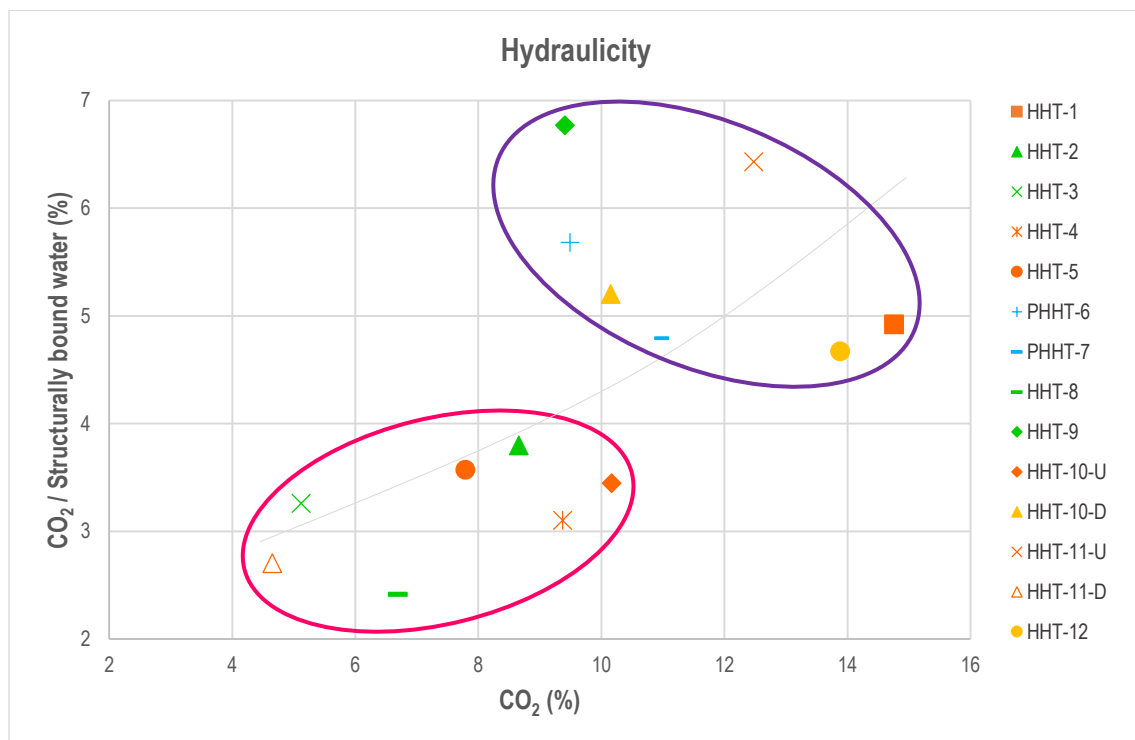


Figure 5.3. CO₂ to structurally bound water ratio in relation to CO₂%. Group 1a=orange; group 1b=yellow; group 2=green; group 3=blue.

6 CONCLUSIONS

This research aimed to carry out the chemical, mineralogical and microstructural characterization of the mortars related to the hydraulic structures from the excavated *pars urbana* of the *villa* Horta da Torre, located in the municipality of Fronteira, Portugal, in order to provide evidence for the assessment of the raw materials used for their manufacture, as well as their provenance, and to establish a chronology amongst the structures. Moreover, valuable information concerning their production techniques was obtained and contrasted with the ancient recipes given by Vitruvius, which can be used for a future outlook with a view to their consolidation and repair.

To achieve this, ten samples were collected from the walls and floors of the tanks, the double apse and the *triclinium*. Additionally, two samples with a chromatic layer were also analyzed and compared against those of the hydraulic structures. A multianalytical approach was required to conduct a complete and more accurate characterization. The samples were analyzed by means of Optical Microscopy (Stereozoom and Petrographic microscope), X-ray Diffraction (XRD, Powder XRD), Variable Pressure Scanning Electron Microscopy coupled to Energy Dispersive X-ray Spectroscopy (VP-SEM-EDS) and Thermogravimetric analysis (TGA-DTG). Acid attack and Granulometric analysis were also performed to determine the binder to aggregate ratios of the mortars, as well as the particle size distribution of the insoluble residue and to hypothesize on the production techniques employed in the mortars' manufacture.

The studied samples were divided in three main groups: 1) wall coatings, subdivided according to their aggregates in a) mortars with ceramics, and b) mortars without ceramics; 2) floors, and 3) mortars with a chromatic layer. The characterization of the materials demonstrates a rather similar composition between every group of samples. Furthermore, an evident similarity between the samples with ceramics was observed, as well as between the samples without ceramics.

In terms of raw materials used in the binder, all the samples proved to be made of a calcitic aerial lime, very likely to be obtained from the calcination of recrystallized limestone. Small angular grains of calcite were also evident within the mixture, that probably resisted the calcination process. Additionally, some impurities were also detected, probably due to the influence of phyllosilicates within this lithology. It is suggested that the raw materials for the binder were quarried from the vicinity (less than a 1 km radius).

The samples showed different aggregate composition. The samples from the groups 1a and 2, used for wall coatings and flooring, show a clear predominance of ceramic fragments, followed by sub-angular to poorly rounded aggregates of a granitic mineralogy (alkaline-feldspars and quartz) and powdered ceramics additives. In comparison, the samples from groups 1b and 3 demonstrate similar granitic aggregates, some rounded metagraywackes grains and predominance of sub-angular quartz grains. These aggregates could have come from the calc-alkaline to alkaline granitic intrusion (Fronreira massif) which outcrops approximately 4 km to the south-west of the site. No “marble chips” were identified within the samples from the group 3 with a chromatic layer, which suggests that Vitruvius’s rules for preparative layers’ production were not followed and siliceous aggregates were used instead.

Some mafic iron-magnesium minerals were mostly associated with the ceramics. Nevertheless, they were also found as isolated crystals within the binder of the samples related to the hydraulic structures. Their presence indicates a relatively close geological provenance and local production, and can be related to the Alter do Chão ultrabasic intrusion of igneous mafic gabbros, outcropping between 1-3 km to the NE of the *villa*. The data acquired was insufficient to determine if these minerals appear in the binder as a consequence of the detachment during the mixing process in the mortars’ preparation. In the case of their provenance, a concentration of local ceramics for construction was found in the neighboring areas of the buildings that could have been used for the mortars production.

Regarding the assessment of the production technologies for the mortars’ manufacture, it was possible to confirm that only four samples (PHHT-7, HHT-10-U, HHT-10-D and HHT-11-U) were made with the binder to aggregate ratios recommended by Vitruvius (1:3). For the rest of the samples, arbitrary ratios were obtained. The samples related to the floors (group 2) showed a small proportion of calcitic binder, displaying high ratios (1:4-1:9), while the ratios of the samples from the walls (group 1) and chromatic layer (group 3) vary from 1:2 to 1:5.

In terms of hydraulicity, although all the samples show a similar level of hydraulicity, two principal patterns could be observed. Most of the samples from the floors and walls with ceramic aggregates (groups 1a and 2) have a higher hydraulicity and higher binder to aggregate ratio in comparison with the samples without ceramics (groups 1b and 3). It can be determined that samples with lower binder to aggregate ratios display a lower hydraulic character, whereas the samples with a large percentage of ceramic aggregates enhance their hydraulicity. It is also suggested that the hydraulicity character is conferred by the addition of artificial pozzolans, such as crushed ceramics.

It is important to draw attention to the samples HHT-11-U and HHT-11-D, taken from the fallen structure of the tank 3, which were supposed to belong to a third wall of the tank. When compared to the samples taken from the preserved walls, they seem to mismatch in terms of composition, for instance, the internal adjacent layer of the standing walls does not include ceramics in their composition. Nevertheless, these samples share more similarities with the analyzed samples of the floors regarding their aggregate characteristics, their binder to aggregate ratio, particle size distribution and hydraulicity. It is possible to assume that the structure is not from collapsed wall, but in fact it probably belongs to the floor of the tank and it was relocated as a result of the agricultural practices carried out in the site before its discovery.

Finally, it can be concluded that the mortars studied present a remarkable uniformity in terms of chemical, mineralogical and microstructural composition and according to their architectural purpose. There are no variations suggesting a different chronology of their manufacture, so it is assumed that they may be contemporaneous. In terms of production, it is evident that the Vitruvius rules were not followed. It can be implied that masons would have been familiar with the ancient recipes for construction, given the fact that homogeneous mixtures of the traditional materials used were employed for every specific purpose, but this knowledge was always linked to their intuition and availability of materials.

The *pars rustica* of *villa* Horta da Torre located to the South of the *pars urbana* still remains buried, and future works will probably be carried out with aims of its characterization and restoration. The data obtained in this thesis will be useful as reference for future analyses, as well as to gather the necessary information for the consolidation and the production of compatible repair materials of the mortars here studied.

BIBLIOGRAPHY

- Almeida, M., Carneiro, A., Rodríguez, F., & Morgado, P. (2011). De Augusta Emerita a Olisipo: proposta de traçado para o primeiro troço da via XII do Itinerário de Antonino. *Arqueologia do Norte Alentejano – Comunicações das 3.as Jornadas, Lisboa*, 193-201.
- Artoli, G. (2010). *Scientific methods and cultural heritage. An introduction to the application of materials sciences to archaeometry and conservation science*. New York, US: Oxford University Press.
- Bakolas, A., Biscontin, G., Moropoulou, A., & Zendri, E. (1995). Characterization of the lumps in the mortars of historic masonry. *Thermochimica Acta* 269/270, 809-816.
- Barker, A. (2014). *A Key for Identification of Rock-forming Minerals in Thin-Section*. University of Southampton, UK: CRC Press.
- Barton, C., & Karathanasis, A. (2002). Clay minerals. Em *Encyclopedia of Soil Science* (pp. 187-192). Marcel Dekker, Inc.
- Borsoi, G., Santos Silva, A., Menezes, P., Candeias, A., & Mirão, J. (2019). Analytical characterization of ancient mortars from the archaeological roman site of Pisões (Beja, Portugal). *Construction and Building Materials* 204, 597–608.
- Cardoso, I., Macedo, M. F., Vermeulen, F., Corsi, C., Santos Silva, A., Rosado, L., . . . Mirao, J. (2014). A multidisciplinary approach to the study of archaeological mortars from the town of Ammaia in the roman province of Lusitana (Portugal). *Archaeometry* 56, 1-24.
- Cardoso, J., de Carvalho Quintela, A., & de Mascarenhas, J. (1997). *Portugal Romano. A exploração dos Recursos Naturais*. Museu Nacional de Arqueologia.
- Carneiro, A. (2014). OTIVM, materialidade e paisagem nas villae do Alto Alentejo português em época romana. *Espacio, tiempo y forma* 27. *Serie II, Historia antigua*, 207-231.
- Carneiro, A. (2016). A villa romana, entre a construção literária e a realidade construída. *Anales de arqueología cordobesa* 27, 77-96.
- Carneiro, A. (2017). *Lusitania Romana: del pasado al presente de la investigación*. Mérida: Museo Nacional de Arte Romano.
- Carneiro, A. (2017). O final das Villae na Lusitânia romana. O exemplo da Horta da Torre (Fronreira). *Urbs Regia*, Nº2, 56-59.
- Carneiro, A. (2017). Urbs in Rure: Decorative Programmes and Architectural Models in Lusitania's Villae. *Journal of Mosaic Research* 10, 117-127.
- Carneiro, A. (2019). *Lugares, tempos e pessoas: povoamento rural romano no Alto Alentejo - vol. I*. Coimbra: Coimbra University Press.
- Carneiro, A., & Carpetudo, C. (2018). Arqueologia 3.0. O património com os olhos postos no futuro. *Encontro Ciência '18*, (pp. 1-21).

- Carneiro, A., García, J., Stek, T., & Kalkers, R. (2019). Primeiros resultados do Fronteira Landscape Project. A arqueologia da paisagem romana no Alto Alentejo. *Al-Madan online II Série* 22, 46-54.
- Carpetudo, C. (22 de May de 2017). *The Roman Villa of Horta da Torre*. Fonte: <https://3dheritage.wordpress.com/2017/05/22/the-roman-villa-of-horta-da-torre/>
- Delatte, N. (2001). Lessons from Roman Cement and Concrete. *Journal of professional issues in engineering education and practice*, 109-115.
- Direção-Geral do Património Cultural. (1 de September de 2019). *Portal do Arqueólogo*. Fonte: <http://arqueologia.patrimoniocultural.pt/index.php?sid=sitios&subsid=57427>
- Elsen, J. (2006). Microscopy of historic mortars - a review. *Cement and Concrete research* 36, 1416-1424.
- Eriksson, L. (2018). Hyperspectral imaging on mortars from the inner walls of Carcassonne. A study on the application of near infrared spectroscopy as a non-destructive classification method on historical mortars. 1-40.
- Fernández , C., & Díaz, M. (2008). Geología de la Zona de Ossa-Morena (Sierra de Huelva). *Geología de Huelva : lugares de interés geológico*". 2ª ed.
- Földvári, M. (2011). *Handbook of thermogravimetric system of minerals and its use in geological practice*. Budapest: Geological Institute of Hungary.
- Gonçalves, A., Morán, E., Posseit, M., & Teichner, F. (1999). New aspects of the romanization of the Alto Alentejo (Portugal). *Arqueologia* 24, 101-110.
- Gonçalves, F., & Peinador, A. (1973). *Notícia explicativa da folha 32-B*. Lisboa: Serviços geológicos de Portugal.
- Gonçalves, F., Zbyszewski, G., & Pinto, A. (1975). *Notícia explicativa da folha 32-D Sousel*. Lisboa: Serviços geológicos de Portugal.
- Groot, C., Bartos, P., & Hughes, J. (1999). Historic mortars: characteristics and tests - Concluding summary and state-of-the-art. *International RILEM Workshop on Historic Mortars: characteristics and Tests*, (pp. 443-454). Paisley.
- Holmstrom, I. (1981). Mortars, cements and grouts for conservation and repair. Some urgent needs for repair. *Mortars, cements and grouts used in the conservation of Historic Buildings*. (pp. 19-24). Rome: ICCROM.
- Hubbard, C., Evans, E., & Smith, D. (1976). The Reference Intensity Ratio, I/I_c, for Computer Simulated Powder Patterns. *J. Appl. Cryst.* 9, 169-174.
- Huggett, J. (2015). *Clay minerals*. Heathfield, UK: The Natural History Museum.
- ICCROM. (1981). Mortars, cements and grouts used in the conservation of historic buildings. *Symposium* 3, (pp. 1-424). Rome.
- Jedrzejewska, H. (2014). Old Mortars in Poland: A New Method of Investigation. *Studies in Conservation*, 5:4, 132-138.
- Lewin, S. Z. (1981). X-Ray Diffraction and Scanning Electron Microscope Analysis of Conventional Mortars. *Mortars, cements and grouts used in the conservation of Historic Buildings* (pp. 101-129). Rome: ICCROM.

- Lugwisha, E. (2011). Identification of clay minerals of the eastern southern region of Lake Victoria by ethylene glycol and heat: Xray Diffraction and Infrared Spectroscopy studies. *Tanz. J. Sci. Vol. 37*, 168-178.
- Middendorf, B., Hughes, J. J., Callebaut, K., Baronio, G., & Papayianni, I. (2005). Investigative methods for the characterisation of historic mortars- Part 1: Mineralogical characterisation. *Materials and Structures* 38, 761-769.
- Middendorf, B., Hughes, J., Callebaut, K., Baronio, G., & Papayianni, I. (2005). Investigative methods for the characterisation of historic mortars- Part 2: Chemical characterisation. *Materials and Structures* 38, 771-780.
- Morgado, P., & Rocha, L. (2014). Caminhos antigos do concelho de Monforte: a Canada do Alicerce. *SCIENTIA ANTIQUITATIS*, 1-22.
- Moropoulou, A., Bakolas, A., & Anagnostopoulou, S. (2005). Composite materials in ancient structures. *Cement & Concrete Composites* 27, 295-300.
- Mosser-Ruck, R., Devineau, K., Charpentier, D., & Cathelineau, M. (2005). Effects of ethylene glycol saturation protocols on XRD patterns: a critical review and discussion. *Clays and Clay Minerals, Vol. 53, No. 6*, 631-638.
- Mukasa-Tebandeke, I., Ssebuwufu, P., Nyanzi, S., Schumann, A., Nyakairu, G., Ntale, M., & Lugolobi, F. (2015). The Elemental, Mineralogical, IR, DTA and XRD Analyses Characterized Clays and Clay Minerals of Central and Eastern Uganda. *Advances in Materials Physics and Chemistry* 5, 67-86.
- Neves, S., Borges, J., Oliveira, R., & Caldeira, B. (2014). Magnetometria e georadar aplicados à arqueologia, O caso da Horta da Torre. *Geonovas* 28, 93-98.
- Oliveira, R., Neves, S., Cladeira, B., Borges, J., & Teixidó, T. (2015). Desenvolvimento de Metodologias eficazes de Prospeção Geofísica Aplicadas a diferentes Ambientes Arqueológicos: o Caso de Horta da Torre (resultados preliminares). 1-9.
- Pavía, S., & Caro, S. (2008). An investigation of Roman mortar technology through the petrographic analysis of archaeological material. *Construction and Building Materials* 22, 1807–1811.
- Pelà, L., Roca, P., & Aprile, A. (2017). Combined In-Situ and Laboratory Minor Destructive Testing of Historical Mortars. *International Journal of Architectural Heritage Vol. 12, No. 3*, 334–349.
- Piovesan, R., Curti, E., Grifa, C., Maritan, L., & Mazzoli, C. (s.d.). Petrographic and microstratigraphic analysis of mortar-based building materials from the Temple of Venus, Pompeii. 66-79.
- Robador, M. D., & Arroyo, F. (2013). Characterisation of Roman coatings from the a Roman house in Mérida (Spain). *Journal of Cultural Heritage* 14S, S52-S58.
- Robador, M., Pérez-Rodríguez, J., & Duran, A. (2010). Hydraulic structures of the Roman Mithraeum house in Augusta emerita, Spain. *Journal of Archaeological Science* 37, 2426-2432.
- Rodríguez-Navarro, C. (2009). Binders in historical buildings: Traditional lime in conservation. *Seminario SEM 09*, 91-112.

- Santos Silva, A., Ricardo, J., Salta, M., Adriano, P., Mirão, J., Candeias, A., & Macias, S. (2004). Characterization of Roman mortars from the historical town of Mertola. 1-6.
- Schulze, D. (2005). Clay minerals. Em *Encyclopedia of soils in the environment* (pp. 246-254). West Lafayette, IN: El Sevier.
- Silva, A., Paiva, M., Ricardo, J., Salta, M., Monteiro, A., & Candeias, A. (2006). Characterisation of roman mortars from the archaeological site of Tróia (Portugal). *Materials Science Forum - MATER SCI FORUM*, 1643-1647.
- Stephens, H. M. (1891). *The story of Portugal*. New York: G. P. Putnam's sons.
- Struers. (2014, April). *Mineralogical specimen preparation*. Retrieved from https://www.als.com.tr/?wpfb_dl=135
- Stuart, B. (2007). *Analytical techniques in materials conservation*. London, UK: Wiley.
- USGS. (n.d.). *Clay Mineral Identification Flow Diagram*. Retrieved from <https://pubs.usgs.gov/of/2001/of01-041/html/docs/flow/start.htm>
- Velosa, A., Coroado, J., Veiga, M., & Rocha, F. (2007). Characterisation of roman mortars from Conímbriga with respect to their repair. *Materials Characterization* 58, 1208-1216.
- Warshaw, C., Rosenberg, P., & Roy, R. (1960). Changes effected in layer silicates by heating below 550. *Clay minerals bulletin Vol. 4, No. 23*, 113-125.
- Wentworth, C. (1922). A Scale of Grade and Class Terms for Clastic Sediments. *The Journal of Geology, Vol. 30, No. 5*, 377-392.

APPENDICES

Appendix 1. Catalogue of collected samples and the fractions used for the elaboration of cross and thin sections.

	
HHT-1.	HHT-2
	
HHT-3	HHT-4



HHT-5





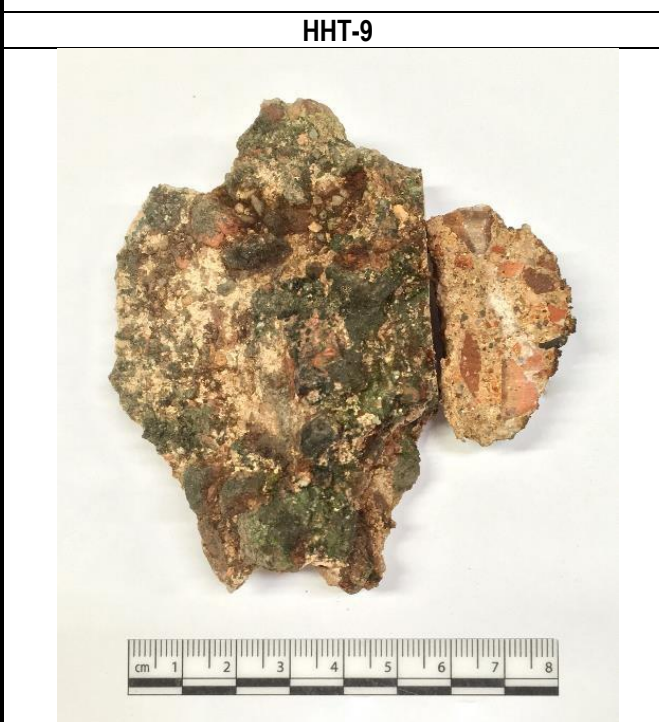
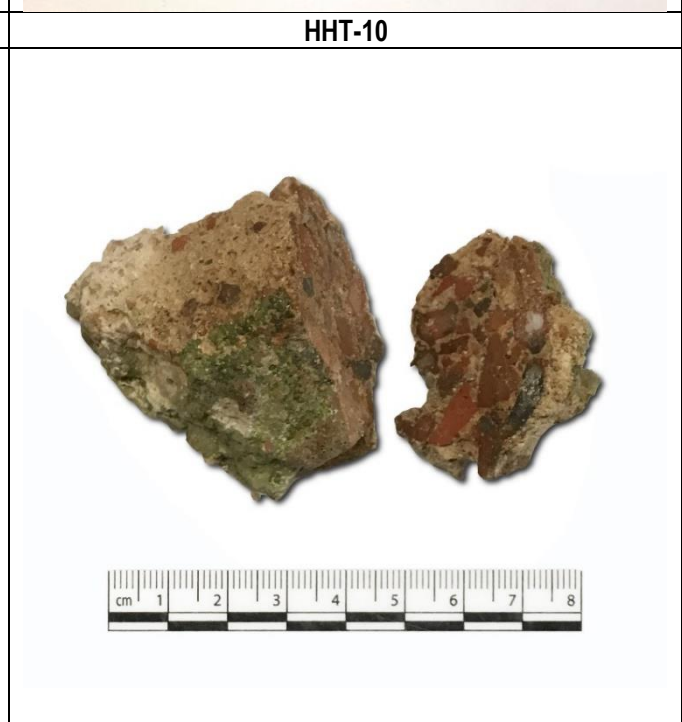

PHHT-6









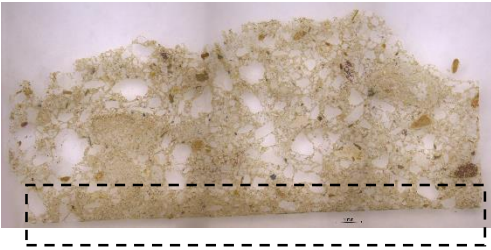
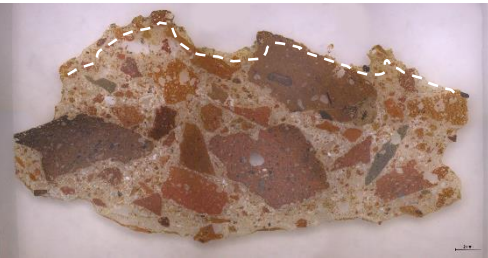
PHHT-7

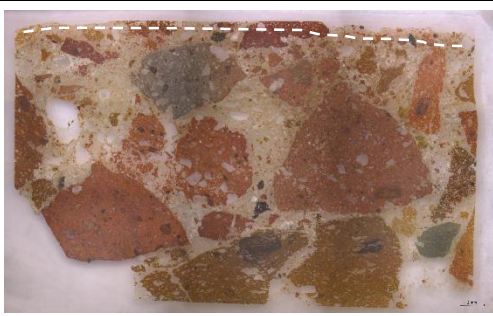




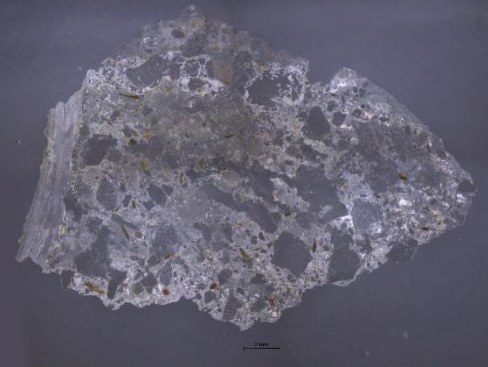


HHT-8

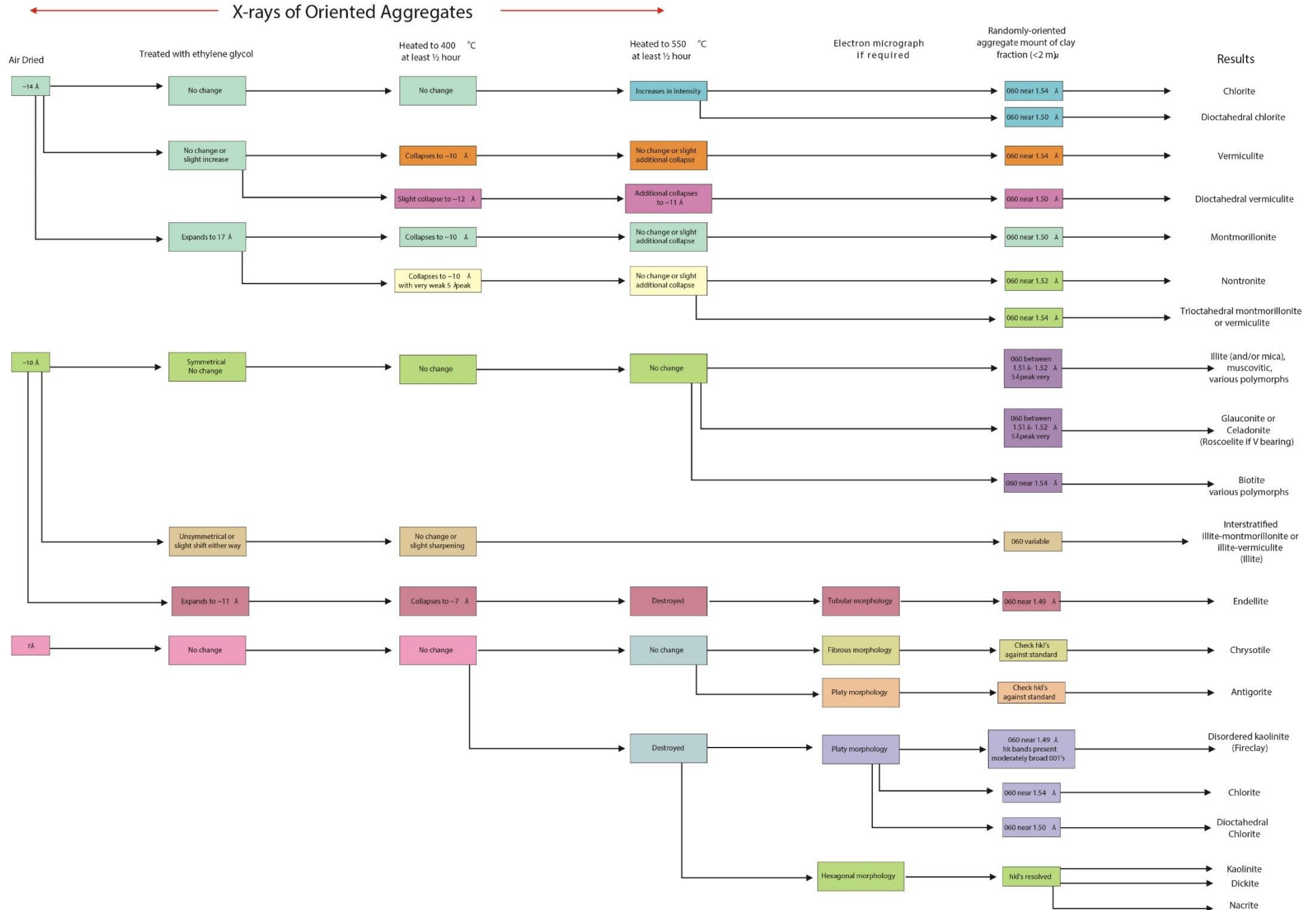
	
HHT-9	HHT-10
	
HHT-11-U	HHT-11-D
	
HHT-12	

Appendix 2. Thin-sections of the samples obtained from cross-sections for OM and VP-SEM-EDS analysis. The white dashed lines indicate the surface in contact with water, and the black dashed squares indicate the surfaces with a chromatic layer. The samples without indication were not in direct contact with water.

			
HHT-1 Interior coating of the double apse	HHT-2 <i>Triclinium</i> floor	HHT-3 Coating of the channel wall	HHT-4 Tank 1 coating
			
HHT-5 Tank 2 coating	PHHT-6 Mural painting with red chromatic layer	PHHT-7 Mural painting with blue chromatic layer	HHT-8 Garden water mirror NE

			
<p>HHT-9-L Garden water mirror SE longitudinal section</p>	<p>HHT-9-T Garden water mirror SE transversal section</p>	<p>HHT-10 Tank 3 North wall</p>	<p>HHT-11-U Tank 3 South wall upper layer</p>
			
<p>HHT-11-D Tank 3 South wall lower layer</p>	<p>HHT-12 Tank 3 East wall</p>		

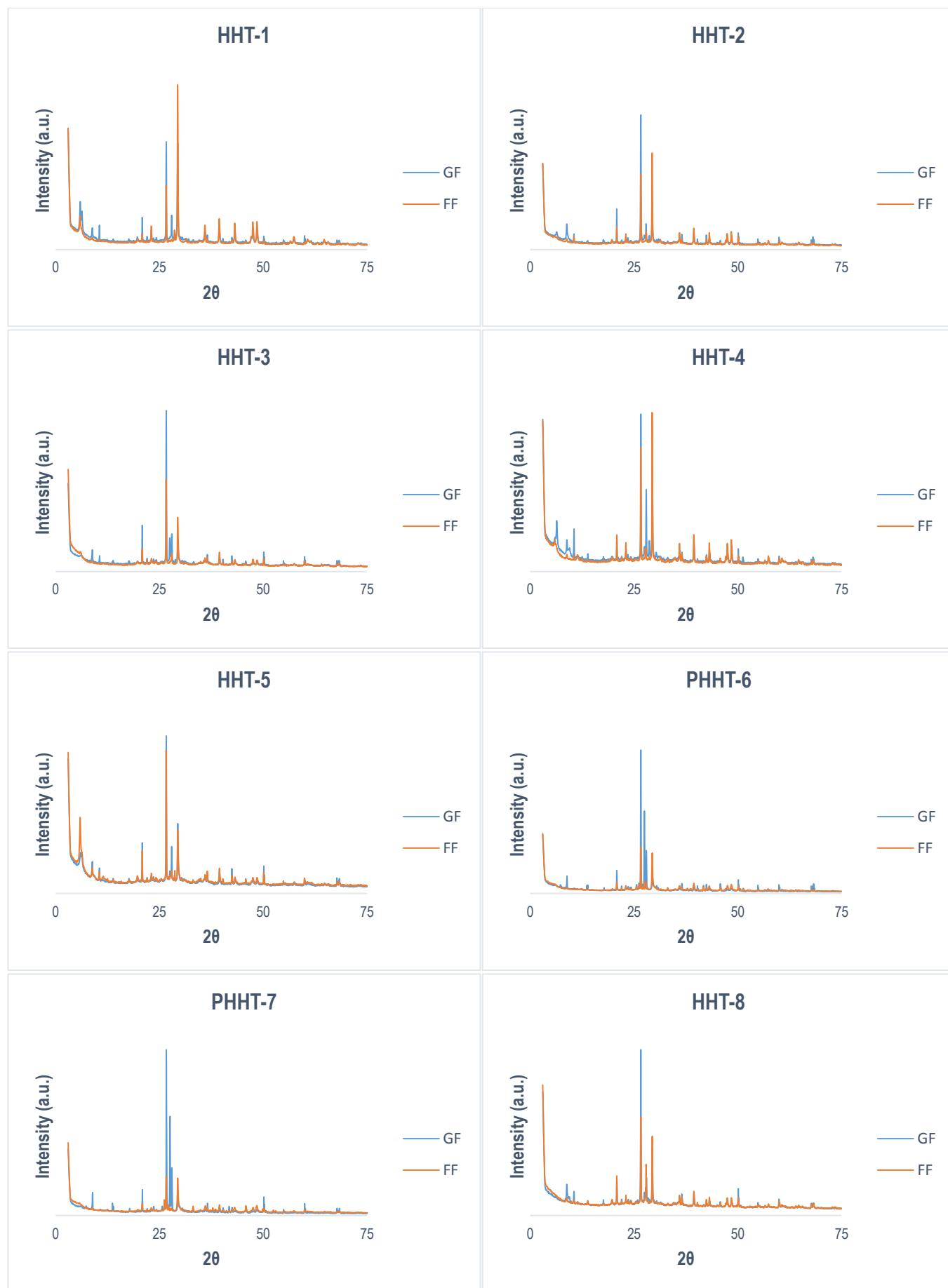
Appendix 3. Clay mineral identification flow diagram from USGS.

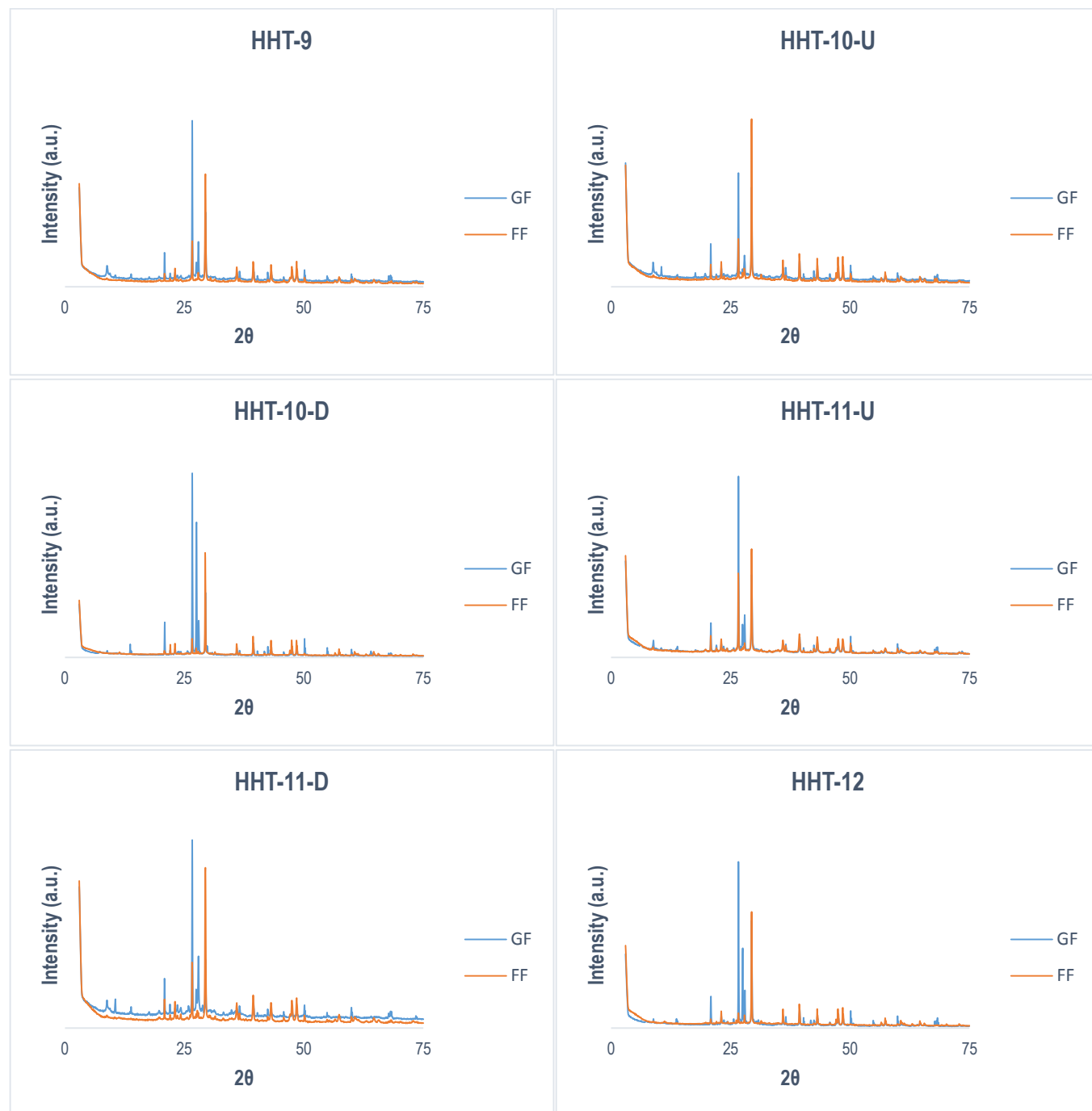


Appendix 4. Results of soluble and insoluble fractions after acid attack, and granulometric analysis performed in insoluble fractions.

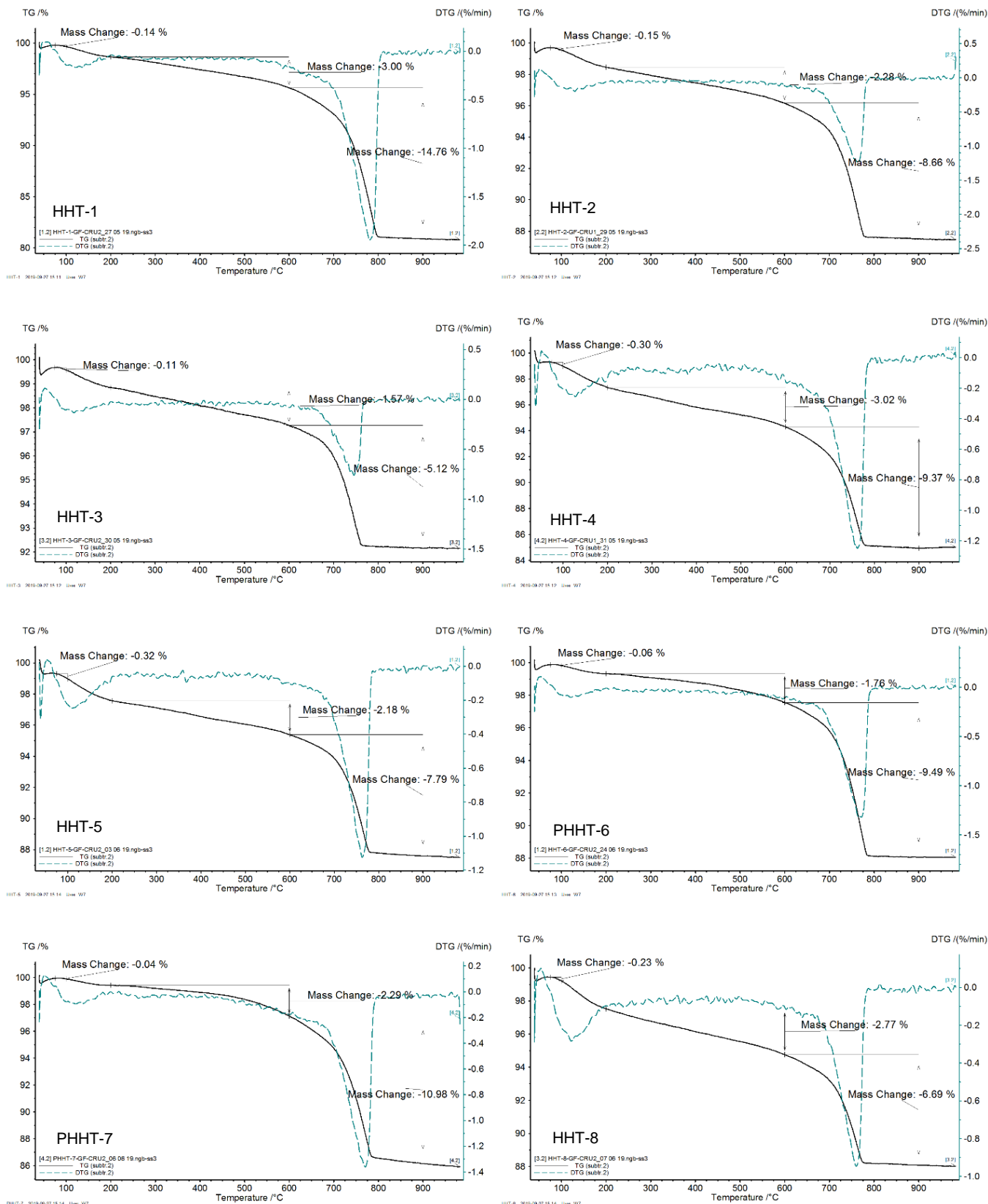
ID			Weight		Fraction (%)		Grain size (%)							
	Sample	Test	Initial	Final	Soluble	Insoluble	> 4 mm	4-2	2-1	1-0.5	0.5-0.25	0.25-0.125	0.125-0.063	< 0.063
1	HHT-1	HCl 1	10.0 g	5.4 g	45.8	54.2	6.4	19.7	24.8	17.1	10.8	5.5	9.9	5.8
2	HHT-1	HCl 2	10.0 g	4.9 g	50.9	49.0	0.0	18.7	21.4	18.4	13.1	12.0	10.4	6.0
3	HHT-2	HCl 1	10.0 g	7.0 g	29.9	70.2	53.6	11.8	7.7	6.3	4.5	5.7	7.5	2.8
4	HHT-2	HCl 2	10.0 g	6.5 g	35.3	64.4	21.0	26.1	15.1	9.6	6.8	7.0	8.4	5.9
5	HHT-3	HCl 1	10.0 g	6.8 g	32.2	67.9	57.6	6.7	8.9	7.7	6.8	4.9	4.1	3.3
6	HHT-3	HCl 2	10.0 g	6.1 g	38.8	60.7	40.2	11.5	7.2	7.4	7.2	10.1	9.2	7.2
7	HHT-4	HCl 1	10.1 g	6.4 g	35.4	63.8	22.5	22.0	11.0	8.6	8.7	10.8	9.7	6.7
8	HHT-4	HCl 2	10.0 g	6.0 g	40.4	59.4	20.9	17.8	12.3	9.3	6.4	9.5	13.8	10.1
10	HHT-5	HCl 2	10.0 g	7.1 g	28.5	71.2	14.0	15.9	10.9	7.8	7.6	12.8	19.9	11.0
11	HHT-5	HCl 3	10.0 g	7.0 g	29.8	69.6	24.7	17.8	12.1	8.9	8.5	10.1	10.7	7.3
12	HHT-6	HCl 1	10.0 g	7.6 g	23.7	76.4	1.7	14.6	31.4	21.5	14.8	7.9	5.0	3.1
13	HHT-6	HCl 2	10.0 g	7.5 g	25.1	74.9	1.4	15.4	28.5	20.7	15.8	8.6	6.0	3.7
14	PPHT-7	HCl 1	10.0 g	7.2 g	27.3	72.2	3.4	14.7	24.0	20.3	14.3	10.9	7.2	5.1
15	PPHT-7	HCl 2	10.0 g	7.0 g	30.2	69.7	0.0	16.0	27.1	20.1	14.2	10.6	7.5	4.6
16	HHT-8	HCl 1	10.0 g	7.4 g	25.8	74.0	48.2	19.1	7.2	4.2	3.6	5.2	6.3	6.2
17	HHT-8	HCl 2	10.1 g	6.6 g	33.7	65.6	43.3	17.2	10.6	6.1	3.9	5.2	7.0	6.5
18	HHT-9	HCl 1	10.0 g	6.7 g	33.5	66.6	61.6	9.1	6.7	4.2	3.7	5.1	5.4	4.1
19	HHT-9	HCl 2	10.0 g	7.5 g	24.6	75.3	65.1	12.9	4.9	3.0	2.1	2.8	4.8	4.5
20	HHT-10-U	HCl 1	10.0 g	6.7 g	33.1	66.6	25.3	22.4	16.2	9.4	6.8	7.3	8.5	4.2
21	HHT-10-U	HCl 2	10.0 g	6.1 g	38.6	61.2	9.9	26.8	19.6	10.5	8.1	8.1	9.1	7.9
22	HHT-10-D	HCl 1	10.0 g	6.9 g	31.3	68.8	11.3	23.4	21.9	18.0	11.2	6.1	4.7	3.4
23	HHT-10-D	HCl 2	10.0 g	6.5 g	34.7	65.3	5.2	17.0	32.8	21.4	11.2	6.6	3.8	1.9
24	HHT-11-U	HCl 1	10.0 g	7.6 g	23.6	76.6	41.4	12.5	13.4	11.5	5.3	5.1	6.0	4.7
25	HHT-11-U	HCl 2	10.0 g	7.6 g	24.5	75.7	49.9	8.7	12.8	9.3	5.4	5.2	5.2	3.5
26	HHT-11-D	HCl 1	10.0 g	7.9 g	21.4	79.1	60.6	11.2	7.2	4.0	2.1	2.5	4.6	7.8
27	HHT-11-D	HCl 2	10.0 g	8.2 g	18.0	82.2	63.4	12.0	6.0	3.4	2.4	2.9	4.0	5.8
28	HHT-12	HCl 1	10.0 g	7.3 g	27.4	72.5	0.0	23.6	30.0	22.8	13.9	5.7	2.7	1.3
29	HHT-12	HCl 2	10.0 g	6.1 g	39.3	60.7	4.2	15.0	27.6	24.0	16.9	7.5	3.2	1.7

Appendix 5. X-ray Diffractograms of the powdered samples from *villa* Horta da Torre. Relationship between global and fine fractions results.

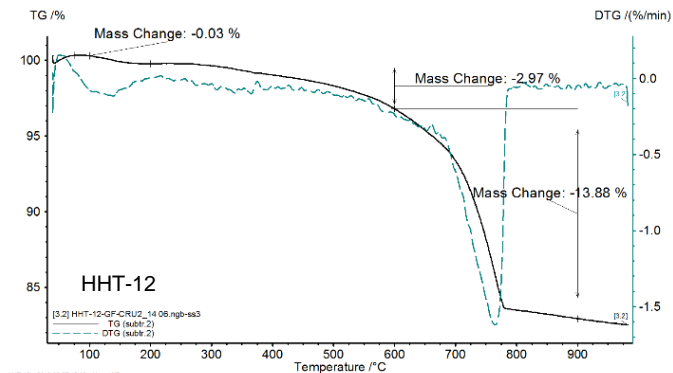
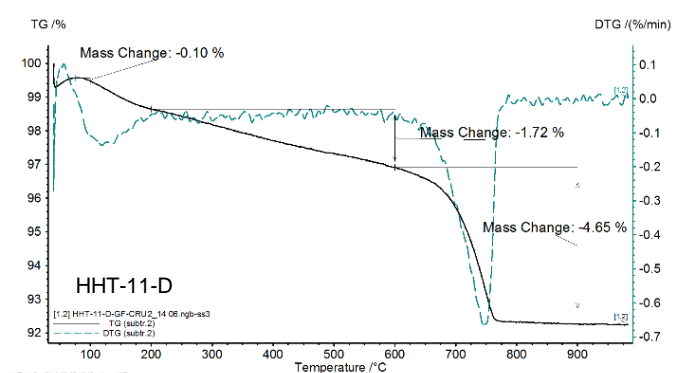
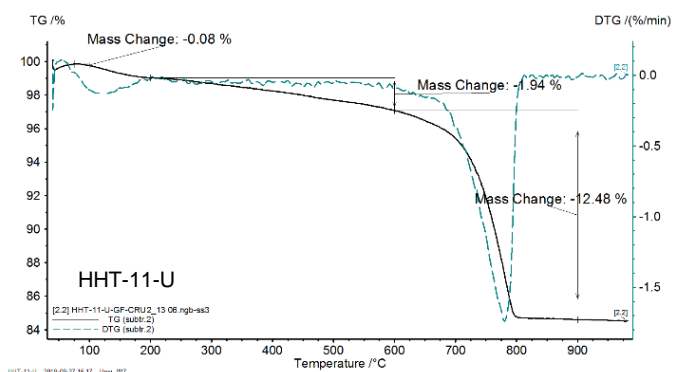
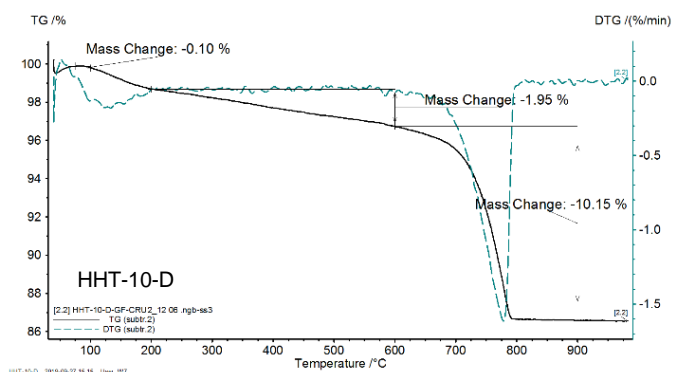
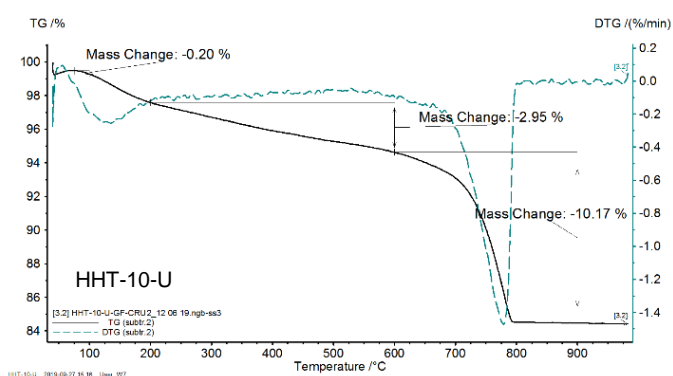
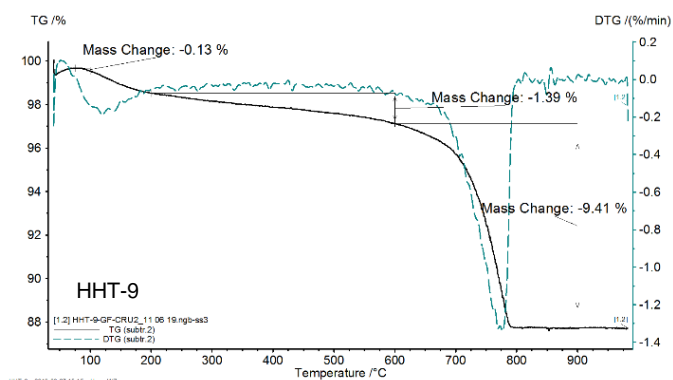




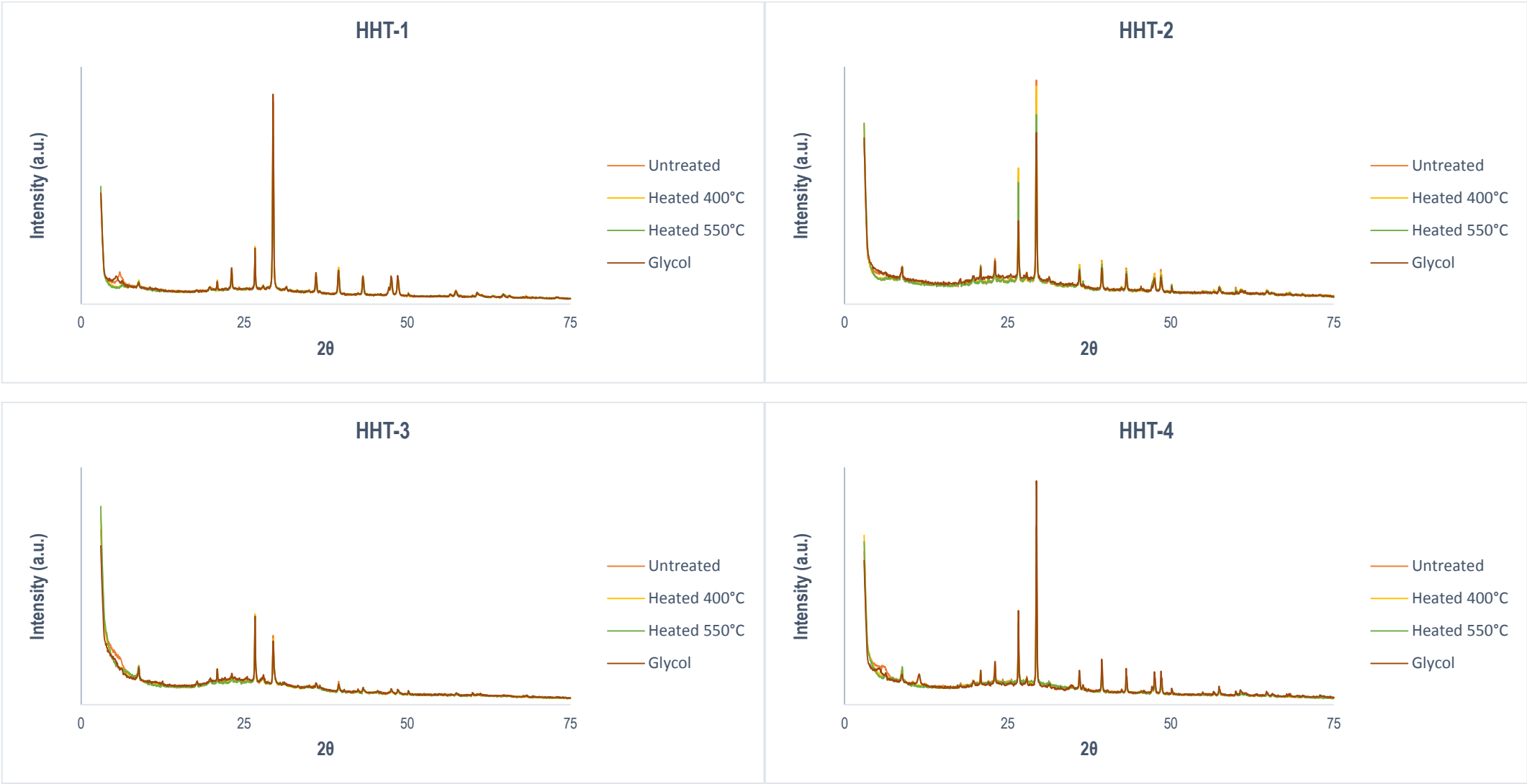
Appendix 6. Thermograms of the results of the global fraction powders of the samples from *villa Horta da Torre*.



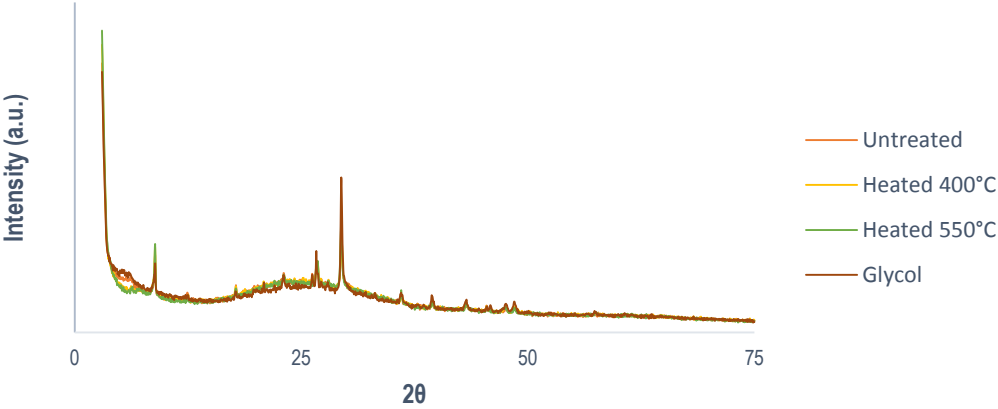
Appendix 6 (continuation).



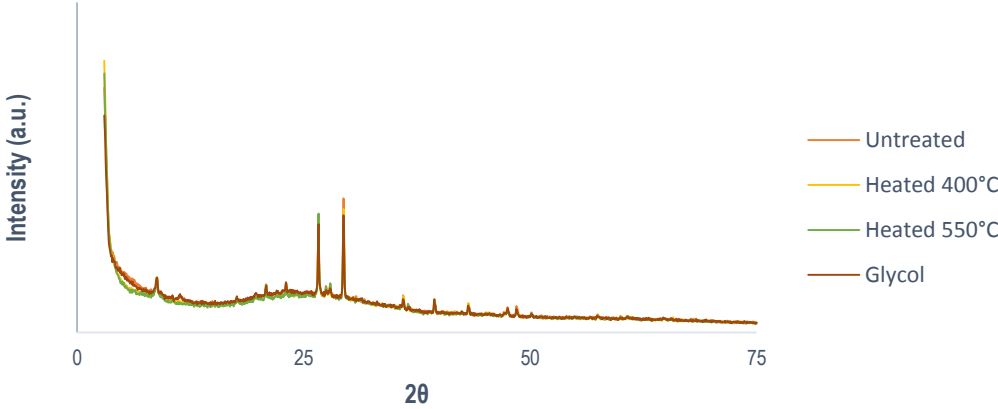
Appendix 7. X-ray diffractograms for clay mineral identification of the samples.



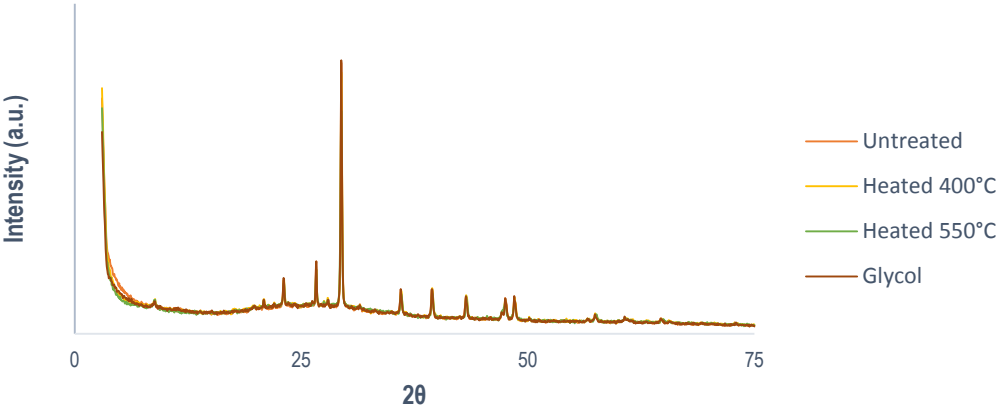
PHHT-6



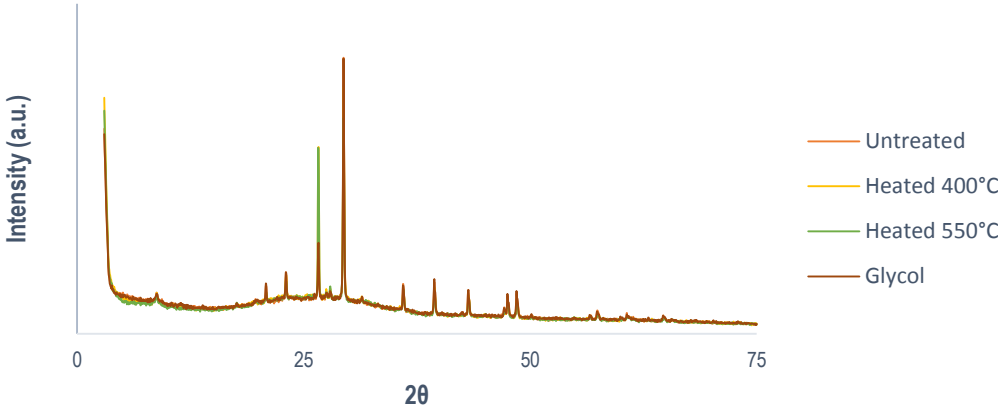
HHT-8



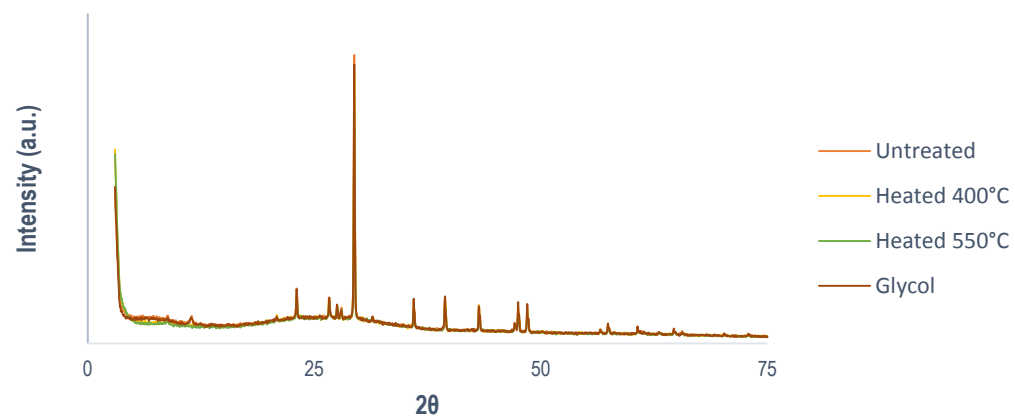
HHT-9



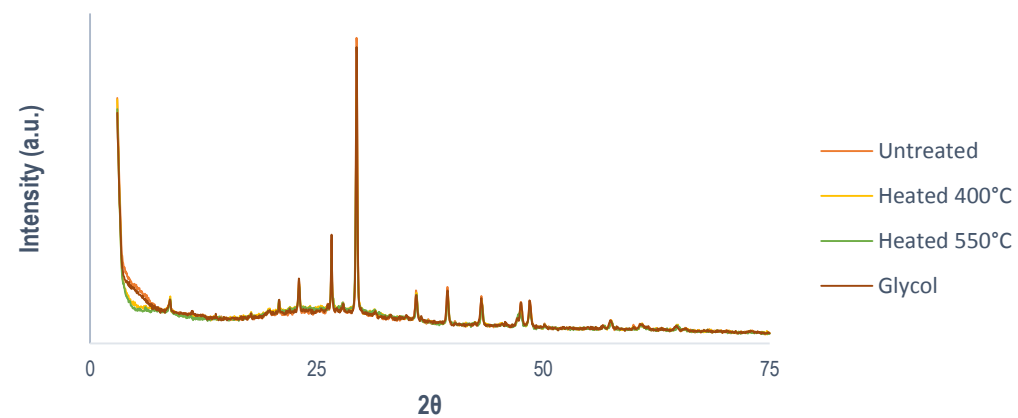
HHT-10-U



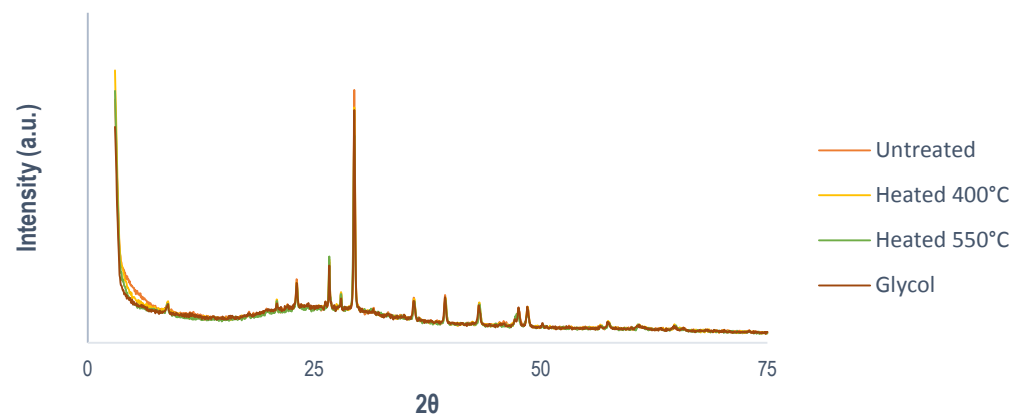
HHT-10-D



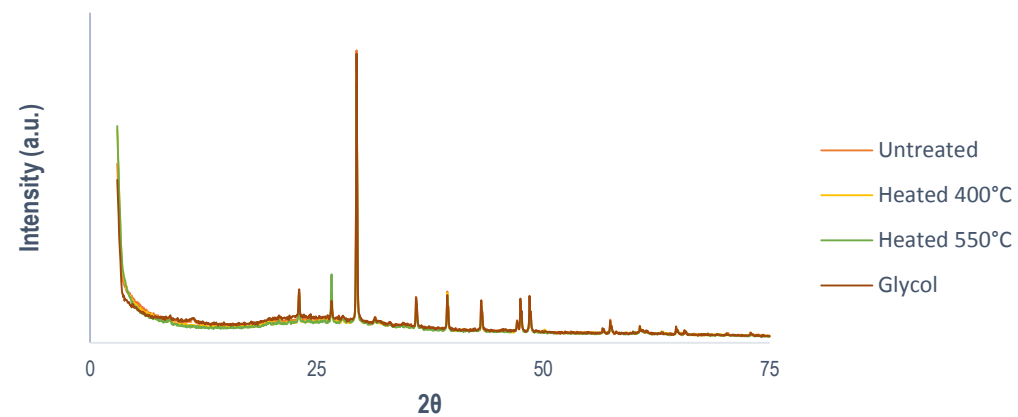
HHT-11-U











HHT-11-D











HHT-12



















Appendix 8. Insoluble residues obtained after acid attack, observed by Stereozoom microscope.

<div> Sample HHT-1 HCl 2 </div>		
	> 4 mm	4-2 mm
		
2-1 mm	1-0.5 mm	0.5-0.25 mm
		
0.25-0.125 mm	0.125-0.063 mm	< 0.063 mm






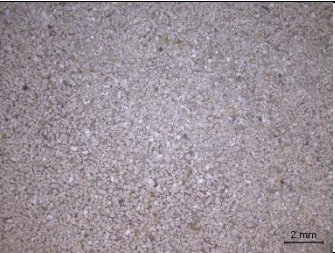

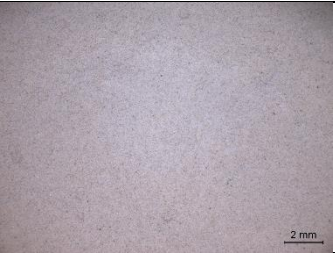
<div> Sample HHT-2 HCl 2 </div>		
	> 4 mm	4-2 mm
		
2-1 mm	1-0.5 mm	0.5-0.25 mm
		
0.25-0.125 mm	0.125-0.063 mm	< 0.063 mm









Appendix 8 (continuation).

Sample HHT-4 HCl 2		
	> 4 mm	4-2 mm
		
2-1 mm	1-0.5 mm	0.5-0.25 mm
		
0.25-0.125 mm	0.125-0.063 mm	< 0.063 mm









Sample HHT-5 HCl 2		
	> 4 mm	4-2 mm
		
2-1 mm	1-0.5 mm	0.5-0.25 mm
		
0.25-0.125 mm	0.125-0.063 mm	< 0.063 mm









Appendix 8 (continuation).

Sample PHHT-7 HCI 1		
	> 4 mm	4-2 mm
		
2-1 mm	1-0.5 mm	0.5-0.25 mm
		
0.25-0.125 mm	0.125-0.063 mm	< 0.063 mm






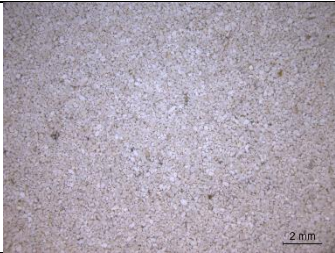
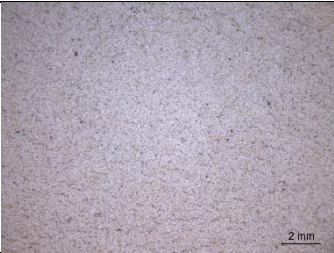
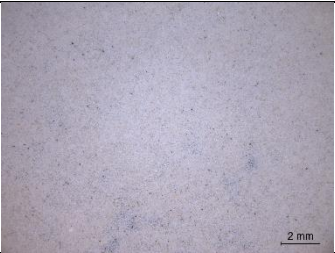
Sample HHT-8 HCI 2		
	> 4 mm	4-2 mm
		
2-1 mm	1-0.5 mm	0.5-0.25 mm
		
0.25-0.125 mm	0.125-0.063 mm	< 0.063 mm









Appendix 8 (continuation).

Sample HHT-9 HCI 1		
	> 4 mm	4-2 mm
		
2-1 mm	1-0.5 mm	0.5-0.25 mm
		
0.25-0.125 mm	0.125-0.063 mm	< 0.063 mm









Sample HHT-10-U HCI 1		
	> 4 mm	4-2 mm
		
2-1 mm	1-0.5 mm	0.5-0.25 mm
		
0.25-0.125 mm	0.125-0.063 mm	< 0.063 mm





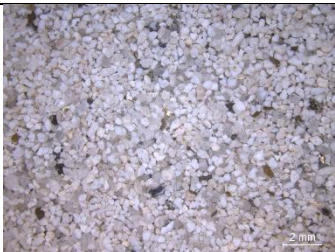

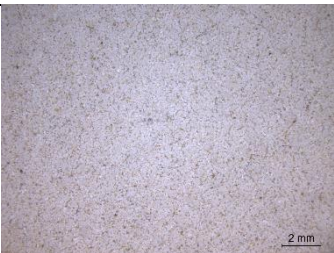
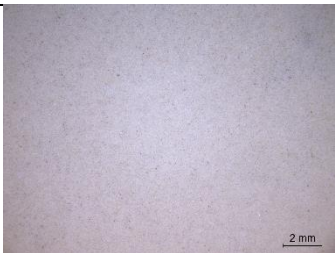
Appendix 8 (continuation).

Sample HHT-10-D HCI 2			
	> 4 mm		4-2 mm
			
2-1 mm	1-0.5 mm	0.5-0.25 mm	
			
0.25-0.125 mm	0.125-0.063 mm	< 0.063 mm	

Sample HHT-11-U HCI 1			
	> 4 mm		4-2 mm
			
2-1 mm	1-0.5 mm	0.5-0.25 mm	
			
0.25-0.125 mm	0.125-0.063 mm	< 0.063 mm	

Appendix 8 (continuation).

<p>Sample HHT-11-D HCl 2</p>				
	> 4 mm		4-2 mm	
				
2-1 mm	1-0.5 mm	0.5-0.25 mm		
				
0.25-0.125 mm	0.125-0.063 mm	< 0.063 mm		

<p>Sample HHT-12 HCl 2</p>				
	> 4 mm		4-2 mm	
				
2-1 mm	1-0.5 mm	0.5-0.25 mm		
				
0.25-0.125 mm	0.125-0.063 mm	< 0.063 mm		